



Search for new phenomena in events containing a same-flavour opposite-sign dilepton pair, jets, and large missing transverse momentum in $\sqrt{s} = 13$ TeV pp collisions with the ATLAS detector

The ATLAS Collaboration

Two searches for new phenomena in final states containing a same-flavour opposite-sign lepton (electron or muon) pair, jets, and large missing transverse momentum are presented. These searches make use of proton–proton collision data, collected during 2015 and 2016 at a centre-of-mass energy $\sqrt{s} = 13$ TeV by the ATLAS detector at the Large Hadron Collider, which correspond to an integrated luminosity of 14.7 fb^{-1} . Both searches target the pair production of supersymmetric particles, squarks or gluinos, which decay to final states containing a same-flavour opposite-sign lepton pair via one of two mechanisms: a leptonically decaying Z boson in the final state, leading to a peak in the dilepton invariant-mass distribution around the Z boson mass; and decays of neutralinos (e.g. $\tilde{\chi}_2^0 \rightarrow \ell^+ \ell^- \tilde{\chi}_1^0$), yielding a kinematic endpoint in the dilepton invariant-mass spectrum. The data are found to be consistent with the Standard Model expectation. Results are interpreted in simplified models of gluino-pair (squark-pair) production, and provide sensitivity to gluinos (squarks) with masses as large as 1.70 TeV (980 GeV).

Contents

| | | |
|-----------|---|-----------|
| 1 | Introduction | 2 |
| 2 | ATLAS detector | 4 |
| 3 | SUSY signal models | 4 |
| 4 | Data and Monte Carlo samples | 6 |
| 5 | Analysis object identification and selection | 8 |
| 6 | Event selection | 9 |
| 7 | Background estimation | 14 |
| 7.1 | Flavour-symmetric backgrounds | 14 |
| 7.2 | Z/γ^* + jets background | 17 |
| 7.3 | Fake-lepton background | 18 |
| 7.4 | Diboson and rare top processes | 20 |
| 7.5 | Results in validation regions | 20 |
| 8 | Systematic uncertainties | 23 |
| 9 | Results | 25 |
| 9.1 | Results in SRZ | 25 |
| 9.2 | Results in the edge SRs | 30 |
| 10 | Interpretation | 35 |
| 11 | Conclusion | 40 |

1 Introduction

Supersymmetry (SUSY) [1–6] is an extension of the Standard Model (SM) that introduces partner particles (called *sparticles*) that differ by half a unit of spin from their SM counterparts. The squarks (\tilde{q}) and sleptons ($\tilde{\ell}$) are the scalar partners of the quarks and leptons, respectively, and the gluinos (\tilde{g}) are the fermionic partners of the gluons. The charginos ($\tilde{\chi}_i^\pm$) and neutralinos ($\tilde{\chi}_i^0$) are the mass eigenstates (where the index i is ordered from the lightest to the heaviest) formed from the linear superpositions of the SUSY partners of the Higgs bosons (higgsinos) and electroweak gauge bosons.

If the masses of the gluino, higgsinos, and top squarks are close to the TeV scale, SUSY may offer a solution to the SM hierarchy problem [7–10]. In this case, strongly interacting sparticles should be produced at a high enough rate to be detected by the experiments at the Large Hadron Collider (LHC). For models with R-parity conservation [11], such sparticles would be pair-produced and are expected to decay into jets, perhaps leptons, and the lightest stable SUSY particle (LSP). The LSP is assumed to be only weakly interacting and therefore escapes the detector, resulting in events with potentially large missing transverse momentum (p_T^{miss} , with magnitude E_T^{miss}). In such a scenario the LSP could be a dark-matter candidate [12, 13].

Final states containing pairs of leptons may arise from the cascade decays of squarks and gluinos via several mechanisms. In this paper, two search channels are considered that target scenarios with same-flavour (SF) opposite-sign (OS) lepton (electron or muon) pairs. The first channel requires a lepton pair with an invariant mass $m_{\ell\ell}$ that is consistent with the Z boson mass m_Z (“on-shell Z ” channel), while the second channel considers all SFOS lepton pairs (“edge” channel). The presence of two leptons in the final state suppresses large SM backgrounds from, e.g., QCD multijet and W + jets production, providing a clean environment in which to search for new physics. As discussed further below, in such events the distribution of dilepton mass $m_{\ell\ell}$ may be used to characterise the nature of the SUSY particle decay and constrain mass differences between SUSY particles.

The SFOS lepton pairs may be produced in the decay $\tilde{\chi}_2^0 \rightarrow \ell^+ \ell^- \tilde{\chi}_1^0$ (or, in models of generalised gauge mediation with a gravitino LSP [14–16], via $\tilde{\chi}_1^0 \rightarrow \ell^+ \ell^- \tilde{G}$). The properties of the $\tilde{\chi}_2^0$ decay depend on the mass difference $\Delta m_\chi \equiv m_{\tilde{\chi}_2^0} - m_{\tilde{\chi}_1^0}$, the mixing of the charginos and neutralinos, and on whether there are additional sparticles with masses less than $m_{\tilde{\chi}_2^0}$ that may be produced in the decay of the $\tilde{\chi}_2^0$ particle. For $\Delta m_\chi > m_Z$, SFOS lepton pairs may be produced in the decay $\tilde{\chi}_2^0 \rightarrow Z \tilde{\chi}_1^0 \rightarrow \ell^+ \ell^- \tilde{\chi}_1^0$, leading to a peak in the invariant-mass distribution near $m_{\ell\ell} \approx m_Z$. Such models are the target of the on-shell Z search. For $\Delta m_\chi < m_Z$, the decay $\tilde{\chi}_2^0 \rightarrow Z^* \tilde{\chi}_1^0 \rightarrow \ell^+ \ell^- \tilde{\chi}_1^0$ leads to a rising $m_{\ell\ell}$ distribution that is truncated at a kinematic endpoint, whose position is given by $m_{\ell\ell}^{\max} = \Delta m_\chi < m_Z$, below the Z boson mass peak. If there are sleptons with masses less than $m_{\tilde{\chi}_2^0}$, the $\tilde{\chi}_2^0$ particle may decay as $\tilde{\chi}_2^0 \rightarrow \tilde{\ell}^\pm \ell^\mp \rightarrow \ell^+ \ell^- \tilde{\chi}_1^0$, also leading to a kinematic endpoint but with a different shape and $m_{\ell\ell}$ endpoint position, given by $m_{\ell\ell}^{\max} = \sqrt{(m_{\tilde{\chi}_2^0}^2 - m_{\tilde{\ell}}^2)(m_{\tilde{\ell}}^2 - m_{\tilde{\chi}_1^0}^2)}/m_{\tilde{\ell}}$, which may occur below, on, or above the Z boson mass peak. The latter two scenarios are targeted by the “edge” search channel, which considers the full $m_{\ell\ell}$ range.

This paper reports on a search for SUSY in the same-flavour dilepton final state with 14.7 fb^{-1} of pp collision data at $\sqrt{s} = 13 \text{ TeV}$ recorded in 2015 and 2016 by the ATLAS detector at the LHC. Searches for SUSY in the Z + jets + E_T^{miss} final state have previously been performed at $\sqrt{s} = 8 \text{ TeV}$ by the CMS [17, 18] and ATLAS [19] collaborations using Run-1 LHC data. In the ATLAS analysis performed with 20.3 fb^{-1} of $\sqrt{s} = 8 \text{ TeV}$ data reported in Ref. [19], an excess of events above the SM background with a significance of 3.0 standard deviations was observed. The event selection criteria for the on-shell Z search in this paper are almost identical, differing only in the details of the analysis object definitions and missing transverse momentum. CMS performed a search with $\sqrt{s} = 13 \text{ TeV}$ data in a similar kinematic region but did not observe evidence to corroborate this excess [20].

Searches for an edge in the $m_{\ell\ell}$ distribution in events with 2ℓ + jets + E_T^{miss} have been performed by the CMS [18, 21] and ATLAS [19] collaborations. In Ref. [18], CMS reported an excess above the SM prediction with a significance of 2.6 standard deviations. In a similar search region, however, the Run-1 ATLAS analysis [19] and Run-2 CMS analysis [20] observed results consistent with the SM prediction.

2 ATLAS detector

The ATLAS detector [22] is a general-purpose detector with almost 4π coverage in solid angle.¹ The detector comprises an inner tracking detector, a system of calorimeters, and a muon spectrometer.

The inner tracking detector (ID) is immersed in a 2 T magnetic field provided by a superconducting solenoid and allows charged-particle tracking out to $|\eta| = 2.5$. It includes silicon-pixel and silicon-strip tracking detectors inside a straw-tube tracking detector. In 2015 the detector received a new innermost layer of silicon pixels, which improves the track impact parameter resolution by almost a factor of two in both the transverse and longitudinal directions [23].

High-granularity electromagnetic and hadronic calorimeters cover the region $|\eta| < 4.9$. All the electromagnetic calorimeters, as well as the endcap and forward hadronic calorimeters, are sampling calorimeters with liquid argon as the active medium and lead, copper, or tungsten as the absorber. The central hadronic calorimeter is a sampling calorimeter with scintillator tiles as the active medium and steel as the absorber.

The muon spectrometer uses several detector technologies to provide precision tracking out to $|\eta| = 2.7$ and triggering in $|\eta| < 2.4$, making use of a system of three toroidal magnets.

The ATLAS detector incorporates a two-level trigger system, with the first level implemented in custom hardware and the second level implemented in software. This trigger system selects events of interest at an output rate of about 1 kHz.

3 SUSY signal models

SUSY-inspired simplified models are considered as signal scenarios for these analyses. In all of these models, squarks or gluinos are directly pair-produced, decaying via an intermediate neutralino, $\tilde{\chi}_2^0$, into the LSP ($\tilde{\chi}_1^0$). All sparticles not directly involved in the decay chains considered are effectively decoupled. Two example decay topologies are shown in Figure 1. For all models with gluino-pair production, a three-body decay for $\tilde{g} \rightarrow q\bar{q}\tilde{\chi}_2^0$ is used. Signal models are generated in a grid over a two-dimensional space, varying the gluino or squark mass and the mass of either the $\tilde{\chi}_2^0$ or the $\tilde{\chi}_1^0$.

Three models, one with squark-pair production and two with gluino-pair production, which result exclusively in events with two on-shell Z bosons in the final state are considered for the on-shell search. For two of these models, signal mass points are generated across the $\tilde{g}\text{-}\tilde{\chi}_2^0$ (or $\tilde{q}\text{-}\tilde{\chi}_2^0$) plane. These models are produced following the decays $\tilde{g} \rightarrow q\bar{q}\tilde{\chi}_2^0$ or $\tilde{q} \rightarrow q\tilde{\chi}_2^0$, with the $\tilde{\chi}_1^0$ (LSP) mass set to 1 GeV, inspired by SUSY scenarios with a low-mass LSP (e.g. generalised gauge mediation). These two models are referred to here as the $\tilde{g}\text{-}\tilde{\chi}_2^0$ on-shell and $\tilde{q}\text{-}\tilde{\chi}_2^0$ on-shell grids, respectively, and are summarised in Table 1. The third model is based on MSSM-inspired topologies [24–26] with potentially higher mass LSPs. Signal points are generated across the $\tilde{g}\text{-}\tilde{\chi}_1^0$ plane, and this model is thus referred to as the $\tilde{g}\text{-}\tilde{\chi}_1^0$ on-shell grid. In this case the $\tilde{\chi}_2^0$ mass is set to be 100 GeV above the $\tilde{\chi}_1^0$ mass, which in many models maximises the

¹ ATLAS uses a right-handed coordinate system with its origin at the nominal interaction point (IP) in the centre of the detector and the z -axis along the beam pipe. The x -axis points from the IP to the centre of the LHC ring, and the y -axis points upward. Cylindrical coordinates (r, ϕ) are used in the transverse plane, ϕ being the azimuthal angle around the z -axis. The pseudorapidity is defined in terms of the polar angle θ as $\eta = -\ln \tan(\theta/2)$ and the rapidity is defined as $y = 1/2 \cdot \ln[(E + p_z)/(E - p_z)]$, where E is the energy and p_z the longitudinal momentum of the object of interest. The opening angle between two analysis objects in the detector is defined as $\Delta R = \sqrt{(\Delta y)^2 + (\Delta\phi)^2}$.

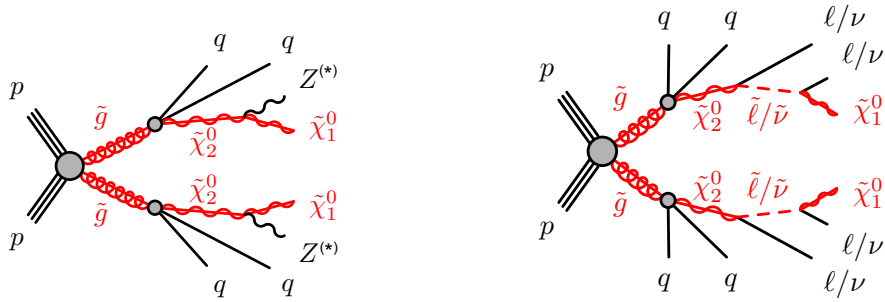


Figure 1: Example decay topologies for two of the simplified models considered, involving gluino-pair production, with the gluinos following an effective three-body decay for $\tilde{g} \rightarrow q\bar{q}\tilde{\chi}_2^0$, with $\tilde{\chi}_2^0 \rightarrow Z^{(*)}\tilde{\chi}_1^0$ (left) and $\tilde{\chi}_2^0 \rightarrow \tilde{\ell}^\mp \ell^\pm/\tilde{\nu}$ (right). For simplicity, no distinction is made between particles and antiparticles.

branching fraction of the $\tilde{\chi}_2^0$ decay to Z bosons. For the two models with gluino-pair production, since the gluino coupling to $q\bar{q}$ is flavour independent and the corresponding flavours of squarks are assumed to be mass degenerate, the branching fractions for $q = u, d, c, s$ are each 25%. Other ATLAS searches are dedicated to final states with two leptons and heavy flavour jets [27, 28]. For the model involving squark-pair production, the superpartners of the u, d, c and s quarks have the same mass, with the superpartners of the b and t quarks being decoupled.

Table 1: Summary of the simplified signal model topologies used in this paper. Here x and y denote the x - y plane across which the signal model masses are varied to construct the signal grid. For the slepton model, the masses of the superpartners of the left-handed leptons are given by $[m(\tilde{\chi}_2^0) + m(\tilde{\chi}_1^0)]/2$, while the superpartners of the right-handed leptons are decoupled.

| Model | Production mode | Quark flavours | $m(\tilde{g})/m(\tilde{q})$ | $m(\tilde{\chi}_2^0)$ | $m(\tilde{\chi}_1^0)$ |
|---------------------------------------|----------------------|-----------------|-----------------------------|--|-----------------------|
| $\tilde{g}-\tilde{\chi}_2^0$ on-shell | $\tilde{g}\tilde{g}$ | u, d, c, s | x | y | 1 GeV |
| $\tilde{g}-\tilde{\chi}_1^0$ on-shell | $\tilde{g}\tilde{g}$ | u, d, c, s | x | $m(\tilde{\chi}_1^0) + 100$ GeV | y |
| $\tilde{q}-\tilde{\chi}_2^0$ on-shell | $\tilde{q}\tilde{q}$ | u, d, c, s | x | y | 1 GeV |
| $Z^{(*)}$ | $\tilde{g}\tilde{g}$ | u, d, c, s, b | x | $[m(\tilde{g}) + m(\tilde{\chi}_1^0)]/2$ | y |
| slepton | $\tilde{g}\tilde{g}$ | u, d, c, s, b | x | $[m(\tilde{g}) + m(\tilde{\chi}_1^0)]/2$ | y |

The edge search considers two scenarios, both of which involve the direct pair production of gluinos and differ by the decay mode of the $\tilde{\chi}_2^0$. These signal models are also summarised in Table 1. In the $Z^{(*)}$ model the $\tilde{\chi}_2^0$ decays as $\tilde{\chi}_2^0 \rightarrow Z^{(*)}\tilde{\chi}_1^0$. For $\Delta m_\chi = m(\tilde{\chi}_2^0) - m(\tilde{\chi}_1^0) > m_Z$, the Z boson is on-shell, leading to a peak in the $m_{\ell\ell}$ distribution at m_Z , while for $\Delta m_\chi < m_Z$, the Z boson is off-shell, leading to an edge in the dilepton mass distribution with a position below m_Z . The slepton model assumes that the sleptons are lighter than the $\tilde{\chi}_2^0$, which decays as $\tilde{\chi}_2^0 \rightarrow \tilde{\ell}^\mp \ell^\pm$ with $\tilde{\ell} \rightarrow \ell\tilde{\chi}_1^0$ or as $\tilde{\chi}_2^0 \rightarrow \tilde{\nu}\nu$ with $\tilde{\nu} \rightarrow \nu\tilde{\chi}_1^0$, each with a branching fraction of 50%, where $\tilde{\ell} = \tilde{e}, \tilde{\mu}, \tilde{\tau}$ and $\tilde{\nu} = \tilde{\nu}_e, \tilde{\nu}_\mu, \tilde{\nu}_\tau$. The endpoint position can occur at any mass, highlighting the need to search over the full dilepton mass distribution. The gluino decays as $\tilde{g} \rightarrow q\bar{q}\tilde{\chi}_2^0$, and both models have equal branching fractions for $q = u, d, c, s, b$. The $\tilde{\chi}_2^0$ mass is set to the average of the gluino and $\tilde{\chi}_1^0$ masses. For the slepton model, the masses of the superpartners of the left-handed leptons are set as the average of the $\tilde{\chi}_2^0$ and $\tilde{\chi}_1^0$ masses, while the superpartners of the right-handed leptons are decoupled. The three slepton flavours are mass-degenerate. In both these models the \tilde{g} and $\tilde{\chi}_1^0$ masses are free parameters that are varied to produce the two-dimensional signal grid. The mass

splittings are chosen to maximise the differences between these simplified models and other models with only one intermediate particle between the gluino and the LSP [29].

4 Data and Monte Carlo samples

The data used in this analysis were collected by ATLAS during 2015 and 2016, with a mean number of additional pp interactions per bunch crossing (*pile-up*) of approximately 14 in 2015 and 21 in 2016, and a centre-of-mass collision energy of 13 TeV. Following requirements based on beam and detector conditions and data quality, the data set corresponds to an integrated luminosity of 14.7 fb^{-1} . The uncertainty in the combined 2015 and 2016 integrated luminosity is $\pm 2.9\%$. It is derived, following a methodology similar to that detailed in Refs. [30] and [31], from a preliminary calibration of the luminosity scale using x - y beam-separation scans performed in August 2015 and May 2016.

Data events are collected using a combination of single-lepton and dilepton triggers [32], in order to maximise the signal acceptance. The dielectron, dimuon, and electron–muon triggers have leading-lepton p_T thresholds in the range 12–24 GeV. Additional single-electron (single-muon) triggers are also used, with trigger p_T thresholds of 60 (50) GeV, to increase the trigger efficiency for models with high- p_T leptons. Events are required to contain at least two selected leptons with $p_T > 25$ GeV, making the selection fully efficient with respect to the trigger p_T thresholds.

An additional control sample of events containing photons is collected using a set of single-photon triggers with p_T thresholds in the range 20–140 GeV. All triggers except for the one with threshold $p_T = 120$ GeV in 2015, or the one with $p_T = 140$ GeV in 2016, are prescaled. Events are required to contain a selected photon with $p_T > 37$ GeV, so that they are selected efficiently by the lowest available p_T trigger in 2015, which had a threshold of $p_T^\gamma = 35$ GeV.

Simulated event samples are used to aid in the estimation of SM backgrounds, validate the analysis techniques, optimise the event selection, and provide predictions for SUSY signal processes. All SM background samples used are listed in Table 2, along with the parton distribution function (PDF) set, the configuration of underlying-event and hadronisation parameters (underlying-event tune) and the cross-section calculation order in α_S used to normalise the event yields for these samples.

Samples simulated using MG5_AMC@NLO v2.2.2 [33], interfaced with PYTHIA 8.186 [34] with the A14 underlying-event tune [35] to simulate the parton shower and hadronisation, are generated at leading order in α_S (LO) with the NNPDF23LO PDF set [36]. For samples generated using POWHEG Box V2 [37–39], PYTHIA 6.428 [40] is used to simulate the parton shower, hadronisation, and the underlying event. The CTEQ6L1 PDF set is used with the corresponding PERUGIA2012 [41] tune. In the case of both the MG5_AMC@NLO and POWHEG samples, the EVTGEN v1.2.0 program [42] is used for properties of the bottom and charm hadron decays. SHERPA 2.1.1 [43] simulated samples use the CT10 PDF set with SHERPA’s own internal parton shower [44] and hadronisation methods, as well as the SHERPA default underlying-event tune. Diboson processes with four charged leptons, three charged leptons and a neutrino or two charged leptons and two neutrinos are simulated using the SHERPA 2.1.1 generator. Matrix elements contain all diagrams with four electroweak vertices. They are calculated for up to one (4ℓ , $2\ell + 2\nu$) or zero ($3\ell + 1\nu$) partons at next-to-leading order in α_S (NLO) and up to three partons at LO using the Comix [45] and OpenLoops [46] matrix element generators and merged with the SHERPA parton shower using the ME+PS@NLO prescription [47]. For the $Z/\gamma^* + \text{jets}$ background, SHERPA 2.1.1 is used to generate a sample with up to two additional partons at NLO and up to four at LO. For Monte Carlo (MC)

closure studies, γ + jets events are generated at LO with up to four additional partons using SHERPA 2.1.1. Additional MC simulation samples of events with a leptonically decaying vector boson and photon ($V\gamma$, where $V = W, Z$) are generated at LO using SHERPA 2.1.1. Matrix elements including all diagrams with three electroweak couplings are calculated with up to three partons. These samples are used to estimate backgrounds with real E_T^{miss} in γ + jets event samples.

The SUSY signal samples are produced at LO using MG5_AMC@NLO with the NNPDF2.3LO PDF set, interfaced with PYTHIA 8.186. The scale parameter for CKKW-L matching [48, 49] is set at a quarter of the mass of the gluino. Up to one additional parton is included in the matrix element calculation. The underlying event is modelled using the A14 tune for all signal samples, and EVTGEN is adopted to describe the properties of bottom and charm hadron decays. Signal cross sections are calculated at NLO in α_S . This includes the resummation of soft gluon emission at next-to-leading-logarithm accuracy (NLO+NLL) [50–54].

All of the SM background MC samples are subject to a full ATLAS detector simulation [55] using GEANT4 [56]. A fast simulation [55], which uses a combination of a parameterisation of the response of the ATLAS electromagnetic and hadronic calorimeters and GEANT4, is used in the case of signal MC samples. This fast simulation is validated by comparing a few chosen signal samples to some fully simulated points. Minimum-bias interactions are generated and overlaid on the hard-scattering process to simulate the effect of multiple pp interactions occurring during the same (in-time) or a nearby (out-of-time) bunch-crossing (pile-up). These are produced using PYTHIA 8.186 with the A2 tune [57] and MSTW 2008 PDF set [58]. The pile-up distribution in MC samples is simulated to match that in data during 2015 and 2016 pp data-taking.

Table 2: Simulated background event samples used in this analysis with the corresponding matrix element and parton shower generators, cross-section order in α_S used to normalise the event yield, underlying-event tune and PDF set.

| Physics process | Generator | Parton Shower | Cross section | Tune | PDF set |
|--|---------------------|---------------|--------------------|----------------|-----------|
| $t\bar{t} + W$ and $t\bar{t} + Z$ [59, 60] | MG5_AMC@NLO | PYTHIA 8.186 | NLO [61, 62] | A14 | NNPDF23LO |
| $t\bar{t} + WW$ [59] | MG5_AMC@NLO | PYTHIA 8.186 | LO [33] | A14 | NNPDF23LO |
| $t\bar{t}$ [63] | POWHEG Box v2 r3026 | PYTHIA 6.428 | NNLO+NNLL [64, 65] | PERUGIA2012 | NLO CT10 |
| Single-top (Wt) [63] | POWHEG Box v2 r2856 | PYTHIA 6.428 | Approx. NNLO [66] | PERUGIA2012 | NLO CT10 |
| WW, WZ and ZZ [67] | SHERPA 2.1.1 | SHERPA 2.1.1 | NLO [68, 69] | SHERPA default | NLO CT10 |
| $Z/\gamma^* (\rightarrow \ell\ell) + \text{jets}$ [70] | SHERPA 2.1.1 | SHERPA 2.1.1 | NNLO [71, 72] | SHERPA default | NLO CT10 |
| γ + jets | SHERPA 2.1.1 | SHERPA 2.1.1 | LO [43] | SHERPA default | NLO CT10 |
| $V (= W, Z)\gamma$ | SHERPA 2.1.1 | SHERPA 2.1.1 | LO [43] | SHERPA default | NLO CT10 |

5 Analysis object identification and selection

All analysis objects are categorised as either “baseline” or “signal” based on various quality and kinematic requirements. *Baseline* objects are used in the calculation of missing transverse momentum and to disambiguate between the analysis objects in the event, while the jets and leptons entering the final analysis selection must pass more stringent *signal* requirements. The selection criteria for both the baseline and signal objects differ from the requirements used in the Run-1 ATLAS $Z + \text{jets} + E_{\text{T}}^{\text{miss}}$ search reported in Ref. [19], owing to the new silicon-pixel tracking layer and significant changes to the reconstruction software since 2012 data-taking. In particular, improvements in the lepton identification criteria have reduced the background due to hadrons misidentified as electrons. The primary vertex in each event is defined as the reconstructed vertex [73] with the highest $\sum p_{\text{T}}^2$, where the summation includes all particle tracks with $p_{\text{T}} > 400$ MeV associated with the vertex.

Electron candidates are reconstructed from energy clusters in the electromagnetic calorimeter matched to ID tracks. Baseline electrons are required to have transverse energy $E_{\text{T}} > 10$ GeV, satisfy the “loose likelihood” criteria described in Ref. [74] and reside within the region $|\eta| < 2.47$. Signal electrons are further required to have $p_{\text{T}} > 25$ GeV, satisfy the “medium likelihood” criteria of Ref. [74], and be consistent with originating from the primary vertex. The signal electrons must originate from within $|z_0 \sin \theta| = 0.5$ mm of the primary vertex along the direction of the beamline.² The transverse-plane distance of closest approach of the electron to the beamline, divided by the corresponding uncertainty, must be $|d_0/\sigma_{d_0}| < 5$. These electrons must also be isolated with respect to other objects in the event, according to a p_{T} -dependent isolation requirement. The isolation uses calorimeter- and track-based information to obtain 95% efficiency at $p_{\text{T}} = 25$ GeV, rising to 99% efficiency at $p_{\text{T}} = 60$ GeV.

Baseline muons are reconstructed from either ID tracks matched to muon segments (collections of hits in a single muon spectrometer layer) or combined tracks formed from the ID and muon spectrometer [75]. They must satisfy the “medium” selection criteria described in Ref. [75], and to satisfy $p_{\text{T}} > 10$ GeV and $|\eta| < 2.5$. Signal muon candidates are further required to have $p_{\text{T}} > 25$ GeV, be isolated, and have $|z_0 \sin \theta| < 0.5$ mm and $|d_0/\sigma_{d_0}| < 3$. Calorimeter- and track-based isolation criteria are used to obtain 95% efficiency at $p_{\text{T}} = 25$ GeV, rising to 99% efficiency at $p_{\text{T}} = 80$ GeV [75]. Further, the relative uncertainties in the q/p of each of the ID track alone and muon spectrometer track alone are required to be less than 80% of the uncertainty in the q/p of the combined track. This reduces the already low rate of grossly mismeasured muons. The combined isolation and identification efficiency for single leptons, after the trigger requirements, is about 70% (80%) for electrons (muons) with $p_{\text{T}} \sim 25$ GeV, rising to about 90% for $p_{\text{T}} > 200$ GeV.

Jets are reconstructed from topological clusters of energy [76] in the calorimeter using the anti- k_t algorithm [77, 78] with a radius parameter of 0.4. Calibration corrections are applied to the jets based on a comparison to jets made of stable particles (those with lifetimes $\tau > 0.3 \times 10^{-10}$ s) in the MC simulation. A residual correction is applied to jets in data, based on studies of p_{T} balance between jets and well-calibrated objects in the MC simulation and data [79, 80]. Baseline jet candidates are required to have $p_{\text{T}} > 20$ GeV and reside within the region $|\eta| < 4.5$. Signal jets are further required to satisfy $p_{\text{T}} > 30$ GeV and reside within the region $|\eta| < 2.5$. Jets with $p_{\text{T}} < 60$ GeV and $|\eta| < 2.4$ must meet additional criteria designed to select jets from the hard-scatter interaction and reject those originating from pile-up. This is enforced by using the jet vertex tagger described in Ref. [81]. Finally, events containing a jet that does

² The distance of closest approach between a particle object and the primary vertex (beamline) in the longitudinal (transverse) plane is denoted by z_0 (d_0).

not pass specific jet quality requirements are vetoed from the analysis selection in order to remove events impacted by detector noise and non-collision backgrounds [82, 83]. The MV2c10 boosted decision tree algorithm [84, 85] identifies jets with $|\eta| < 2.5$ containing b -hadrons (b -jets) based on quantities such as the impact parameters of associated tracks and any reconstructed secondary vertices. A selection that provides 77% efficiency for tagging b -jets in simulated $t\bar{t}$ events is used. These tagged jets are called b -tagged jets.

Photon candidates must satisfy “tight” selection criteria described in Ref. [86], have $p_T > 25$ GeV and reside within the region $|\eta| < 2.37$, excluding the transition region $1.37 < |\eta| < 1.6$ where there is a discontinuity in the calorimeter. Signal photons are further required to have $p_T > 37$ GeV and to be isolated from other objects in the event, using p_T -dependent requirements on both track- and calorimeter-based isolation.

To avoid the duplication of analysis objects in more than one baseline selection, an overlap removal procedure is applied. Any baseline jet within $\Delta R = 0.2$ of a baseline electron is removed, unless the jet is b -tagged, in which case the electron is identified as originating from a heavy-flavour decay and is removed instead. Remaining electrons residing within $\Delta R = 0.4$ of a baseline jet are then removed from the event. Subsequently, any baseline muon residing within $\Delta R = 0.2$ of a remaining baseline b -tagged jet is discarded. If such a jet is not b -tagged then the jet is removed instead. Any remaining muon found within $\min(0.04 + (10 \text{ GeV})/p_T, 0.4)$ of a jet is also discarded. This stage of the overlap removal procedure differs from that used in Ref. [19]. It was improved to retain muons near jet candidates mostly containing calorimeter energy from final-state radiation from muons, while still rejecting muons from heavy-flavour decays. Finally, to remove electron candidates originating from muon bremsstrahlung, any baseline electron within $\Delta R = 0.01$ of any remaining baseline muon is removed from the event. Photons are removed if they reside within $\Delta R = 0.4$ of a baseline electron, and any jet within $\Delta R = 0.4$ of any remaining photon is discarded.

The E_T^{miss} is defined as the magnitude of the negative vector sum, $\mathbf{p}_T^{\text{miss}}$, of the transverse momenta of all baseline electrons, muons, jets, and photons [87, 88]. Low-momentum contributions from particle tracks from the primary vertex that are not associated with reconstructed analysis objects are included in the calculation of E_T^{miss} . This contribution to the E_T^{miss} is referred to as the “soft term”.

Models with large hadronic activity are targeted by placing additional requirements on the quantity H_T , defined as the scalar sum of the p_T values of all signal jets, or on H_T^{incl} , the scalar sum of the p_T values of all signal jets and the two leptons with largest p_T .

All MC samples have correction factors applied to take into account small differences between data and MC simulation in identification, reconstruction and trigger efficiencies for leptons. The p_T values of leptons in MC samples are additionally smeared to match the momentum resolution in data.

6 Event selection

For each search channel, signal regions (SRs) are designed to target events from specific SUSY signal models. Control regions (CRs) are defined to be depleted in SUSY signal events and enriched in specific SM backgrounds, and they are used to assist in estimating these backgrounds in the SRs. To validate the background estimation procedures, various validation regions (VRs) are defined to be analogous to the CRs and SRs, but with less stringent requirements than the SRs on E_T^{miss} , H_T^{incl} or H_T . Other VRs with

additional requirements on the number of leptons are used to validate the modelling of backgrounds in which more than two leptons are expected.

Events in SRs are required to contain at least two signal leptons (electrons or muons). If more than two signal leptons are present in a given event, the selection process continues based on the two leptons with the highest p_T values in the event.

The selected events must pass at least one of the leptonic triggers. If an event is selected by a dilepton trigger, the two leading, highest p_T , leptons must be matched to one of the objects that triggered the event. These leptons must also have p_T higher than the threshold of the trigger in question. For events selected by a single-lepton trigger, at least one of the two leading leptons must be matched to the trigger object in the same way. The leading two leptons in the event must have $p_T > 25$ GeV, and form an SFOS pair.

As at least two jets are expected in all signal models studied, selected events are further required to contain at least two signal jets. Furthermore, events in which the azimuthal opening angle between either of the leading two jets and the E_T^{miss} satisfies $\Delta\phi(\text{jet}_{1,2}, \mathbf{p}_T^{\text{miss}}) < 0.4$ are rejected so as to remove events with E_T^{miss} from jet mismeasurements. This requirement also suppresses $t\bar{t}$ events in which the top quark, the anti-top quark, or the entire $t\bar{t}$ system has a large Lorentz boost.

The various methods used to predict the background in the SRs are discussed in Section 7. The selection criteria for the CRs, VRs, and SRs are summarised in Tables 3 and 4. The most important of these regions are shown graphically in Figure 2.

For the on-shell Z search, the leading-lepton p_T threshold is raised to 50 GeV to increase the sensitivity to signal models with final-state Z bosons. This is an increased leading-lepton p_T threshold relative to Ref. [19] and is found to better reject fake-lepton candidates from misidentified jets, photon conversions and b -hadron decays, while retaining high efficiency for signal events, which tend to produce boosted Z bosons. To select events containing a leptonically decaying Z boson, the invariant mass of the dilepton system is required to be $81 < m_{\ell\ell} < 101$ GeV. In the CRs and VRs that use the Z mass sidebands, only events with $m_{\ell\ell} > 45$ GeV are used to reject the lower $m_{\ell\ell}$ region dominated by Drell–Yan (DY) production. In Ref. [19] an “on- Z ” SR, denoted SRZ, is defined requiring $E_T^{\text{miss}} > 225$ GeV and $H_T^{\text{incl}} > 600$ GeV. The region is motivated by SUSY signals with high gluino or squark mass and high jet activity. Since b -jets are not always expected in the simplified models considered here, no requirement is placed on b -tagged jet multiplicity ($n_{b\text{-jets}}$) so as to be as inclusive as possible and to be consistent with Ref. [19]. Dedicated CRs are defined, with selection criteria similar to those of SRZ, to estimate the contribution from the dominant SM backgrounds in SRZ. These CRs are discussed in more detail in Section 7.

The edge selection requires at least two leptons with $p_T > 25$ GeV. The search is performed across the full $m_{\ell\ell}$ spectrum, with the exception of the region with $m_{\ell\ell} < 12$ GeV, which is vetoed to reject low-mass DY events and the J/ψ and Υ resonances. Three regions are defined to target signal models with low, medium and high values of $\Delta m_{\tilde{g}} = m(\tilde{g}) - m(\tilde{\chi}_1^0)$, denoted SR-low, SR-medium, and SR-high, respectively. All these regions require $E_T^{\text{miss}} > 200$ GeV. SR-medium and SR-high also include the requirements $H_T > 400$ GeV and $H_T > 700$ GeV, respectively, to further isolate high- $\Delta m_{\tilde{g}}$ events. Here the leptons are not included in the H_T definition to avoid introducing any bias in the $m_{\ell\ell}$ distribution. Events selected in SR-low, SR-medium and SR-high are further grouped into non-orthogonal $m_{\ell\ell}$ windows, which represent the search regions used in the edge analysis. The dilepton mass ranges of these are chosen to maximise sensitivity to the targeted signal models, with the window boundaries being motivated by the dilepton mass endpoints of generated signal points. In total, 24 $m_{\ell\ell}$ windows are defined by selecting ranges with the best expected sensitivity to signal models. Of these windows, nine are in SR-low, eight are in SR-medium and seven are in SR-high. Details of the $m_{\ell\ell}$ definitions in these regions are given along with

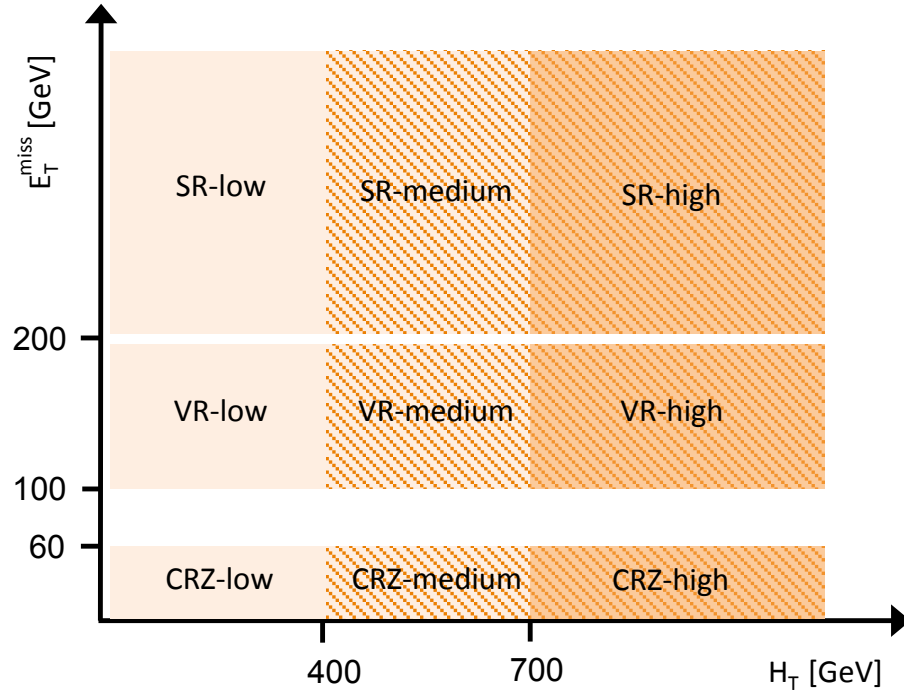
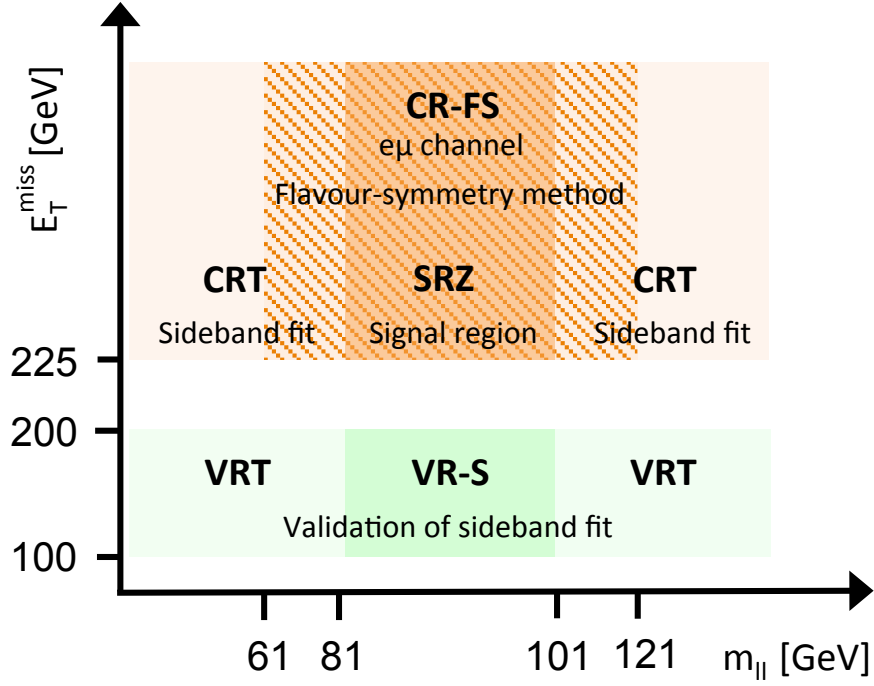


Figure 2: Schematic diagrams of the control (CR), validation (VR) and signal regions (SR) for the on-shell Z (top) and edge (bottom) searches. For the on-shell Z search the various regions are shown in the $m_{\ell\ell} - E_T^{\text{miss}}$ plane, whereas in the case of the edge search the signal and validation regions are depicted in the $H_T - E_T^{\text{miss}}$ plane. The flavour-symmetry and sideband-fit background estimation methods are described further in Section 7.1.

Table 3: Overview of all signal (SR), control (CR) and validation regions (VR) used in the on-shell Z search. The flavour combination of the dilepton pair is denoted as either “SF” for same-flavour or “DF” for different-flavour. All regions require at least two leptons, unless otherwise indicated. In the case of $\text{CR}\gamma$, VR-WZ , VR-ZZ , and VR-3L the number of leptons, rather than a specific flavour configuration, is indicated. More details are given in the text. The main requirements that distinguish the control and validation regions from the signal region are indicated in bold. The kinematic quantities used to define these regions are discussed in the text. The quantity $m_{\text{T}}(\ell_3, E_{\text{T}}^{\text{miss}})$ indicates the transverse mass formed by the $E_{\text{T}}^{\text{miss}}$ and the lepton which is not assigned to either of the Z -decay leptons.

| On-shell Z regions | $E_{\text{T}}^{\text{miss}}$ [GeV] | $H_{\text{T}}^{\text{incl}}$ [GeV] | n_{jets} | $m_{\ell\ell}$ [GeV] | SF/DF | $\Delta\phi(\text{jet}_{12}, p_{\text{T}}^{\text{miss}})$ | $m_{\text{T}}(\ell_3, E_{\text{T}}^{\text{miss}})$ [GeV] | $n_{b\text{-jets}}$ |
|----------------------|------------------------------------|------------------------------------|-------------------|--|------------------------------------|---|--|---------------------|
| Signal region | | | | | | | | |
| SRZ | > 225 | > 600 | ≥ 2 | $81 < m_{\ell\ell} < 101$ | SF | > 0.4 | – | – |
| Control regions | | | | | | | | |
| CRZ | < 60 | > 600 | ≥ 2 | $81 < m_{\ell\ell} < 101$ | SF | > 0.4 | – | – |
| CR-FS | > 225 | > 600 | ≥ 2 | $61 < m_{\ell\ell} < 121$ | DF | > 0.4 | – | – |
| CRT | > 225 | > 600 | ≥ 2 | > 45, $m_{\ell\ell} \notin [81, 101]$ | SF | > 0.4 | – | – |
| $\text{CR}\gamma$ | – | > 600 | ≥ 2 | – | $0\ell, 1\gamma$ | – | – | – |
| Validation regions | | | | | | | | |
| VRZ | < 225 | > 600 | ≥ 2 | $81 < m_{\ell\ell} < 101$ | SF | > 0.4 | – | – |
| VRT | 100–200 | > 600 | ≥ 2 | > 45, $m_{\ell\ell} \notin [81, 101]$ | SF | > 0.4 | – | – |
| VR-S | 100–200 | > 600 | ≥ 2 | $81 < m_{\ell\ell} < 101$ | SF | > 0.4 | – | – |
| VR-FS | 100–200 | > 600 | ≥ 2 | $61 < m_{\ell\ell} < 121$ | DF | > 0.4 | – | – |
| VR-WZ | 100–200 | – | – | – | 3ℓ | – | < 100 | 0 |
| VR-ZZ | < 100 | – | – | – | 4ℓ | – | – | 0 |
| VR-3L | 60–100 | > 200 | ≥ 2 | $81 < m_{\ell\ell} < 101$ | 3ℓ | > 0.4 | – | – |

the results in Section 9. Models without light sleptons are targeted by windows with $m_{\ell\ell} < 60$ GeV or $m_{\ell\ell} < 80$ GeV for $\Delta m_\chi < m_Z$ leading to off-shell Z bosons, and by the window with $81 < m_{\ell\ell} < 101$ GeV for $\Delta m_\chi > m_Z$ leading to on-shell Z bosons. Models with light sleptons are targeted by the remaining $m_{\ell\ell}$ windows, which cover the full $m_{\ell\ell}$ range. The edge selection and on-shell Z selection are not orthogonal. In particular, SR-medium in the range $81 < m_{\ell\ell} < 101$ GeV overlaps significantly with SRZ.

For the combined $ee + \mu\mu$ channels, the typical signal acceptance times efficiency values for the signal models considered in SRZ are 2–8%. They are 8–40%, 3–35%, and 1–35%, inclusively in $m_{\ell\ell}$, for SR-low, SR-medium and SR-high, respectively. The on-shell Z and edge analyses are each optimised for different signal models. There are models in which signal contamination in CRs or VRs can become significant. For example, CRT in Table 3 is used to normalise the $t\bar{t}$ MC sample to data as a cross-check in the on-shell Z search, but it is a region where the signal contamination from signal models targeted by the edge search can be up to 80% relative to the expected background. In addition, the contamination from on-shell Z signals in the region used to validate the $Z/\gamma^* + \text{jets}$ and flavour-symmetric estimates, VR-S, is up to 60% for models with $m(\tilde{g}) < 1$ TeV. The signal contamination from the slepton models in the DF regions used to estimate the flavour-symmetric backgrounds in the edge search, CR-FS-low/medium/high in Table 4, is less than 20% for models with $m(\tilde{g}) > 600$ GeV. It is only the contamination in these $e\mu$ CRs that is relevant in terms of the model-dependent interpretation of the results, and its impact is further

Table 4: Overview of all signal (SR), control (CR) and validation regions (VR) used in the edge search. The flavour combination of the dilepton pair is denoted as either “SF” for same-flavour or “DF” for different-flavour. The charge combination of the leading lepton pairs are given as “SS” for same-sign or “OS” for opposite-sign. All regions require *at least* two leptons, with the exception of CR-real, which requires *exactly* two leptons, and the three γ CRs, which require no leptons and one photon. More details are given in the text. The main requirements that distinguish the control and validation regions from the signal regions are indicated in bold. The kinematic quantities used to define these regions are discussed in the text.

| Edge regions | E_T^{miss} [GeV] | H_T [GeV] | n_{jets} | $m_{\ell\ell}$ [GeV] | SF/DF | OS/SS | $\Delta\phi(\text{jet}_{12}, p_T^{\text{miss}})$ | $m_{\ell\ell}$ ranges |
|---------------------|------------------------------|----------------|-------------------|---|---|-----------|--|-----------------------|
| Signal regions | | | | | | | | |
| SR-low | > 200 | – | ≥ 2 | > 12 | SF | OS | > 0.4 | 9 |
| SR-medium | > 200 | > 400 | ≥ 2 | > 12 | SF | OS | > 0.4 | 8 |
| SR-high | > 200 | > 700 | ≥ 2 | > 12 | SF | OS | > 0.4 | 7 |
| Control regions | | | | | | | | |
| CRZ-low | < 60 | – | ≥ 2 | > 12 | SF | OS | > 0.4 | – |
| CRZ-medium | < 60 | > 400 | ≥ 2 | > 12 | SF | OS | > 0.4 | – |
| CRZ-high | < 60 | > 700 | ≥ 2 | > 12 | SF | OS | > 0.4 | – |
| CR-FS-low | > 200 | – | ≥ 2 | > 12 | DF | OS | > 0.4 | – |
| CR-FS-medium | > 200 | > 400 | ≥ 2 | > 12 | DF | OS | > 0.4 | – |
| CR-FS-high | > 200 | > 700 | ≥ 2 | > 12 | DF | OS | > 0.4 | – |
| CR γ -low | – | – | ≥ 2 | – | 0ℓ, 1γ | – | – | – |
| CR γ -medium | – | > 400 | ≥ 2 | – | 0ℓ, 1γ | – | – | – |
| CR γ -high | – | > 700 | ≥ 2 | – | 0ℓ, 1γ | – | – | – |
| CR-real | – | > 200 | ≥ 2 | 81–101 | 2 ℓ SF | OS | – | – |
| CR-fake | < 125 | – | – | $\in [12, \infty]$, $\notin [81, 101](\text{SF})$ | 2ℓ SF/DF | SS | – | – |
| Validation regions | | | | | | | | |
| VR-low | 100–200 | – | ≥ 2 | > 12 | SF | OS | > 0.4 | – |
| VR-medium | 100–200 | > 400 | ≥ 2 | > 12 | SF | OS | > 0.4 | – |
| VR-high | 100–200 | > 700 | ≥ 2 | > 12 | SF | OS | > 0.4 | – |
| VR-fake | > 50 | – | ≥ 2 | $\in [12, \infty]$, $\notin [81, 101](\text{SF})$ | SF/DF | SS | – | – |

discussed in Section 10. In general, for models giving substantial contamination in the CRs, the signal-to-background ratio in the SRs is found to be large enough for this contamination to have negligible impact on the sensitivity of the search.

7 Background estimation

The dominant background processes in the SRs are “flavour-symmetric” (FS) backgrounds, where the ratio of ee , $\mu\mu$ and $e\mu$ dileptonic branching fractions is 1:1:2 because the two leptons originate from independent $W \rightarrow \ell\nu$ decays. This background is dominated by $t\bar{t}$ (50–70%) and also includes WW , Wt , and $Z \rightarrow \tau\tau$ processes. The FS background constitutes 60–90% of the expected background in the SRs, and is estimated using control samples of $e\mu$ events.

As all the SRs have a high- E_T^{miss} requirement, $Z/\gamma^* + \text{jets}$ events only enter the SRs when there is large E_T^{miss} originating from instrumental effects or from neutrinos in jet fragments. This background is generally small, but it is difficult to model with MC simulation and can mimic signal, particularly for the on-shell Z search. This background is estimated using a control sample of $\gamma + \text{jets}$ events in data, which are kinematically similar to $Z/\gamma^* + \text{jets}$ and have similar sources of E_T^{miss} .

The production of WZ/ZZ dibosons contributes approximately 30% of the SM background in SRZ and up to 20% of the background in the edge SR $m_{\ell\ell}$ windows. These backgrounds are estimated from MC simulation, after validation in dedicated 3ℓ (WZ) and 4ℓ (ZZ) VRs. Rare top backgrounds, which include $t\bar{t}W$, $t\bar{t}Z$ and $t\bar{t}WW$ processes, constitute $< 5\%$ of the expected SM background in all SRs, and are estimated from MC simulation. The contribution from events with fake or misidentified leptons is at most 15% (in one of the edge $m_{\ell\ell}$ ranges in SR-low), but is generally $< 5\%$ of the expected SM background in most SRs.

7.1 Flavour-symmetric backgrounds

The flavour-symmetric background is dominant in all SRs. To estimate the contribution of this background to each SR, the so-called “flavour-symmetry” method, detailed in Ref. [19], is used. In this method, data events from a DF control sample, which is defined with the same kinematic requirements as the SR, are used to determine the expected event yields in the SF channels. In the on-shell Z analysis, the method is used to predict the background yield in the Z mass window, defined as $81 < m_{\ell\ell} < 101$ GeV. In the edge analysis, the method is extended to predict the full dilepton mass shape, such that a prediction can be extracted in any of the predefined $m_{\ell\ell}$ windows.

For the edge search, the flavour-symmetric contribution to each $m_{\ell\ell}$ bin of the signal regions is predicted using data from the corresponding bin in an $e\mu$ control region. All edge CR-FS regions (definitions can be seen in Table 4) are 88–97% pure in flavour-symmetric processes (this purity is calculated from MC simulation).

For the on-shell search, this method is complicated slightly by a widening of the $m_{\ell\ell}$ window used in CR-FS, the $e\mu$ control region (defined in Table 3). The window is enlarged to $61 < m_{\ell\ell} < 121$ GeV to approximately triple the amount of data in the control region and thus increase the statistical precision of the method. This results in a region that is $\sim 95\%$ pure in flavour-symmetric processes (the expected composition of this 95% is $\sim 80\%$ $t\bar{t}$, $\sim 10\%$ Wt , $\sim 10\%$ WW and $< 1\%$ $Z \rightarrow \tau\tau$).

Apart from the $m_{\ell\ell}$ widening in CR-FS, the method used is identical for the on-shell and edge regions. Events in the control regions are subject to lepton p_T - and η -dependent correction factors measured in data and MC simulation. Because the triggers used are not identical in 2015 and 2016, these factors are measured separately for each year and account for the different identification and reconstruction efficiencies for electrons and muons, as well as the different trigger efficiencies for the dielectron, dimuon and electron–muon selections. The estimated numbers of events in the SF channels, $N_{ee/\mu\mu}^{\text{est}}$, are given by:

$$N_{ee}^{\text{est}} = \frac{1}{2} \cdot f_{\text{FS}} \cdot f_{Z\text{-mass}} \cdot \sum_i^{N_{e\mu}^{\text{data}}} k_e(p_T^{i,\mu}, \eta^{i,\mu}) \cdot \alpha(p_T^{i,\mu}, \eta^{i,\mu}), \quad (1)$$

$$N_{\mu\mu}^{\text{est}} = \frac{1}{2} \cdot f_{\text{FS}} \cdot f_{Z\text{-mass}} \cdot \sum_i^{N_{e\mu}^{\text{data}}} k_\mu(p_T^{i,e}, \eta^{i,e}) \cdot \alpha(p_T^{i,e}, \eta^{i,e}), \quad (2)$$

where $N_{e\mu}^{\text{data}}$ is the number of data events observed in a given control region, $\alpha(p_T^i, \eta^i)$ accounts for the different trigger efficiencies for SF and DF events, and $k_e(p_T^{i,\mu}, \eta^{i,\mu})$ and $k_\mu(p_T^{i,e}, \eta^{i,e})$ are electron and muon selection efficiency factors for the kinematics of the lepton being replaced, in event i . The trigger and selection efficiency correction factors are derived from the events in an inclusive on-Z selection ($81 < m_{\ell\ell} < 101$ GeV, ≥ 2 jets), according to:

$$k_e(p_T, \eta) = \sqrt{\frac{N_{ee}^{\text{meas}}(p_T, \eta)}{N_{\mu\mu}^{\text{meas}}(p_T, \eta)}} \quad (3)$$

$$k_\mu(p_T, \eta) = \sqrt{\frac{N_{\mu\mu}^{\text{meas}}(p_T, \eta)}{N_{ee}^{\text{meas}}(p_T, \eta)}} \quad (4)$$

$$\alpha(p_T, \eta) = \frac{\sqrt{\epsilon_{ee}^{\text{trig}}(p_T^{\ell_1}, \eta^{\ell_1}) \times \epsilon_{\mu\mu}^{\text{trig}}(p_T^{\ell_1}, \eta^{\ell_1})}}{\epsilon_{e\mu}^{\text{trig}}(p_T^{\ell_1}, \eta^{\ell_1})} \quad (5)$$

where $\epsilon_{ee/\mu\mu}^{\text{trig}}$ is the trigger efficiency and $N_{ee/\mu\mu}^{\text{meas}}$ is the number of $ee/\mu\mu$ events in the inclusive on-Z region outlined above. Here $k_e(p_T, \eta)$ and $k_\mu(p_T, \eta)$ are calculated separately for leading and sub-leading leptons, while α is calculated for the leading lepton, ℓ_1 . The correction factors are typically within 10% of unity, except in the region $|\eta| < 0.1$ where, because of the lack of coverage by the muon spectrometer, they are up to 50% from unity. For all background estimates based on the flavour-symmetry method, results are computed separately for ee and $\mu\mu$ and then summed to obtain the combined predictions. The resulting estimates from the DF channels are scaled according to the fraction of flavour-symmetric backgrounds in each $e\mu$ control sample, f_{FS} (95% in CR-FS), which is determined by subtracting non-flavour-symmetric backgrounds taken from MC simulation from the data observed in the corresponding $e\mu$ region. In the on-shell case, the result is also scaled by the fraction of events in CR-FS expected to be contained within $81 < m_{\ell\ell} < 101$ GeV, $f_{Z\text{-mass}}$ (38%), which is otherwise set to 100% for the edge regions. The validity of extrapolating in $m_{\ell\ell}$ between CR-FS and SRZ was checked by comparing the $m_{\ell\ell}$ shapes in data and MC simulation in a region similar to VR-S, but with the $m_{\ell\ell}$ requirement relaxed and $H_T^{\text{incl}} > 300$ GeV to obtain a sample with a large number of events. The resulting on-Z fractions in MC simulation were found

to agree with data within statistical uncertainties, which are summed in quadrature to assign a systematic uncertainty. In the case of the edge search the full $m_{\ell\ell}$ distribution is validated by applying a flavour-symmetry method to $t\bar{t}$ MC evnets in VR-low, VR-medium and VR-high. This procedure results in good closure, which is further discussed in Section 7.5. The difference between the prediction and the observed distribution is used to assign an MC non-closure uncertainty to the estimate.

The flavour-symmetry method in SRZ is further cross-checked by performing a profile likelihood fit [89] of MC yields to data in the Z-mass sidebands ($m_{\ell\ell} \notin [81, 101]$ GeV), the region denoted CRT in Table 3, which is dominated by $t\bar{t}$ (with a purity of $> 75\%$) and contains 273 events in data. The other flavour-symmetric processes in this region contribute $\sim 12\%$ (Wt), 10% (WW) and $< 1\%$ ($Z \rightarrow \tau\tau$). All SM background processes are taken directly from MC simulation in this cross-check, including backgrounds also estimated using the flavour-symmetry method. The normalisation of the dominant $t\bar{t}$ background is a free parameter and is the only parameter affected by the fit. For this cross-check, the contamination from Beyond Standard Model processes in the Z-mass sidebands is assumed to be negligible. The fit results in a scale factor of 0.64 for the $t\bar{t}$ yield predicted by simulation. This result is extrapolated from the Z-mass sidebands to SRZ and gives a prediction of 29 ± 7 events, which is consistent with the nominal flavour-symmetry background estimate of 33 ± 4 in this region.

The sideband fit is repeated at lower E_T^{miss} in VRT, with the results being propagated to VR-S, so as to test the $m_{\ell\ell}$ extrapolation used in the sideband fit method. The normalisation to data in this region, which is at lower E_T^{miss} relative to CRT, results in a scale factor of 0.80 for the $t\bar{t}$ yield predicted by simulation. The number of FS events predicted in VR-S using the sideband fit in VRT is compatible with the number estimated by applying the FS method to data in VR-FS. The results of the background estimate in both VR-S and SRZ obtained from the flavour-symmetry method are compared with the values obtained by the sideband fit cross-check in Table 5. The methods result in consistent estimates in both regions. Further results in the edge VRs are discussed in Section 7.5.

Table 5: Comparison of the predicted yields for the flavour-symmetric backgrounds in SRZ and VR-S as obtained from the nominal data-driven method using CR-FS and the Z-mass sideband method. The quoted uncertainties include statistical and systematic contributions.

| Region | Flavour-symmetry | Sideband fit |
|--------|------------------|--------------|
| SRZ | 33 ± 4 | 29 ± 7 |
| VR-S | 99 ± 8 | 92 ± 25 |

A potential cause of the low scale factors obtained from the sideband fit at large H_T and E_T^{miss} is mis-modelling of the top-quark p_T distribution, where measurements of $t\bar{t}$ differential cross sections by the ATLAS and CMS experiments indicate that the top-quark p_T distribution predicted by most generators is harder than that observed in data [90, 91]. Corrections to the MC predictions according to NNLO calculations provided in Ref. [92] indicate an improvement in the top-quark pair modelling at high H_T , which should lead to scale factors closer to unity. With the data-driven method used to estimate $t\bar{t}$ contributions in this analysis, the results do not depend on these corrections. They are therefore not applied to the $t\bar{t}$ MC sample for the sideband-fit cross-check.

7.2 $Z/\gamma^* + \text{jets}$ background

The $Z/\gamma^* + \text{jets}$ background estimate is based on a data-driven method that uses $\gamma + \text{jets}$ events in data to model the E_T^{miss} distribution of $Z/\gamma^* + \text{jets}$. The $\gamma + \text{jets}$ and $Z/\gamma^* + \text{jets}$ processes have similar event topologies, with a well-measured object recoiling against a hadronic system, and both tend to have E_T^{miss} that stems from jet mismeasurements and neutrinos in hadronic decays. In this method, which has been used by CMS in a search in this final state [17], a sample of data events containing at least one photon and no leptons is constructed using the same kinematic selection as each of the SRs, without the E_T^{miss} and $\Delta\phi(\text{jet}_{12}, \mathbf{p}_T^{\text{miss}})$ requirements (the CR γ regions defined in Tables 3 and 4).

The requirement $\Delta\phi(\text{jet}_{12}, \mathbf{p}_T^{\text{miss}}) > 0.4$ applied in the SRs suppresses E_T^{miss} from jet mismeasurements and increases the relative contributions to E_T^{miss} from the photon, electrons, and muons. The difference in resolution between photons, electrons, and muons can be significant at high p_T . Therefore, before the $\Delta\phi(\text{jet}_{12}, \mathbf{p}_T^{\text{miss}}) > 0.4$ requirement is applied, the photon p_T is smeared according to a $Z \rightarrow ee$ or $Z \rightarrow \mu\mu$ resolution function. The smearing function is derived by comparing the E_T^{miss} -projection along the boson momentum in $Z/\gamma^* + \text{jets}$ and $\gamma + \text{jets}$ MC events in a 1-jet control region with no other event-level kinematic requirements. A deconvolution is applied to avoid including the photon resolution in the Z resolution. For each event, a photon p_T smearing Δp_T is obtained by sampling the smearing function. The photon p_T is shifted by Δp_T , with the parallel component of the E_T^{miss} being correspondingly adjusted by $-\Delta p_T$.

The smeared $\gamma + \text{jets}$ events are then reweighted to match the boson p_T distribution of the $Z/\gamma^* + \text{jets}$ events. This reweighting is applied separately in each region and accounts for small differences between the $\gamma + \text{jets}$ events and $Z/\gamma^* + \text{jets}$ events, which arise mainly from the mass of the Z boson. The reweighting is done using $Z/\gamma^* + \text{jets}$ events in data, and is checked using $Z/\gamma^* + \text{jets}$ MC simulation in an MC closure test, as described further below. Following this smearing and reweighting procedure, the E_T^{miss} of each $\gamma + \text{jets}$ event is recalculated, and the final E_T^{miss} distribution is obtained after applying the $\Delta\phi(\text{jet}_{12}, \mathbf{p}_T^{\text{miss}}) > 0.4$ requirement. For each SR, the resulting E_T^{miss} distribution is normalised to data in a CRZ with the same requirements except that the SR E_T^{miss} requirement is replaced by $E_T^{\text{miss}} < 60$ GeV.

The shape of the $Z/\gamma^* + \text{jets}$ $m_{\ell\ell}$ distribution is extracted from MC simulation and validated by comparing to data in events with lower E_T^{miss} requirements and a veto on b -tagged jets, to suppress the background from $t\bar{t}$. The $m_{\ell\ell}$ distribution is modelled by parameterising the $m_{\ell\ell}$ in $Z/\gamma^* + \text{jets}$ events as a function of the difference between reconstructed and true Z boson p_T in MC simulation. This parameterization ensures that the correlation between lepton momentum mismeasurement and observed $m_{\ell\ell}$ values far from the Z boson mass is preserved. Each photon event is assigned an $m_{\ell\ell}$ via a random sampling of the corresponding distribution, equating photon Δp_T and the difference between true and reconstructed Z boson p_T . The resulting $m_{\ell\ell}$ distribution in $\gamma + \text{jets}$ MC simulation is compared to that extracted from $Z/\gamma^* + \text{jets}$ MC simulation and the difference is assessed as a systematic uncertainty in the background prediction for each $m_{\ell\ell}$ bin.

The full smearing, reweighting, and $m_{\ell\ell}$ assignment procedure is applied to the $V\gamma$ MC sample in parallel with the $\gamma + \text{jets}$ data sample. After applying all corrections to both samples, the $V\gamma$ contribution to the $\gamma + \text{jets}$ data sample is subtracted to remove contamination from backgrounds with real E_T^{miss} . Contamination by events with fake photons in these $\gamma + \text{jets}$ data samples is small, and this contribution is therefore neglected.

In the H_T -inclusive region corresponding to VR-low, there is a non-negligible contribution expected from $Z/\gamma^* + \text{jets}$ events with $p_T^Z < 37$ GeV. Given the photon trigger strategy discussed in Section 4, no photons

with $p_T < 37$ GeV are included in the event selection. To account for this photon p_T threshold, a boson- p_T correction of up to 50% is applied as a function of E_T^{miss} in VR-low. This correction uses the fraction of $Z/\gamma^* + \text{jets}$ events in a given E_T^{miss} bin expected to have $p_T^Z < 37$ GeV, according to MC simulation. The $\gamma + \text{jets}$ data are then scaled according to this fraction, as a function of E_T^{miss} , to correct for the missing $p_T^Z < 37$ GeV contribution. The correction is found to be negligible in all signal regions.

The distribution of E_T^{miss} obtained in SHERPA $Z/\gamma^* + \text{jets}$ MC simulation is compared to that obtained by applying this background estimation technique to SHERPA $\gamma + \text{jets}$ MC samples. In this check the $\gamma + \text{jets}$ MC simulation is reweighted according to the p_T distribution given by the $Z/\gamma^* + \text{jets}$ MC simulation. The result of this MC closure check is shown in Figure 3(a) for events in VRZ (without an upper E_T^{miss} cut), where good agreement between $Z/\gamma^* + \text{jets}$ and corrected $\gamma + \text{jets}$ MC simulation can be seen across the entire E_T^{miss} spectrum. A comparison between the full E_T^{miss} spectrum in data and the $Z/\gamma^* + \text{jets}$ background estimated via the $\gamma + \text{jets}$ method is also shown in Figure 3(b) for events in VRZ. The systematic uncertainties associated with this method are described in Section 8.

7.3 Fake-lepton background

Semileptonic $t\bar{t}$, $W \rightarrow \ell\nu$ and single top (s - and t -channel) events enter the dilepton channels via “fake” leptons. These can include misidentified hadrons, converted photons or non-prompt leptons from b -hadron decays. The extent of this background is estimated using the matrix method, detailed in Ref. [93]. Its contribution in regions with high lepton p_T and dilepton invariant mass is negligible, but in the edge search, where lower- p_T leptons are selected and events can have low $m_{\ell\ell}$, the fake-lepton background can make up to 15% of the total background. In this method a control sample is constructed using baseline leptons, thereby enhancing the probability of selecting a fake lepton due to the looser lepton selection and identification criteria relative to the signal lepton selection. For each relevant CR, VR or SR, the region-specific kinematic requirements are placed upon this sample of baseline leptons. The number of events in this sample in which the selected leptons subsequently pass (N_{pass}) or fail (N_{fail}) the signal lepton requirements in Section 5 are then counted. In the case of a one-lepton selection, the number of fake-lepton events in a given region is then estimated according to:

$$N_{\text{pass}}^{\text{fake}} = \frac{N_{\text{fail}} - (1/\epsilon^{\text{real}} - 1) \times N_{\text{pass}}}{1/\epsilon^{\text{fake}} - 1/\epsilon^{\text{real}}}. \quad (6)$$

Here ϵ^{real} is the relative identification efficiency (from baseline to signal) for genuine, prompt (“real”) leptons and ϵ^{fake} is the relative identification efficiency (again from baseline to signal) with which non-prompt leptons or jets might be misidentified as prompt leptons. This principle is then expanded to a dilepton selection by using a four-by-four matrix to account for the various possible real–fake combinations for the two leading leptons in an event.

The real-lepton efficiency, ϵ^{real} , is measured in $Z \rightarrow \ell\ell$ data events using a tag-and-probe method in CR-real, defined in Table 4. In this region the p_T of the leading lepton is required to be > 40 GeV, and only events with exactly two SFOS leptons are selected. The fake-lepton efficiency, ϵ^{fake} , is measured in CR-fake, a region enriched with fake leptons by requiring same-sign lepton pairs. The lepton p_T requirements are the same as those in CR-real, with the leading lepton being tagged as the “real” lepton and the fake efficiency being evaluated based on the sub-leading lepton in the event. An E_T^{miss} requirement of < 125 GeV is used to reduce possible contamination from Beyond Standard Model processes. In this

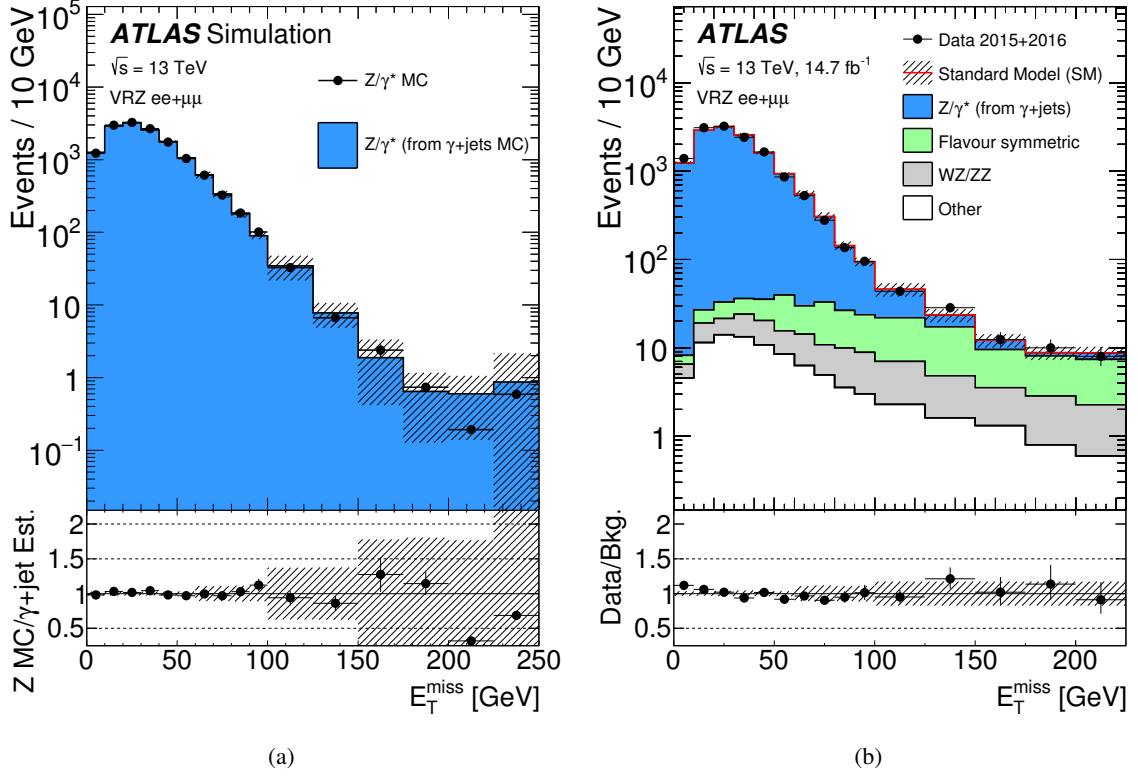


Figure 3: Left, the E_T^{miss} spectrum in SHERPA $Z/\gamma^* + \text{jets}$ MC simulation compared to that of the $\gamma + \text{jets}$ background estimation technique applied to SHERPA $\gamma + \text{jets}$ MC simulation in VRZ. The error bars on the points indicate the statistical uncertainty of the $Z/\gamma^* + \text{jets}$ MC simulation, and the hashed uncertainty bands indicate the statistical and reweighting systematic uncertainties of the $\gamma + \text{jet}$ background method. For this MC comparison the upper E_T^{miss} cut has been removed from VRZ and the overflow is included in the rightmost bin. Right, the E_T^{miss} spectrum when the method is applied to data in VRZ. Here the flavour-symmetric background is estimated using the data-driven flavour-symmetry method, and the fake-lepton background is estimated using the data-driven method explained in Section 7.3. Rare top and diboson backgrounds are taken from MC simulation. The rare top and data-driven fake-lepton backgrounds are grouped under “other” backgrounds. The hashed bands indicate the systematic uncertainty of only the $\gamma + \text{jets}$ and flavour-symmetric backgrounds below 100 GeV and the full uncertainty of the VR-S prediction above 100 GeV. The bottom panel of each figure shows the ratio of the observation (left, in MC simulation; right, in data) to the prediction.

region the background due to prompt-lepton production, estimated from MC simulation, is subtracted from the total data contribution. Prompt-lepton production makes up 7% (11%) of the baseline electron (muon) sample and 10% (61%) of the signal electron (muon) sample in CR-fake. From the resulting data sample the fraction of events in which the baseline leptons pass a signal-like selection yields the fake efficiency. Both the real- and fake-lepton efficiencies are binned as a function of lepton p_T and calculated separately for the 2015 and 2016 data sets.

This method is validated by checking the closure in MC simulation and data–background agreement in VR-fake.

7.4 Diboson and rare top processes

The remaining SM background contribution in the SRs is due to WZ/ZZ diboson production and rare top processes ($t\bar{t}Z$, $t\bar{t}W$ and $t\bar{t}WW$). The rare top processes compose $< 5\%$ of the expected SM background in the SRs and are taken directly from MC simulation.

Production of WZ/ZZ dibosons constitutes about 30% of the expected background in SRZ and up to 20% in some edge SR $m_{\ell\ell}$ windows. In SRZ, this background is composed of roughly 70% WZ , about 40% of which is $WZ \rightarrow \ell\ell\tau\nu$. This is the largest background contribution that is estimated from MC simulation, and must be carefully validated, especially because these backgrounds contain Z bosons and can thus mimic a signal by producing a peak at $m_{\ell\ell} \approx m_Z$. To validate the MC modelling of these backgrounds, VRs with three leptons (VR-WZ) and four leptons (VR-ZZ) are defined (selection shown in Table 3). In VR-WZ, from the three selected leptons in an event, the SFOS pair with $m_{\ell\ell}$ most consistent with the Z mass is identified as the Z candidate. The transverse mass of the remaining lepton and the E_T^{miss} , $m_T(\ell_3, E_T^{\text{miss}})$, is then required to be < 100 GeV, forming the W candidate. In VR-ZZ an $E_T^{\text{miss}} < 100$ GeV requirement is used to suppress WZ and top processes. The yields and kinematic distributions observed in these regions are well-modelled by MC simulation. In particular, the E_T^{miss} , H_T , jet multiplicity, and boson p_T distributions show good agreement. An additional three-lepton VR (VR-3L) is defined to provide validation of the diboson background in a region of phase space closer to the SR; good agreement is observed in this region as well.

7.5 Results in validation regions

The expected background yields in VR-S are shown in Table 6 and compared with the observed data yield. Agreement between the data and the expected Standard Model background is observed. The expected background yields in the three diboson VRs are also shown in Table 6. The data are consistent with the expected background. Similar information for the edge VRs is provided in Table 7. Data and background estimates are in agreement within uncertainties.

Figure 4 shows the observed and expected $m_{\ell\ell}$ distributions in the same edge VRs. The same background estimation methods are applied to both MC simulation and data. In the MC studies, the flavour-symmetry method of Section 7.1 is applied to $t\bar{t}$ MC simulation, and the observed SF $m_{\ell\ell}$ distribution is compared to the prediction based on DF events. In the data studies, the observed SF $m_{\ell\ell}$ distribution is compared to the sum of FS backgrounds from the extended flavour-symmetry method, the $Z/\gamma^* + \text{jets}$ background from the $\gamma + \text{jets}$ method, and the WZ/ZZ diboson, rare top, and fake-lepton backgrounds.

The observed MC closure is good in all validation regions. The data agree with the expected background in the validation regions as well. No significant discrepancies or trends are apparent.

Table 6: Expected and observed event yields in the four validation regions, VR-S, VR-WZ, VR-ZZ, and VR-3L. The flavour-symmetric, Z/γ^* + jets, and fake-lepton contributions to VR-S are derived using the data-driven estimates described in Section 7. All remaining backgrounds, and all backgrounds in the diboson validation regions, are taken from MC simulation. The quoted uncertainties in VR-S include statistical and all systematic contributions. In VR-WZ, VR-ZZ, and VR-3L, the rare top and diboson uncertainties include statistical and all theoretical uncertainties described in Section 8. The fake-lepton contribution in these three regions is predominantly due to Z/γ^* + jets, and in this case only the statistical uncertainty is given. The individual uncertainties can be correlated and do not necessarily add up in quadrature to the total systematic uncertainty.

| | VR-S | VR-WZ | VR-ZZ | VR-3L |
|---|--------------|--------------|-----------------|---------------|
| Observed events | 236 | 698 | 132 | 32 |
| Total expected background events | 224 ± 41 | 622 ± 66 | 139 ± 25 | 35 ± 10 |
| Flavour-symmetric ($t\bar{t}$, Wt , WW , $Z \rightarrow \tau\tau$) | 99 ± 8 | - | - | - |
| WZ/ZZ events | 27 ± 13 | 573 ± 66 | 139 ± 25 | 25 ± 10 |
| Rare top events | 11 ± 3 | 14 ± 3 | 0.44 ± 0.11 | 9.1 ± 2.3 |
| Z/γ^* + jets events | 84 ± 37 | - | - | - |
| Fake-lepton events | 4 ± 4 | 35 ± 6 | - | 0.6 ± 0.3 |

Table 7: Expected and observed event yields in the three validation regions, VR-low, VR-medium and VR-high. The quoted uncertainties include statistical and systematic contributions. The individual uncertainties can be correlated and do not necessarily add up in quadrature to the total systematic uncertainty.

| | VR-low | VR-medium | VR-high |
|---|-----------------|----------------|---------------|
| Observed events | 16253 | 1917 | 314 |
| Total expected background events | 16500 ± 700 | 1990 ± 150 | 340 ± 60 |
| Data-driven flavour-symmetry events | 14700 ± 600 | 1690 ± 120 | 250 ± 50 |
| WZ/ZZ events | 250 ± 80 | 40 ± 19 | 9 ± 6 |
| Data-driven Z/γ^* + jets (γ + jets) events | 1100 ± 400 | 130 ± 70 | 50 ± 29 |
| Rare top events | 87 ± 23 | 27 ± 7 | 6.5 ± 1.8 |
| Data-driven fake-lepton events | 270 ± 100 | 98 ± 35 | 20 ± 11 |

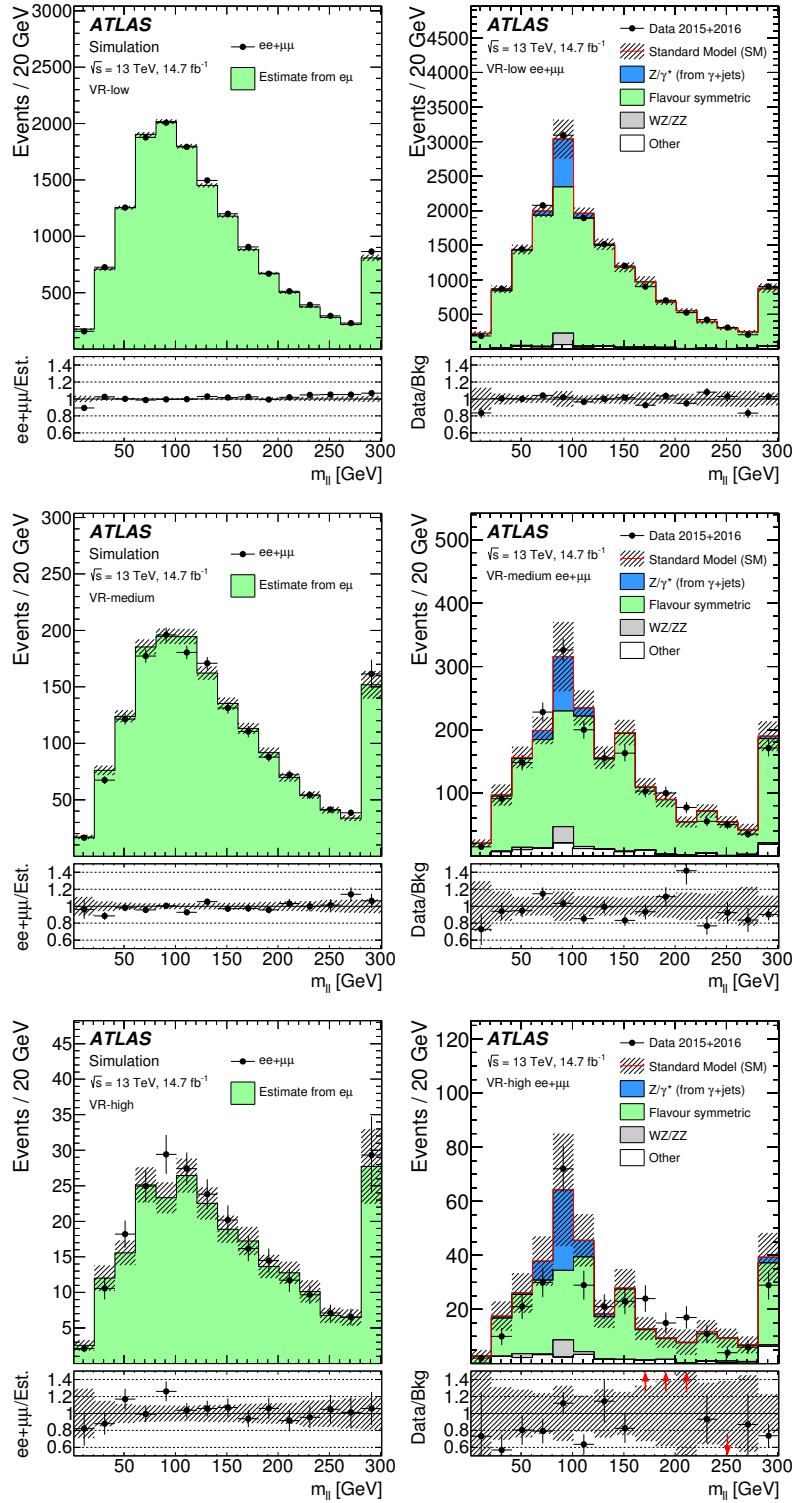


Figure 4: Validation of the flavour-symmetry method for the edge search using MC events (left) and data (right), in the VR-low (top), VR-medium (middle), and VR-high (bottom) regions. In the MC plots the flavour-symmetry estimate from $e\mu t\bar{t}$ MC samples is compared with the observed SF distribution from these MC samples, with the MC statistical uncertainty indicated by the hashed bands. In the data plots, all uncertainties in the background prediction are included in the hashed band. The rare top and data-driven fake-lepton backgrounds are grouped under “other” backgrounds. The bottom panel of each figure shows the ratio of the observation (left, in MC simulation; right, in data) to the prediction. In cases where the data point is not accommodated by the scale of this panel, a red arrow indicates the direction in which the point is out of range. The last bin contains the overflow.

8 Systematic uncertainties

The data-driven background estimates are subject to uncertainties associated with the methods employed and the limited number of events used in their estimation. The dominant uncertainty (10%) for the flavour-symmetry-based background estimate in SRZ is due to the limited number of events in CR-FS. Other systematic uncertainties assigned to this background estimate include those due to MC closure (3%), the measurement of the efficiency correction factors (3%) and the extrapolation in $m_{\ell\ell}$ (1%). In the case of the edge SRs the statistical uncertainty is also the dominant uncertainty in the flavour-symmetric background estimate in the case of SR-high, but for both SR-medium and SR-low the uncertainties from the MC non-closure and efficiency correction factors are comparable in size, or in some cases larger. These uncertainties can contribute up to 5% in SR-low and SR-medium and 10% in SR-high.

Several sources of systematic uncertainty are assessed for the $Z/\gamma^* + \text{jets}$ background. The boson p_T reweighting procedure is assigned an uncertainty based on a comparison of the nominal results with those obtained by reweighting using three other kinematic variables, namely H_T , Z -boson E_T and jet multiplicity. For the smearing function, which is measured using MC events in a 1-jet control region, an uncertainty is derived by comparing the results obtained using the nominal smearing function with those obtained using a smearing function from a 2-jet sample of MC events, and also using a smearing function measured in a 1-jet data sample. An uncertainty of between 40–100% is assigned to account for different reweighting procedures and between 20–100% for the smearing procedure applied to $\gamma + \text{jets}$ events. The smearing uncertainty dominates in SR-high, while the reweighting uncertainty dominates in SR-low and SR-medium, with both being around 60% in SRZ. The full reweighting and smearing procedure is carried out using $\gamma + \text{jets}$ MC events such that an MC non-closure uncertainty can be derived by comparing the resulting $\gamma + \text{jets}$ MC E_T^{miss} distribution to that in $Z/\gamma^* + \text{jets}$ MC events. The resulting uncertainty of up to 35% is calculated in the VRs, so as to maximise the number of events that contribute. An uncertainty of 16% is assessed for the $V\gamma$ backgrounds, based on data-to-MC agreement in a $V\gamma$ -enriched control region. This uncertainty is propagated to the final $Z/\gamma^* + \text{jets}$ estimate following the subtraction of the $V\gamma$ background. In VR-low, a correction is applied to the E_T^{miss} distribution in $\gamma + \text{jets}$ events to account for the fraction of $Z/\gamma^* + \text{jets}$ events in this H_T -inclusive region expected to have boson p_T less than 37 GeV. The full size of this correction (up to 50% for $E_T^{\text{miss}} = 150$ GeV) is applied as a systematic uncertainty. The $m_{\ell\ell}$ distribution assigned to $\gamma + \text{jets}$ MC events is compared to that of $Z/\gamma^* + \text{jets}$ MC events, and the relative difference in a given $m_{\ell\ell}$ bin is assigned as an uncertainty. Finally, the statistical precision of the estimate also enters as a systematic uncertainty of $\sim 10\%$ in the final background estimate. After applying the correction procedure, differences in the number of b -tagged jets between $Z/\gamma^* + \text{jets}$ and $\gamma + \text{jets}$ are found to be negligible, indicating good agreement in heavy-flavour content.

The uncertainties in the fake-lepton background stem from the number of events in the regions used to measure the real- and fake-lepton efficiencies, the limited size of the inclusive loose-lepton sample, and from varying the region used to measure the fake-lepton efficiency. The nominal fake-lepton efficiency is compared with those measured in a region with b -tagged jets and a region with a b -jet, as well as a region with the prompt-lepton subtraction varied by 20%. Varying the sample composition via b -jet tagging gives the largest uncertainty. The uncertainty for the edge SRs from the statistical component of the lepton efficiencies is 30–45%, and from varying the region for the fake-lepton efficiency it is 50–75%. The uncertainties in SRZ are generally larger due to the small number of events contributing to the estimate in this region.

Theoretical and experimental uncertainties are taken into account for the signal models, as well as background processes that rely on MC simulation. The estimated uncertainty in the luminosity measurement

is 2.9% [30, 31]. The jet energy scale is subject to uncertainties associated with the jet flavour composition, the pile-up and the jet and event kinematics [80]. Uncertainties in the jet energy resolution are included to account for differences between data and MC simulation [80]. An uncertainty in the E_T^{miss} soft-term resolution and scale is taken into account [87], and uncertainties due to the lepton energy scales and resolutions, as well as trigger, reconstruction, and identification efficiencies, are also considered.

The WZ/ZZ processes are assigned a cross-section uncertainty of 6% and an additional uncertainty based on comparisons between SHERPA and POWHEG MC samples, which is up to 50% in the SRs. Uncertainties due to the choice of factorisation and renormalisation scales are calculated by varying the nominal values up and down by a factor of two and can be up to 23%. For rare top processes, a 13% PDF and scale variation uncertainty is applied [33] in addition to a 22% cross-section uncertainty [60–62].

For signal models, the nominal cross section and the uncertainty are taken from an envelope of cross-section predictions using different PDF sets and factorisation and renormalisation scales, as described in Refs. [94, 95]. These are calculated at next-to-leading-logarithm accuracy (NLO+NLL) [50–54], and the resulting uncertainties range from 16% to 30%.

A breakdown of the dominant uncertainties in the background prediction in the SRs is provided in Table 8 for the on-shell Z and edge searches. Here these uncertainties are quoted relative to the total background. In the case of the edge regions a range is quoted, taking into account the relative contribution of the given uncertainty in each of the $m_{\ell\ell}$ ranges in SR-low, SR-medium and SR-high. The largest uncertainties in the signal regions are due to the size of the $e\mu$ data sample in CR-FS, used to provide the flavour-symmetric background estimate, the combined systematic uncertainty in the same background, the systematic uncertainty in γ + jets, or, in the case of SRZ, the WZ/ZZ generator uncertainty. The statistical component of the uncertainty from the flavour-symmetry estimate is largest for the edge analysis in SR-medium and SR-high in the highest $m_{\ell\ell}$ regions. In the edge SRs the uncertainty in the WZ/ZZ background tends to be highest in the $m_{\ell\ell}$ ranges that include the Z window. The uncertainty in the fake-lepton background is largest in SR-high, where fake leptons can compose a larger fraction of the background. Experimental uncertainties have a far lower impact on the systematic uncertainty of the total background ($< 2\%$).

Table 8: Overview of the dominant sources of systematic uncertainty in the total background estimate in the signal regions. The values shown are relative to the total background estimate, shown in %. The systematic uncertainties for the edge search are quoted as a range across the $m_{\ell\ell}$ regions used for statistical interpretations.

| Source | Relative systematic uncertainty [%] | | | |
|-----------------------------------|-------------------------------------|--------|-----------|---------|
| | SRZ | SR-low | SR-medium | SR-high |
| Total systematic uncertainty | 17 | 8–30 | 6–34 | 10–45 |
| WZ/ZZ generator uncertainty | 13 | 0–7 | 0–6 | 0–10 |
| Flavour symmetry (statistical) | 7 | 3–16 | 5–16 | 7–28 |
| WZ/ZZ scale uncertainty | 6 | 0–1 | 0–1 | 0–2 |
| Z/γ^* + jets (systematic) | 4 | 0–15 | 0–25 | 0–15 |
| Flavour symmetry (systematic) | 3 | 2–23 | 2–15 | 4–25 |
| Z/γ^* + jets (statistical) | 2 | 0–3 | 0–5 | 0–1 |
| Fake leptons | 1 | 0–17 | 2–18 | 2–20 |

Table 9: Expected and observed event yields in SRZ, inclusively, in the ee channel, and in the $\mu\mu$ channel, along with the discovery p -value for zero signal strength ($p(s = 0)$) [96], Gaussian significance, 95% confidence level (CL) observed and expected upper limits on the number of signal events (S^{95}), and the corresponding observed upper limit on the visible cross section ($\langle\epsilon\sigma\rangle_{\text{obs}}^{95}$). For regions in which the data yield is less than expected, the discovery p -value is truncated at 0.5 and the significance is set to zero. The flavour-symmetric, $Z/\gamma^* + \text{jets}$ and fake-lepton components are all derived using data-driven estimates described in Section 7. All remaining backgrounds are taken from MC simulation. The quoted uncertainties include statistical and systematic contributions. The individual uncertainties can be correlated and do not necessarily add up in quadrature to the total systematic uncertainty.

| | SRZ | SRZ ee | SRZ $\mu\mu$ |
|--|-------------------------------|-------------------------------|-------------------------------|
| Observed events | 60 | 35 | 25 |
| Total expected background events | 53.5 ± 9.3 | 27.1 ± 5.1 | 26.8 ± 4.4 |
| Flavour-symmetric ($t\bar{t}$, Wt , WW and $Z \rightarrow \tau\tau$) events | 33.2 ± 3.9 | 16.5 ± 2.1 | 16.7 ± 2.0 |
| $Z/\gamma^* + \text{jets}$ events | 3.1 ± 2.8 | $1.0^{+1.3}_{-1.0}$ | 2.1 ± 1.4 |
| WZ/ZZ events | 14.2 ± 7.7 | 7.8 ± 4.3 | 6.4 ± 3.5 |
| Rare top events | 2.9 ± 0.8 | 1.4 ± 0.4 | 1.5 ± 0.4 |
| Fake-lepton events | $0.1^{+0.8}_{-0.1}$ | $0.5^{+0.7}_{-0.5}$ | $0^{+0.2}$ |
| $p(s = 0)$ | 0.32 | 0.15 | 0.5 |
| Significance (σ) | 0.47 | 1.02 | 0 |
| Observed (Expected) S^{95} | 28.2 ($24.5^{+8.9}_{-6.7}$) | 22.0 ($15.8^{+6.5}_{-4.5}$) | 12.9 ($14.0^{+5.7}_{-3.9}$) |
| $\langle\epsilon\sigma\rangle_{\text{obs}}^{95}$ [fb] | 1.9 | 1.5 | 0.88 |

9 Results

9.1 Results in SRZ

For the on-shell Z search, the expected background and observed yields in the SR are shown in Table 9. A total of 60 events are observed in data with a predicted background of 53.5 ± 9.3 events. There are 35 events observed in data in the ee channel, and 25 events observed in the $\mu\mu$ channel. The probability for the background to produce a fluctuation greater than or equal to that observed in the data, called the significance when expressed in terms of the number of standard deviations, corresponds to 0.47σ (details of the significance calculation are presented in Section 10). The level of agreement between the observed event yields in data and the background predictions in the VRs, shown previously in Table 6, is also displayed in Figure 5, along with the results in SRZ.

The dilepton invariant-mass distribution for the $ee + \mu\mu$ and $e\mu$ channels with the kinematic requirements of SRZ, but over the full $m_{\ell\ell}$ range, is shown in Figure 6. Here the data are consistent with the expected background over the full $m_{\ell\ell}$ range. The dilepton invariant-mass, jet and b -tagged jet multiplicity, $E_{\text{T}}^{\text{miss}}$, $H_{\text{T}}^{\text{incl}}$ and $p_{\text{T}}^{\ell\ell}$ distributions in SRZ are shown in Figure 7. The shapes of the background distributions in these figures are obtained from MC simulation, where the MC simulation is normalised according to the data-driven estimates in the SR. Here two representative examples of $\tilde{g}-\tilde{\chi}_2^0$ on-shell signal models, with $(m(\tilde{g}), m(\tilde{\chi}_2^0)) = (1095, 205)$ GeV and $(m(\tilde{g}), m(\tilde{\chi}_2^0)) = (1240, 960)$ GeV, are overlaid. To demonstrate the modelling of the $Z/\gamma^* + \text{jets}$ background in VR-S and SRZ, Figure 8 shows the minimum $\Delta\phi(\text{jet}_{12}, \mathbf{p}_{\text{T}}^{\text{miss}})$

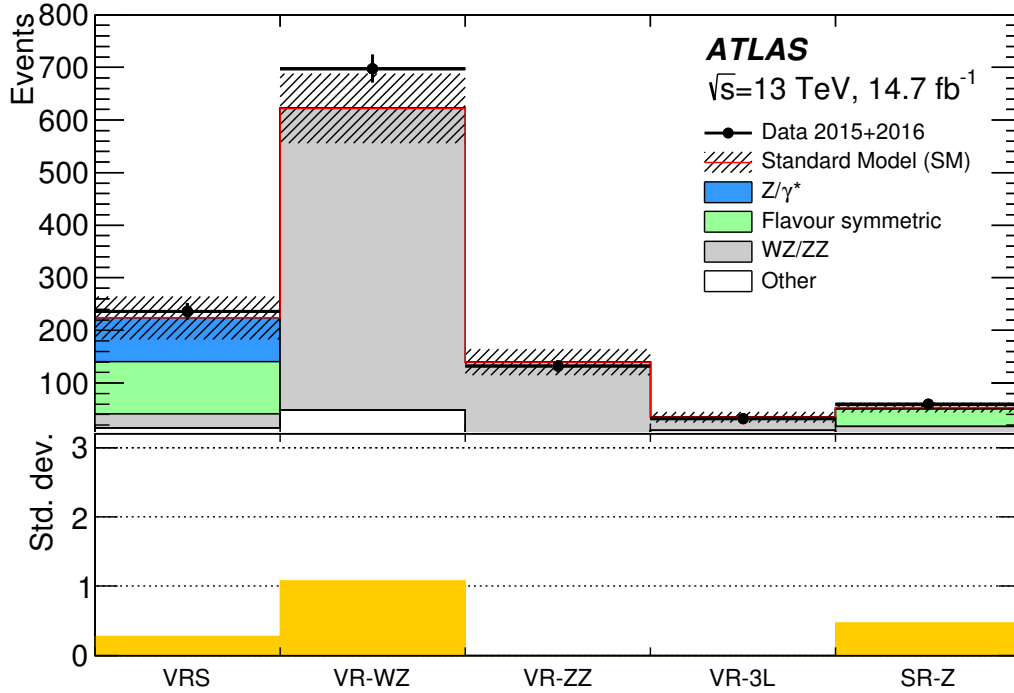


Figure 5: The expected and observed yields in the validation regions and signal region of the on-shell Z search. The rare top and data-driven fake-lepton backgrounds are grouped under “other” backgrounds. The significance of the difference between the data and the expected background (see text for details) is shown in the bottom plot; for regions in which the data yield is less than expected, the significance is set to zero. The hashed uncertainty bands include the statistical and systematic uncertainties in the background prediction.

distribution over the full range, where $\Delta\phi(\text{jet}_{12}, \mathbf{p}_T^{\text{miss}}) > 0.4$ is required in VR-S and SRZ. Here the $Z/\gamma^* + \text{jets}$ distribution is modelled using the full data-driven prediction from $\gamma + \text{jets}$. Two of the events in the SR contain a third signal lepton.

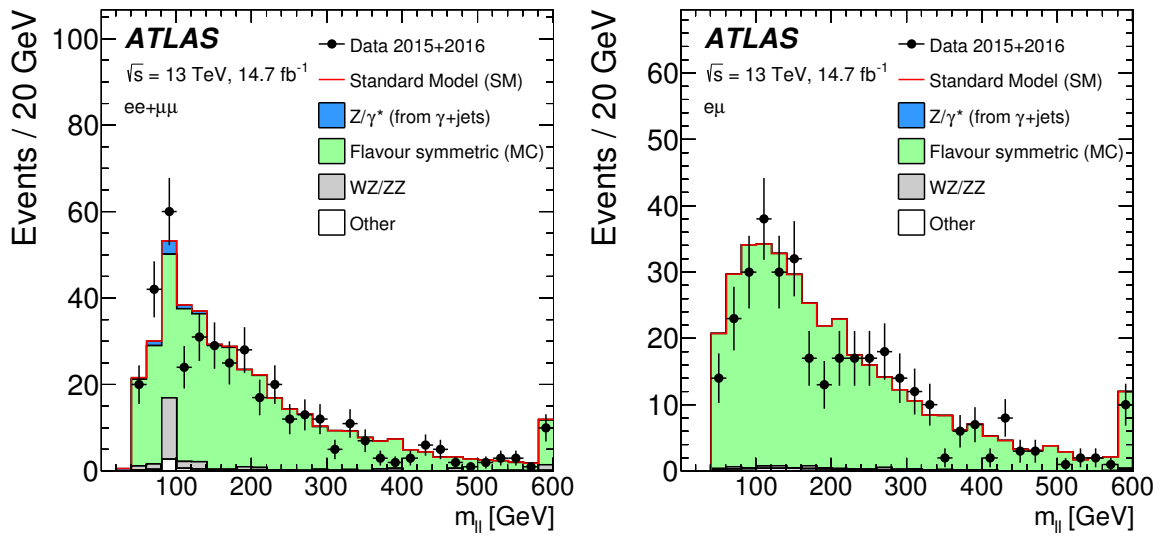


Figure 6: The dilepton invariant-mass distribution for an SRZ-like selection, but with the Z mass requirement removed, in the same-flavour (left) and different-flavour (right) channels. With the exception of the $Z/\gamma^* + \text{jets}$ background, MC simulation is used to show the expected shapes of the $m_{\ell\ell}$ distributions, with the backgrounds being normalised according to their SRZ prediction. For the $Z/\gamma^* + \text{jets}$ background, the $m_{\ell\ell}$ shape is taken from the $\gamma + \text{jets}$ method. The rare top and data-driven fake-lepton backgrounds are grouped under “other” backgrounds. The last bin includes the overflow.

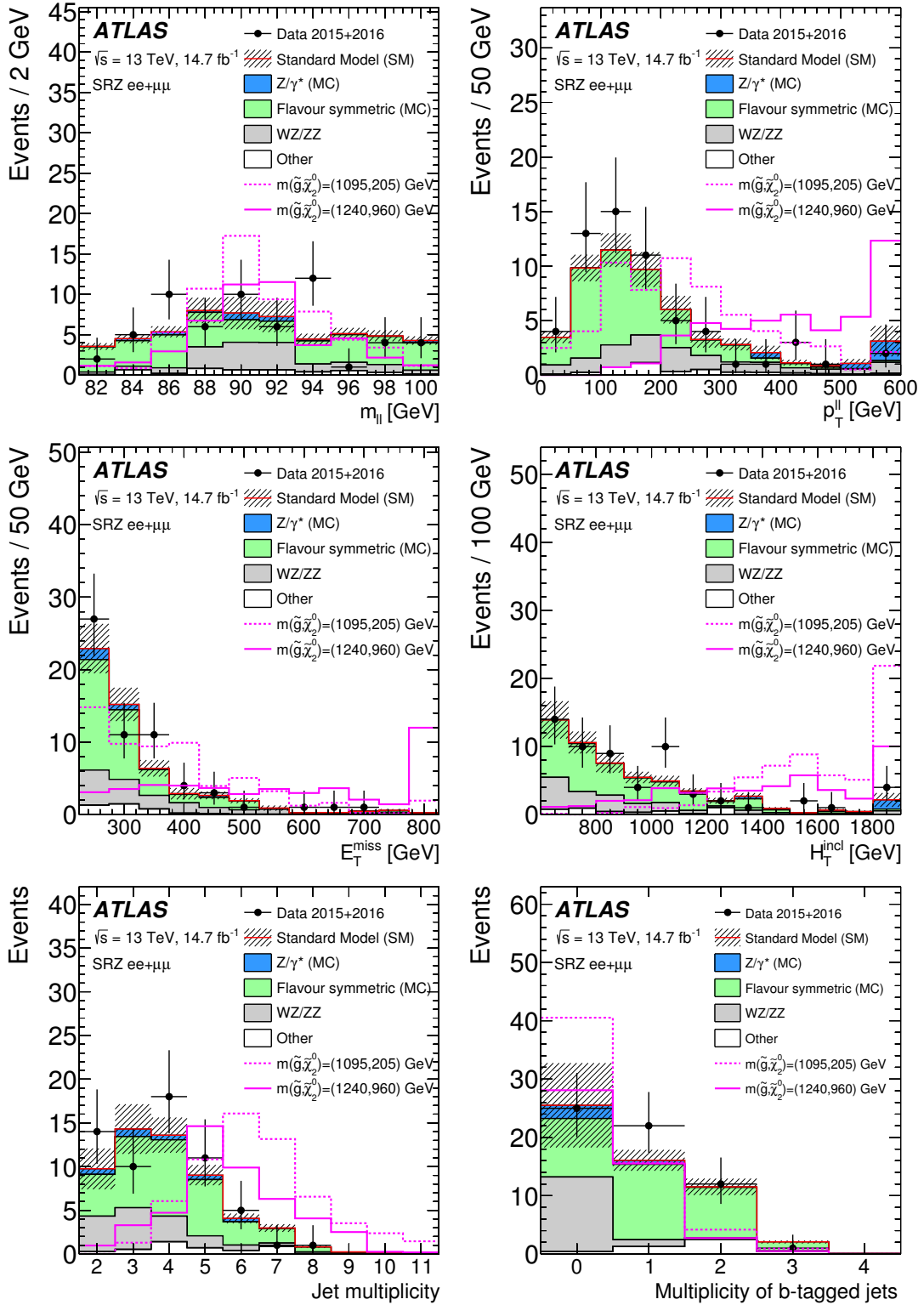


Figure 7: The $m_{\ell\ell}$ (top left), $p_T^{\ell\ell}$ (top right), E_T^{miss} (middle left), H_T^{incl} (middle right), jet multiplicity (bottom left) and b -tagged jet multiplicity (bottom right) distributions in SRZ. Two examples of signal models from the $\tilde{g}-\tilde{\chi}_2^0$ on-shell grid, described in Section 4, with $(m(\tilde{g}), m(\tilde{\chi}_2^0)) = (1095, 205)$ GeV and $(m(\tilde{g}), m(\tilde{\chi}_2^0)) = (1240, 960)$ GeV, are overlaid. In the case of the E_T^{miss} , H_T^{incl} and $p_T^{\ell\ell}$ distributions, the last bin contains the overflow. The flavour-symmetric and Z/γ^* + jets backgrounds are taken from MC simulation and scaled to match their SRZ data-driven predictions. The rare top and data-driven fake-lepton backgrounds are grouped under “other” backgrounds. The hashed uncertainty bands include the statistical and systematic uncertainties in the background prediction.

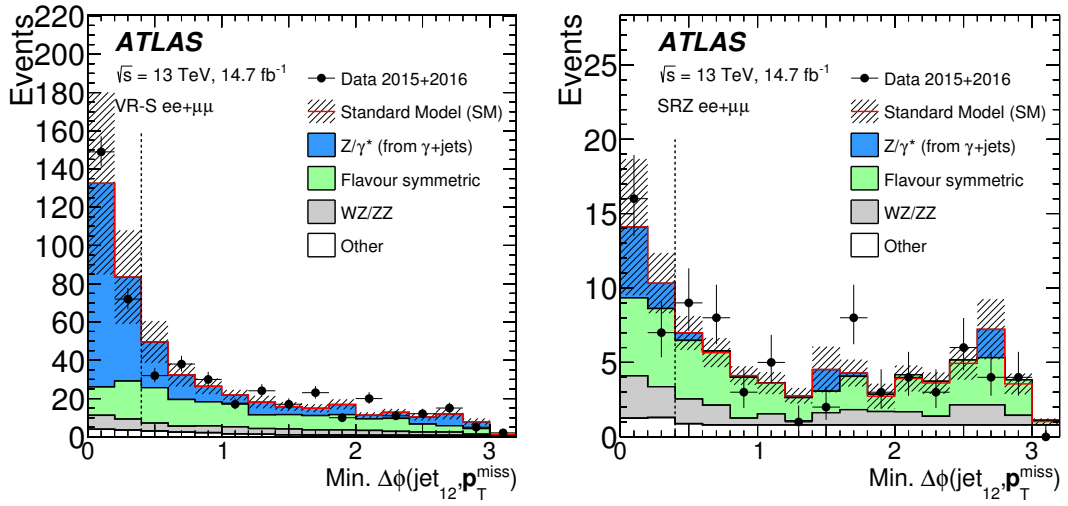


Figure 8: The $\text{min. } \Delta\phi(\text{jet}_{12}, \mathbf{p}_T^{\text{miss}})$ distribution in (left) VR-S and (right) SRZ, where the $\text{min. } \Delta\phi(\text{jet}_{12}, \mathbf{p}_T^{\text{miss}}) > 0.4$ requirement has been lifted. The vertical dashed lines indicate the requirement in each region. The flavour-symmetric and Z/γ^* + jets distributions are taken completely from the data-driven estimate. The rare top and data-driven fake-lepton backgrounds are grouped under “other” backgrounds. The hashed uncertainty bands include the statistical and systematic uncertainties in the background prediction.

Table 10: Breakdown of the expected background and observed data yields for SR-low, SR-medium and SR-high, integrated over the $m_{\ell\ell}$ spectrum. The flavour-symmetric, $Z/\gamma^* + \text{jets}$ and fake-lepton components are all derived using data-driven estimates described in Section 7. All remaining backgrounds are taken from MC simulation. The quoted uncertainties include statistical and systematic contributions.

| | SR-low | SR-medium | SR-high |
|--|----------------|----------------|---------------|
| Observed events | 1394 | 689 | 212 |
| Total expected background events | 1500 ± 100 | 700 ± 60 | 171 ± 18 |
| Flavour-symmetric ($t\bar{t}$, Wt , WW and $Z \rightarrow \tau\tau$) events | 1270 ± 70 | 584 ± 32 | 148 ± 14 |
| $Z/\gamma^* + \text{jets}$ events | 90 ± 50 | 50 ± 40 | 3^{+7}_{-3} |
| WZ/ZZ events | 68 ± 31 | 26 ± 11 | 7 ± 4 |
| Rare top events | 19 ± 5 | 11.3 ± 3.2 | 4.2 ± 1.4 |
| Fake-lepton events | 59 ± 34 | 32 ± 19 | 10 ± 8 |

9.2 Results in the edge SRs

The integrated yields in the edge signal regions are compared to the expected background in Table 10. To allow for the visualisation of a potential edge, the full $m_{\ell\ell}$ distributions in the three search regions are compared to the expected background in Figure 9. In addition, the observed $m_{\ell\ell}$ distributions are compared to the predictions from MC simulation in Figure 10, in which the $t\bar{t}$ background is scaled such that the total MC expected yield matches the data in the $e\mu$ CR. The $t\bar{t}$ normalisation factors are $\mu_{t\bar{t}} = 0.85 \pm 0.03$, 0.75 ± 0.04 , and 0.57 ± 0.07 in SR-low, SR-medium, and SR-high, respectively, where the uncertainty is the data statistical uncertainty. The data-driven flavour-symmetry prediction is used for the quantitative results of the analysis. This prediction does not rely on the $t\bar{t}$ normalisation scale factors discussed above. The MC-based cross-check method is used to examine the $m_{\ell\ell}$ distribution in finer bins than can be achieved with the flavour-symmetry method, due to the limited statistical precision of the $e\mu$ CR.

As signal models may produce kinematic endpoints at any value of $m_{\ell\ell}$, any excess must be searched for across the $m_{\ell\ell}$ distribution. To do this a ‘‘sliding window’’ approach is used. The binning in the SRs, shown in Figure 9, defines many possible dilepton mass windows. The 24 $m_{\ell\ell}$ ranges (9 for SR-low, 8 for SR-medium, and 7 for SR-high) are chosen because they are the most sensitive for at least one grid point in the signal model parameter space. Some of the ranges overlap. The results in these regions are summarised in Figure 11, and the expected and observed yields in the combined $ee + \mu\mu$ channel for all 24 $m_{\ell\ell}$ ranges are presented in Table 11. In SR-low and SR-medium, the data are consistent with the expected background across the full $m_{\ell\ell}$ range. In SR-high the data show a slight excess above the background at low $m_{\ell\ell}$. Of these 24 $m_{\ell\ell}$ ranges, the largest excess is observed in SR-high with $12 < m_{\ell\ell} < 101$ GeV. Here a total of 90 events are observed in data, compared to an expectation of 65 ± 10 events, corresponding to a local significance of 1.7σ .

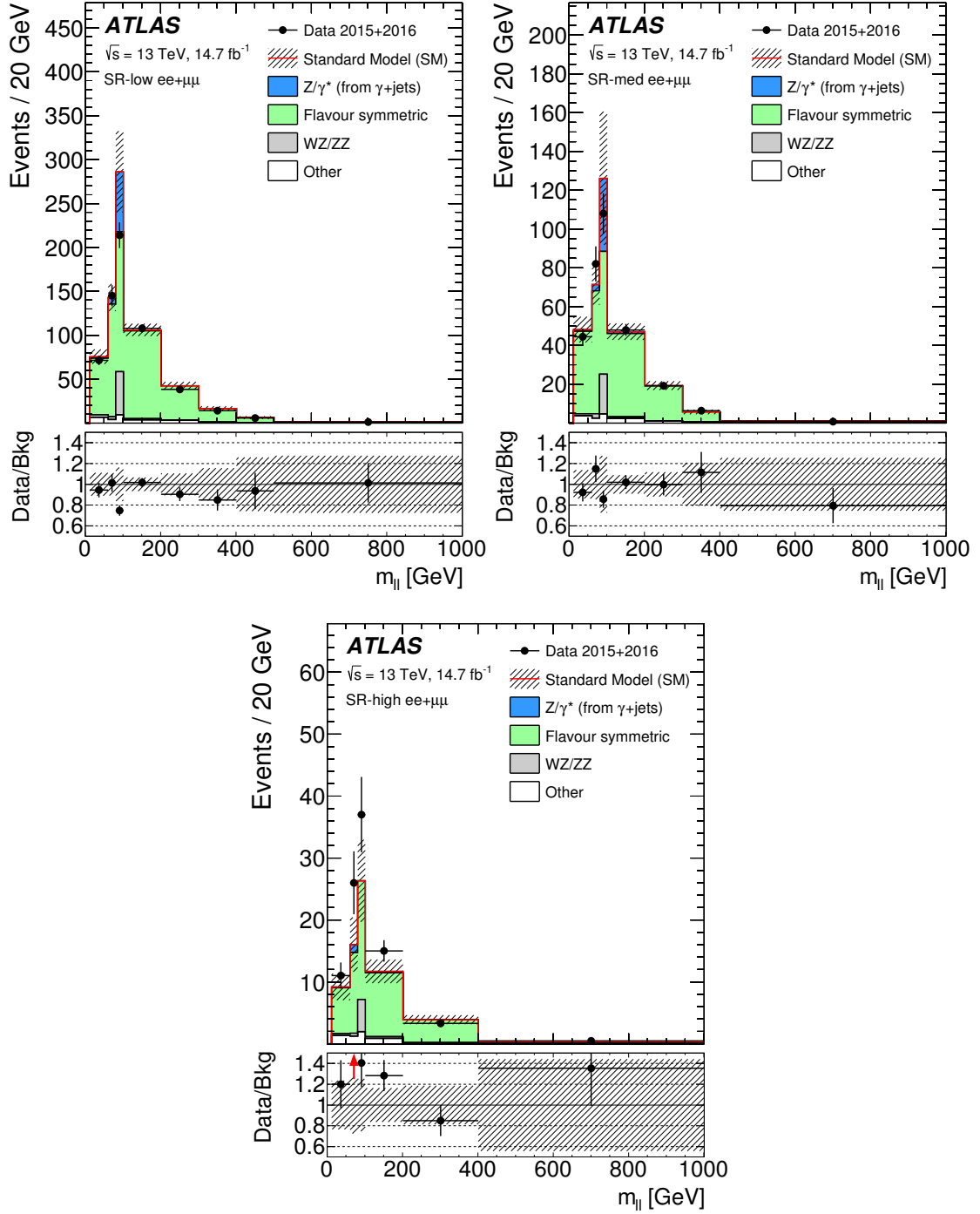


Figure 9: Expected and observed dilepton mass distributions, with the bin boundaries considered for the interpretation, in (top left) SR-low, (top-right) SR-medium, and (bottom) SR-high of the edge search. These bins, and sets of neighbouring bins, make up the $m_{\ell\ell}$ windows used for the interpretation. The flavour-symmetric and $Z/\gamma^* + \text{jets}$ distributions are taken completely from the data-driven estimate. The rare top and data-driven fake-lepton backgrounds are grouped under “other” backgrounds. All statistical and systematic uncertainties are included in the hashed bands. The ratio of data to predicted background is shown in the bottom panels. In cases where the data point is not accommodated by the scale of this panel, a red arrow indicates the direction in which the point is out of range.

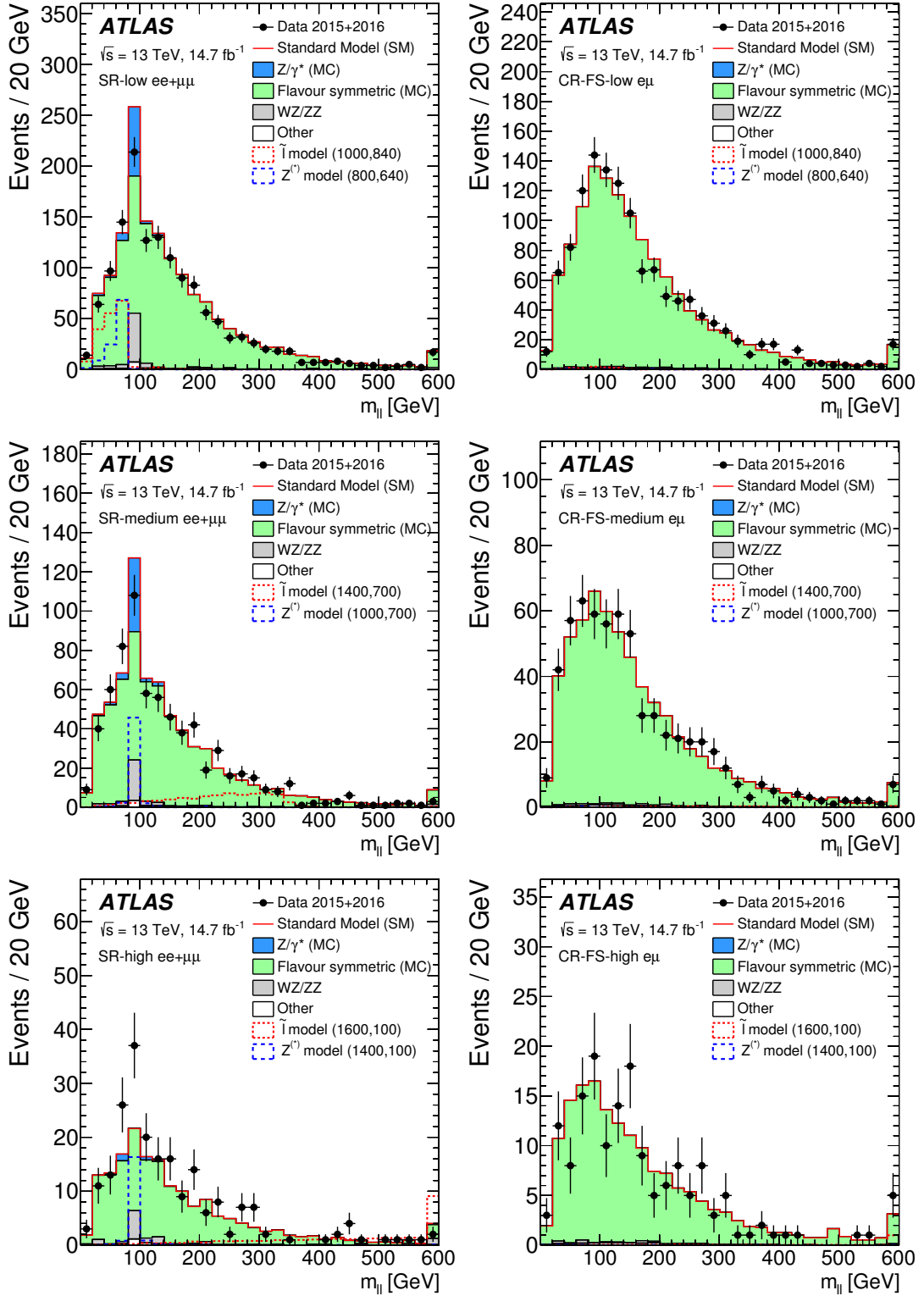


Figure 10: The dilepton mass distributions in the (top) SR-low (left) and CR-FS-low (right), (middle) SR-medium (left) and CR-FS-medium (right), and (bottom) SR-high (left) and CR-FS-high (right) regions of the edge search. The $t\bar{t}$ MC sample is normalised such that the total MC prediction matches data in the $e\mu$ channel for each region. The $m_{\ell\ell}$ shape and normalisation for the Z/γ^* + jets background is taken from the γ + jets method. The rare top and data-driven fake-lepton backgrounds are grouped under “other” backgrounds. Example signal benchmarks from the slepton and $Z^{(*)}$ models are overlaid on the distributions. The first (second) number in parentheses is the gluino (LSP) mass. The overflow is included in the last bin.

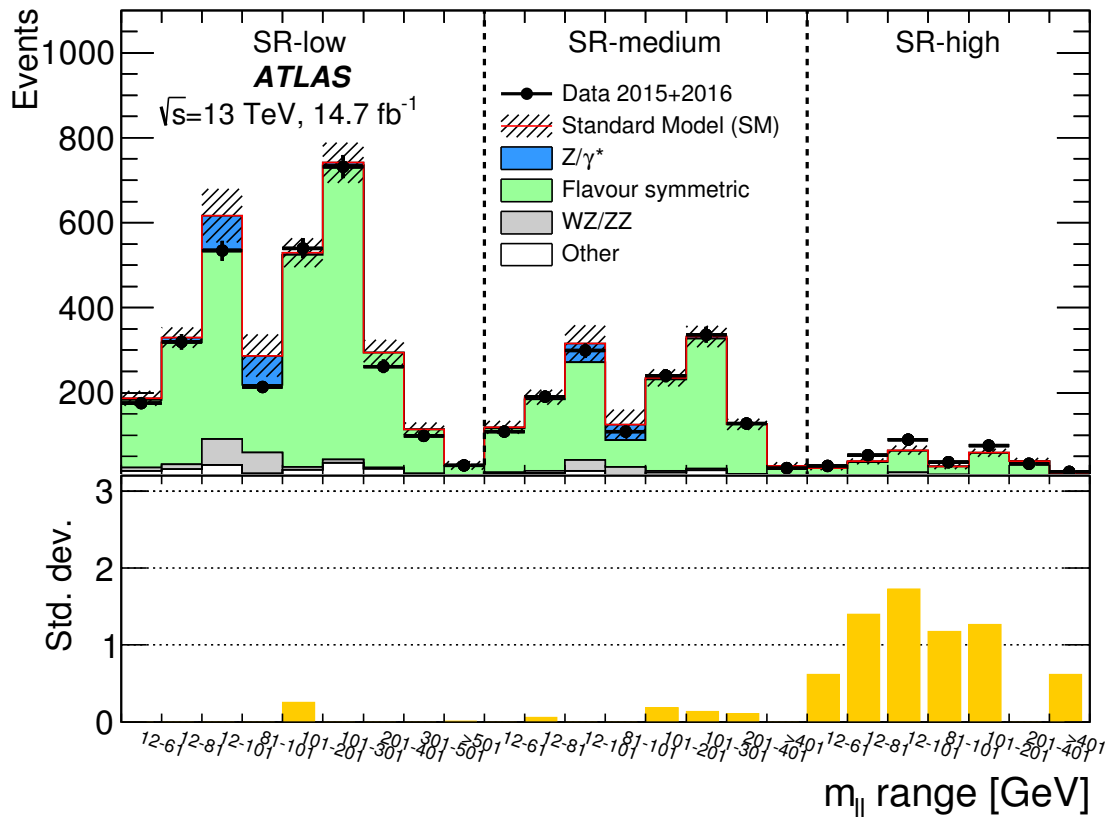


Figure 11: The expected and observed yields in the 24 (overlapping) $m_{\ell\ell}$ ranges of SR-low, SR-medium, and SR-high. The data are compared to the sum of the expected backgrounds. The rare top and data-driven fake-lepton backgrounds are grouped under “other” backgrounds. The significance of the difference between the data and the expected background (see text for details) is shown in the bottom plots; for regions in which the data yield is less than expected, the significance is set to zero. The hashed uncertainty bands include the statistical and systematic uncertainties in the background prediction.

Table 11: Breakdown of the expected background and observed data yields in the edge signal regions. The results are given for SR-low, SR-medium and SR-high in all 24 $m_{\ell\ell}$ ranges. The $m_{\ell\ell}$ range in units of GeV is indicated in the leftmost column of the table. Left to right: the total expected background, with combined statistical and systematic uncertainties, observed data, 95% CL upper limits on the visible cross section ($\langle\epsilon\sigma\rangle_{\text{obs}}^{95}$) and on the number of signal events (S_{obs}^{95}). The sixth column (S_{exp}^{95}) shows the expected 95% CL upper limit on the number of signal events, given the expected number (and $\pm 1\sigma$ excursions) of background events. The last two columns indicate the discovery p -value ($p(s=0)$) [96], and the Gaussian significance ($Z(s=0)$). For an observed number of events lower than expected, the discovery p -value is truncated at 0.5 and the significance is set to zero.

| Signal Region | Total Bkg. | Data | $\langle\epsilon\sigma\rangle_{\text{obs}}^{95}$ [fb] | S_{obs}^{95} | S_{exp}^{95} | $p(s=0)$ | $Z(s=0)$ |
|---------------|--------------|------|---|-----------------------|-----------------------|----------|----------|
| SR-low | | | | | | | |
| 12–61 | 187 ± 18 | 175 | 2.68 | 39.4 | 48_{-14}^{+23} | 0.50 | 0.00 |
| 12–81 | 330 ± 24 | 320 | 3.88 | 57.1 | 64_{-19}^{+30} | 0.50 | 0.00 |
| 12–101 | 617 ± 63 | 534 | 4.64 | 68.2 | 98_{-26}^{+36} | 0.50 | 0.00 |
| 81–101 | 287 ± 50 | 214 | 2.73 | 40.2 | 62_{-16}^{+22} | 0.50 | 0.00 |
| 101–201 | 529 ± 34 | 540 | 6.80 | 99.9 | 91_{-29}^{+52} | 0.40 | 0.26 |
| 101–301 | 741 ± 48 | 732 | 7.28 | 107 | 113_{-33}^{+53} | 0.50 | 0.00 |
| 201–401 | 295 ± 30 | 262 | 3.43 | 50.5 | 70_{-21}^{+37} | 0.50 | 0.00 |
| 301–501 | 113 ± 17 | 99 | 2.37 | 34.8 | 46_{-16}^{+41} | 0.50 | 0.00 |
| > 501 | 29 ± 10 | 29 | 1.88 | 27.7 | 27_{-10}^{+34} | 0.50 | 0.01 |
| SR-medium | | | | | | | |
| 12–61 | 119 ± 15 | 109 | 2.38 | 35.1 | 43_{-14}^{+29} | 0.50 | 0.00 |
| 12–81 | 190 ± 18 | 191 | 3.57 | 52.5 | 51_{-15}^{+31} | 0.48 | 0.06 |
| 12–101 | 315 ± 43 | 299 | 5.12 | 75.3 | 81_{-20}^{+29} | 0.50 | 0.00 |
| 81–101 | 125 ± 35 | 108 | 3.18 | 46.7 | 51_{-12}^{+17} | 0.50 | 0.00 |
| 101–201 | 235 ± 20 | 240 | 4.26 | 62.6 | 58_{-19}^{+37} | 0.42 | 0.19 |
| 101–301 | 332 ± 25 | 336 | 4.92 | 72.3 | 69_{-22}^{+39} | 0.45 | 0.14 |
| 201–401 | 126 ± 13 | 128 | 3.27 | 48.0 | 46_{-16}^{+52} | 0.46 | 0.11 |
| > 401 | 28 ± 8 | 22 | 1.09 | 16.1 | 21_{-7}^{+19} | 0.50 | 0.00 |
| SR-high | | | | | | | |
| 12–61 | 23 ± 5 | 27 | 1.84 | 27.0 | 20_{-8}^{+31} | 0.27 | 0.62 |
| 12–81 | 39 ± 7 | 53 | 3.32 | 48.9 | 26_{-10}^{+28} | 0.08 | 1.40 |
| 12–101 | 65 ± 10 | 90 | 4.00 | 58.8 | 31_{-10}^{+17} | 0.04 | 1.73 |
| 81–101 | 26 ± 6 | 37 | 2.17 | 31.9 | 20_{-7}^{+13} | 0.12 | 1.18 |
| 101–201 | 59 ± 9 | 75 | 3.68 | 54.1 | 31_{-11}^{+29} | 0.10 | 1.27 |
| 201–401 | 39 ± 7 | 33 | 1.82 | 26.7 | 28_{-7}^{+14} | 0.50 | 0.00 |
| > 401 | 10 ± 5 | 14 | 2.04 | 30.0 | 21_{-10}^{+79} | 0.27 | 0.62 |

10 Interpretation

In this section, exclusion limits are shown for the SUSY models detailed in Section 3. The asymptotic CL_S prescription [89, 97], implemented in the HistFitter program [96], is used to determine cross-section upper limits at 95% confidence level (CL) for the on-Z search. For the edge search, pseudo-experiments are used to evaluate the cross-section upper limits. A Gaussian model for nuisance parameters is used for all signal and background uncertainties. Exceptions are the statistical uncertainties of the flavour-symmetry method, $\gamma + \text{jets}$ method and MC-based backgrounds, all of which are treated as Poissonian nuisance parameters. The different experimental uncertainties are treated as correlated between signal and background events. The theoretical uncertainty of the signal cross section is not accounted for in the limit-setting procedure. Instead, following the initial limit determination, the impact of varying the signal cross section within its uncertainty is evaluated separately and indicated in the exclusion results. Limits are based on the combined $ee + \mu\mu$ results. Possible signal contamination in the CRs is neglected in the limit-setting procedure; the contamination is found to be negligible for signal points near the exclusion boundaries. Far from the exclusion boundary, although the signal contamination can be significant, the number of events appearing in the signal region is large enough that the points are still excluded, due to the relative branching fractions for the signal in the CR and SR. For example, for models with signal contamination of 50% in CR-FS the signal-to-background ratio in SRZ is ~ 10 .

The results of the on-shell Z search are interpreted in a simplified model with gluino-pair production, where each gluino decays as $\tilde{g} \rightarrow q\bar{q}\tilde{\chi}_2^0, \tilde{\chi}_2^0 \rightarrow Z\tilde{\chi}_1^0$ and the $\tilde{\chi}_1^0$ mass is set to 1 GeV. The expected and observed exclusion contours for this $\tilde{g}\text{-}\tilde{\chi}_2^0$ on-shell grid are shown in the $m(\tilde{g})\text{-}m(\tilde{\chi}_2^0)$ plane in Figure 12. The expected (observed) lower limit on the gluino mass is about 1.35 TeV (1.30 TeV) for a $\tilde{\chi}_2^0$ with a mass of 1.1 TeV in this model. The impact of the systematic uncertainties in the background and the experimental uncertainties in the signal, shown with a coloured band, is about 100 GeV on the gluino mass limit. The systematic uncertainty of the signal cross section, shown as dotted lines around the observed contour, has an impact of about 40 GeV. Figure 12 also shows the expected and observed exclusion limits for the $\tilde{q}\text{-}\tilde{\chi}_2^0$ on-shell model. This is a simplified model with squark-pair production, where each squark decays to a quark and a neutralino, with the neutralino subsequently decaying to a Z boson and an LSP with a mass of 1 GeV. In this model, exclusion is expected (observed) for squarks with masses below 1040 GeV (980 GeV) for a $\tilde{\chi}_2^0$ mass of 600 GeV.

Figure 13 shows the expected and observed exclusion contours for the $\tilde{g}\text{-}\tilde{\chi}_1^0$ on-shell model, in which the produced gluinos follow the same decay chain as in the model above. In this case the mass difference $\Delta m = m(\tilde{\chi}_2^0) - m(\tilde{\chi}_1^0)$ is set to 100 GeV.

The results of the edge search are interpreted in two simplified models with gluino-pair production, in which each gluino decays as $\tilde{g} \rightarrow q\bar{q}\tilde{\chi}_2^0$. For each point in the signal-model parameter space, limits on the signal strength are calculated using the $m_{\ell\ell}$ window with the best expected sensitivity. Details of the windows are described in Section 9.

The excluded regions in the $m(\tilde{g})\text{-}m(\tilde{\chi}_1^0)$ plane are presented in Figure 14 for the slepton model. In this model, pair-produced gluinos each decay as $\tilde{g} \rightarrow q\bar{q}\tilde{\chi}_2^0, \tilde{\chi}_2^0 \rightarrow \ell^\pm \tilde{\ell}^\mp, \tilde{\ell}^\mp \rightarrow \ell^\pm \tilde{\chi}_1^0$. Here, the results exclude gluinos with masses as large as 1.7 TeV, with an expected limit of 1.75 TeV for small $m(\tilde{\chi}_1^0)$. The results probe kinematic endpoints as small as $m_{\ell\ell}^{\text{max}} = m(\tilde{\chi}_2^0) - m(\tilde{\chi}_1^0) = 1/2(m(\tilde{g}) - m(\tilde{\chi}_1^0)) = 50$ GeV.

The $Z^{(*)}$ exclusion limits from the results in the edge SRs are compared with the same limits derived using the results in SRZ in Figure 15. In this model, pair-produced gluinos each decay as $\tilde{g} \rightarrow q\bar{q}\tilde{\chi}_2^0, \tilde{\chi}_2^0 \rightarrow$

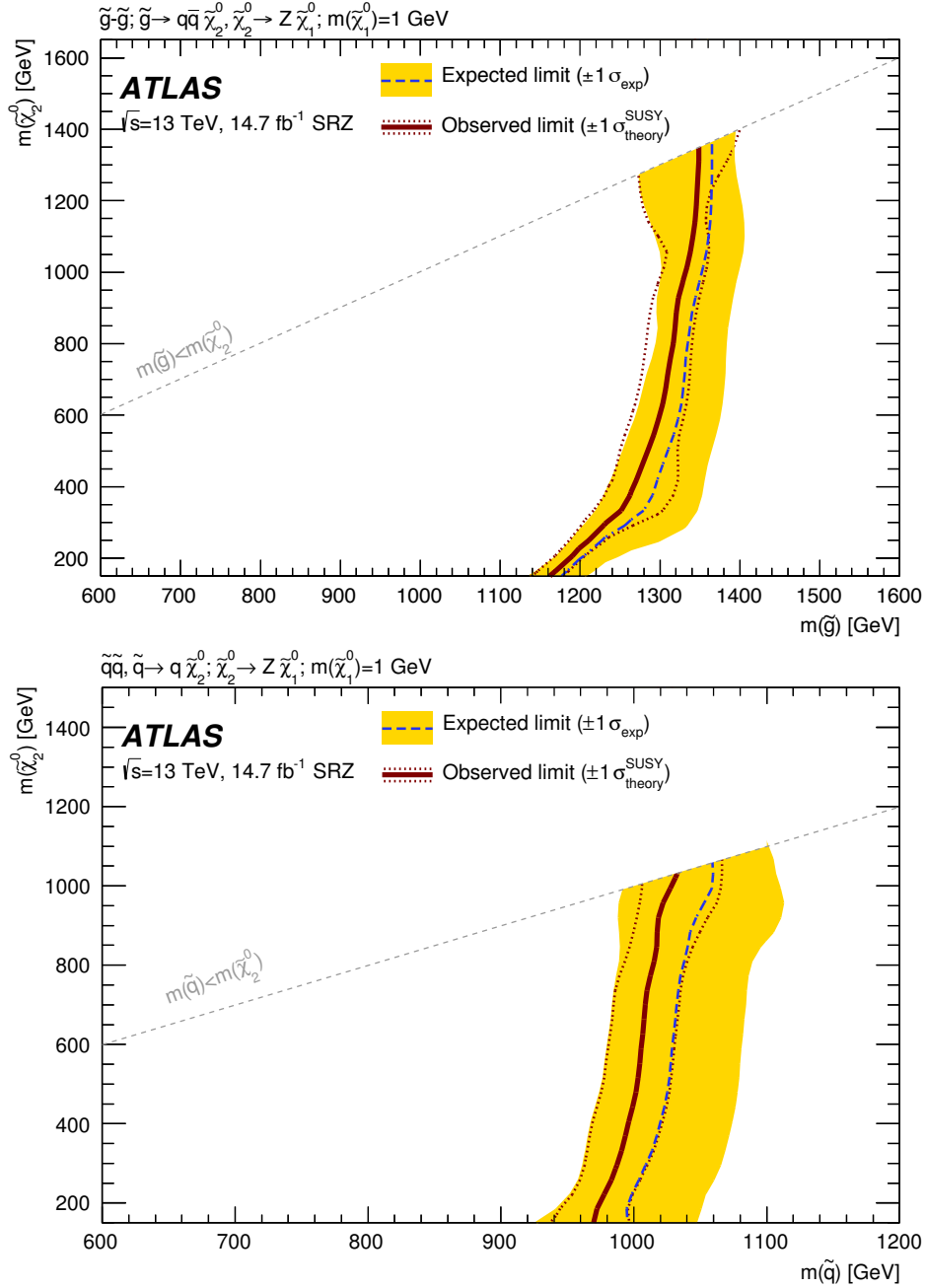


Figure 12: Expected and observed exclusion contours derived from the results in SRZ for the (top) $\tilde{g}\text{-}\tilde{\chi}_2^0$ on-shell grid and (bottom) $\tilde{q}\text{-}\tilde{\chi}_2^0$ on-shell grid. The dashed blue line indicates the expected limits at 95% CL and the yellow band shows the 1σ variation of the expected limit as a consequence of the uncertainties in the background prediction and the experimental uncertainties in the signal ($\pm 1\sigma_{\text{exp}}$). The observed limits are shown by the solid red line, with the dotted red lines indicating the variation resulting from changing the signal cross section within its uncertainty ($\pm 1\sigma_{\text{theory}}^{\text{SUSY}}$).

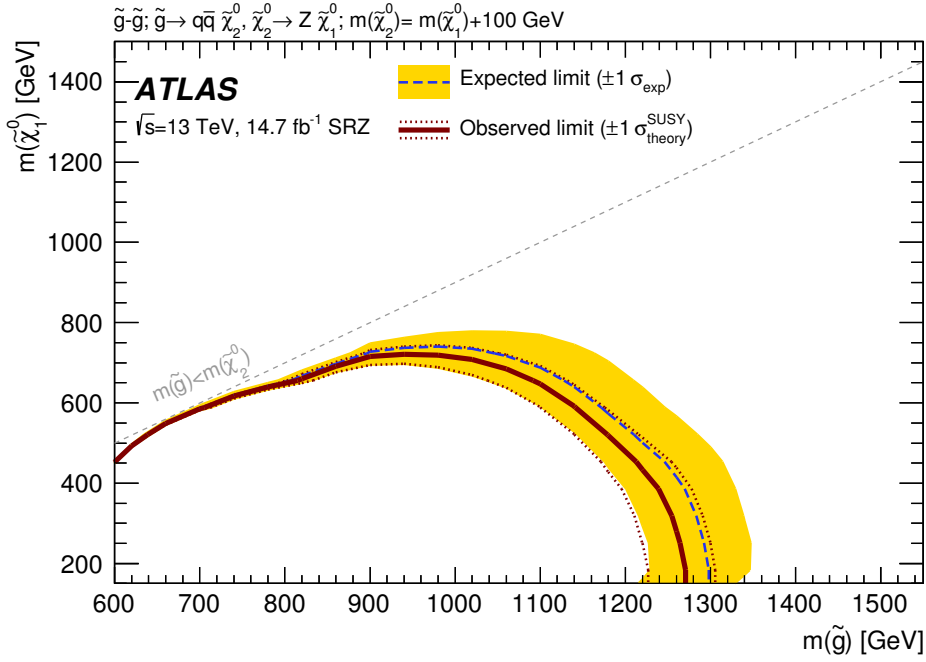


Figure 13: Expected and observed exclusion contours derived from the results in SRZ for the $\tilde{g}-\tilde{\chi}_1^0$ on-shell grid. The dashed blue line indicates the expected limits at 95% CL and the yellow band shows the 1σ variation of the expected limit as a consequence of the uncertainties in the background prediction and the experimental uncertainties in the signal ($\pm 1\sigma_{\text{exp}}$). The observed limits are shown by the solid red line, with the dotted red lines indicating the variation resulting from changing the signal cross section within its uncertainty ($\pm 1\sigma_{\text{theory}}^{\text{SUSY}}$).

$Z^{(*)}\tilde{\chi}_1^0$, and the mass splitting between the $\tilde{\chi}_2^0$ and the $\tilde{\chi}_1^0$ determines whether the Z boson is produced on-shell. Here the edge limits extend into the more compressed region, whereas the expected SRZ exclusion probes higher $\tilde{\chi}_1^0$ masses in the on-shell regime. At high gluino masses, the edge SRs provide stronger limits. For the $Z^{(*)}$ model, the expected and observed gluino mass limits are 1.4 TeV and 1.34 TeV (1.35 and 1.3 TeV for the on- Z signal region), respectively, for $\tilde{\chi}_1^0$ masses below 400 GeV. The sensitivity in the $Z^{(*)}$ model is smaller than that of the slepton model because the leptonic branching fraction of the Z boson suppresses the signal production rate.

Model-independent upper limits at 95% CL on the number of events that could be attributed to non-SM sources (S^{95}) for SRZ are derived using the CL_s prescription and neglecting possible signal contamination in the CRs. For these upper limits, pseudo-experiments are used rather than the asymptotic approximation. The expected and observed upper limits are given in Table 9. The same information is given for the 24 $m_{\ell\ell}$ ranges of the edge search in Table 11.

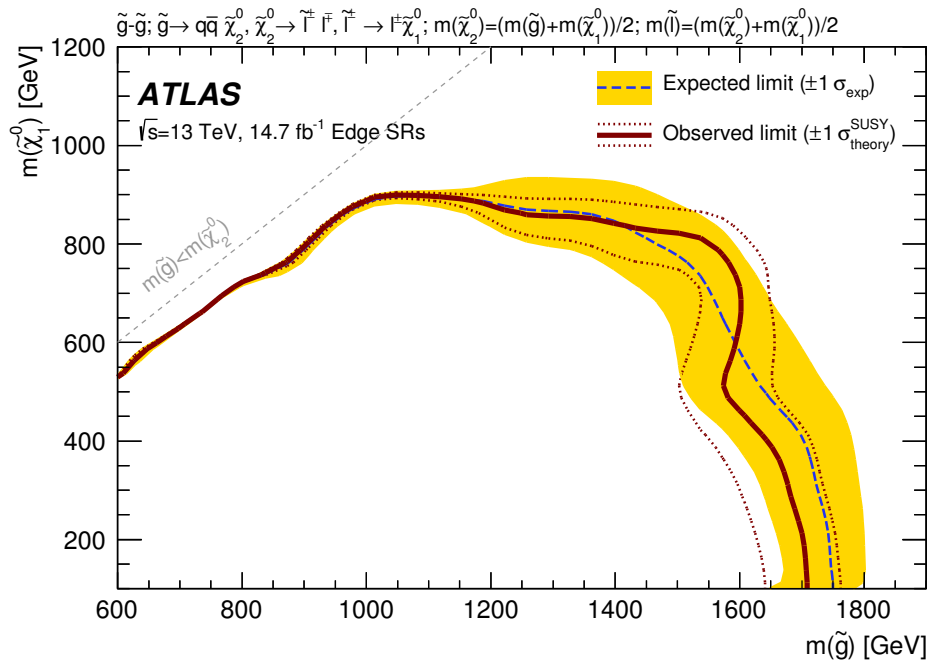


Figure 14: Expected and observed exclusion contours derived from the results in the edge search SRs for the slepton signal model. The dashed blue line indicates the expected limits at 95% CL and the yellow band shows the 1σ variation of the expected limit as a consequence of the uncertainties in the background prediction and the experimental uncertainties in the signal ($\pm 1\sigma_{\text{exp}}$). The observed limits are shown by the solid red lines, with the dotted red lines indicating the variation resulting from changing the signal cross section within its uncertainty ($\pm 1\sigma_{\text{theory}}^{\text{SUSY}}$).

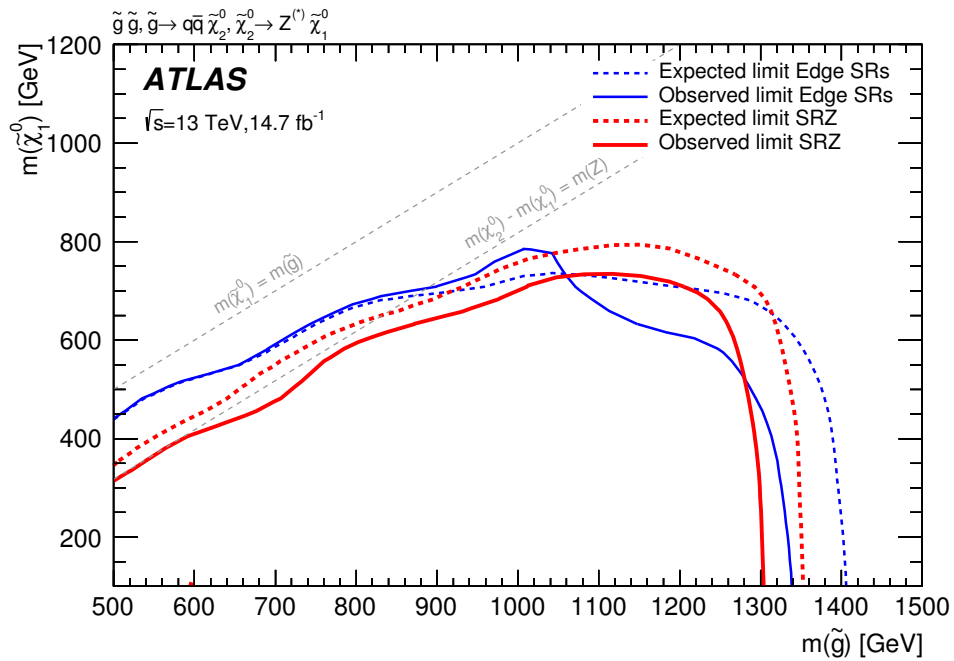


Figure 15: Expected and observed exclusion contours derived from the results in the edge search SRs and SRZ for the $Z^{(*)}$ model. The dashed and solid blue lines indicate the expected and observed limits at 95% CL from the results in the edge SRs, while the thick dashed and solid red lines indicate the expected and observed limits at 95% CL from the results in SRZ.

11 Conclusion

This paper presents two searches for new phenomena in final states containing a same-flavour opposite-sign lepton (electron or muon) pair, jets, and large missing transverse momentum using 14.7 fb^{-1} of ATLAS data collected during 2015 and 2016 at the LHC at $\sqrt{s} = 13 \text{ TeV}$. The first search (on-shell Z search) targets lepton pairs consistent with Z boson decay, while the second search (edge search) targets a kinematic endpoint feature in the dilepton mass distribution. For the edge search, a set of 24 mass ranges are considered, with different requirements on E_T^{miss} and H_T , and different kinematic endpoint values in the dilepton invariant-mass distribution. The data in both searches are found to be consistent with the Standard Model prediction. The results are interpreted in simplified models of gluino-pair production and squark-pair production, and exclude gluinos (squarks) with masses as large as 1.7 TeV (980 GeV).

Acknowledgements

We thank CERN for the very successful operation of the LHC, as well as the support staff from our institutions without whom ATLAS could not be operated efficiently.

We acknowledge the support of ANPCyT, Argentina; YerPhI, Armenia; ARC, Australia; BMWFW and FWF, Austria; ANAS, Azerbaijan; SSTC, Belarus; CNPq and FAPESP, Brazil; NSERC, NRC and CFI, Canada; CERN; CONICYT, Chile; CAS, MOST and NSFC, China; COLCIENCIAS, Colombia; MSMT CR, MPO CR and VSC CR, Czech Republic; DNRF and DNSRC, Denmark; IN2P3-CNRS, CEA-DSM/IRFU, France; GNSF, Georgia; BMBF, HGF, and MPG, Germany; GSRT, Greece; RGC, Hong Kong SAR, China; ISF, I-CORE and Benoziyo Center, Israel; INFN, Italy; MEXT and JSPS, Japan; CNRST, Morocco; FOM and NWO, Netherlands; RCN, Norway; MNiSW and NCN, Poland; FCT, Portugal; MNE/IFA, Romania; MES of Russia and NRC KI, Russian Federation; JINR; MESTD, Serbia; MSSR, Slovakia; ARRS and MIZŠ, Slovenia; DST/NRF, South Africa; MINECO, Spain; SRC and Wallenberg Foundation, Sweden; SERI, SNSF and Cantons of Bern and Geneva, Switzerland; MOST, Taiwan; TAEK, Turkey; STFC, United Kingdom; DOE and NSF, United States of America. In addition, individual groups and members have received support from BCKDF, the Canada Council, CANARIE, CRC, Compute Canada, FQRNT, and the Ontario Innovation Trust, Canada; EPLANET, ERC, ERDF, FP7, Horizon 2020 and Marie Skłodowska-Curie Actions, European Union; Investissements d’Avenir Labex and Idex, ANR, Région Auvergne and Fondation Partager le Savoir, France; DFG and AvH Foundation, Germany; Herakleitos, Thales and Aristeia programmes co-financed by EU-ESF and the Greek NSRF; BSF, GIF and Minerva, Israel; BRF, Norway; CERCA Programme Generalitat de Catalunya, Generalitat Valenciana, Spain; the Royal Society and Leverhulme Trust, United Kingdom.

The crucial computing support from all WLCG partners is acknowledged gratefully, in particular from CERN, the ATLAS Tier-1 facilities at TRIUMF (Canada), NDGF (Denmark, Norway, Sweden), CC-IN2P3 (France), KIT/GridKA (Germany), INFN-CNAF (Italy), NL-T1 (Netherlands), PIC (Spain), ASGC (Taiwan), RAL (UK) and BNL (USA), the Tier-2 facilities worldwide and large non-WLCG resource providers. Major contributors of computing resources are listed in Ref. [98].

References

- [1] Yu. A. Golfand and E. P. Likhtman, *Extension of the Algebra of Poincare Group Generators and Violation of p Invariance*, JETP Lett. **13** (1971) 323, [Pisma Zh. Eksp. Teor. Fiz. 13 (1971) 452].
- [2] D. V. Volkov and V. P. Akulov, *Is the Neutrino a Goldstone Particle?*, Phys. Lett. B **46** (1973) 109.
- [3] J. Wess and B. Zumino, *Supergauge Transformations in Four-Dimensions*, Nucl. Phys. B **70** (1974) 39.
- [4] J. Wess and B. Zumino, *Supergauge Invariant Extension of Quantum Electrodynamics*, Nucl. Phys. B **78** (1974) 1.
- [5] S. Ferrara and B. Zumino, *Supergauge Invariant Yang-Mills Theories*, Nucl. Phys. B **79** (1974) 413.
- [6] A. Salam and J. A. Strathdee, *Supersymmetry and Nonabelian Gauges*, Phys. Lett. B **51** (1974) 353.
- [7] N. Sakai, *Naturalness in Supersymmetric GUTS*, Z. Phys. C **11** (1981) 153.
- [8] S. Dimopoulos, S. Raby and F. Wilczek, *Supersymmetry and the Scale of Unification*, Phys. Rev. D **24** (1981) 1681.
- [9] L. E. Ibanez and G. G. Ross, *Low-Energy Predictions in Supersymmetric Grand Unified Theories*, Phys. Lett. B **105** (1981) 439.
- [10] S. Dimopoulos and H. Georgi, *Softly Broken Supersymmetry and $SU(5)$* , Nucl. Phys. B **193** (1981) 150.
- [11] G. R. Farrar and P. Fayet, *Phenomenology of the Production, Decay, and Detection of New Hadronic States Associated with Supersymmetry*, Phys. Lett. B **76** (1978) 575.
- [12] H. Goldberg, *Constraint on the Photino Mass from Cosmology*, Phys. Rev. Lett. **50** (1983) 1419, [Erratum: Phys. Rev. Lett. 103 (2009) 099905].
- [13] J. R. Ellis et al., *Supersymmetric Relics from the Big Bang*, Nucl. Phys. B **238** (1984) 453.
- [14] M. Dine and W. Fischler, *A Phenomenological Model of Particle Physics Based on Supersymmetry*, Phys. Lett. B **110** (1982) 227.
- [15] L. Alvarez-Gaume, M. Claudson and M. B. Wise, *Low-Energy Supersymmetry*, Nucl. Phys. B **207** (1982) 96.
- [16] C. R. Nappi and B. A. Ovrut, *Supersymmetric Extension of the $SU(3) \times SU(2) \times U(1)$ Model*, Phys. Lett. B **113** (1982) 175.
- [17] CMS Collaboration, *Search for physics beyond the standard model in events with a Z boson, jets, and missing transverse energy in pp collisions at $\sqrt{s} = 7$ TeV*, Phys. Lett. B **716** (2012) 260, arXiv: 1204.3774 [hep-ex].
- [18] CMS Collaboration, *Search for physics beyond the standard model in events with two leptons, jets, and missing transverse momentum in pp collisions at $\sqrt{s} = 8$ TeV*, JHEP **04** (2015) 124, arXiv: 1502.06031 [hep-ex].

- [19] ATLAS Collaboration, *Search for supersymmetry in events containing a same-flavour opposite-sign dilepton pair, jets, and large missing transverse momentum in $\sqrt{s} = 8$ TeV pp collisions with the ATLAS detector*, *Eur. Phys. J. C* **75** (2015) 318, arXiv: [1503.03290 \[hep-ex\]](#).
- [20] CMS Collaboration, *Search for new physics in final states with two opposite-sign same-flavor leptons, jets and missing transverse momentum in pp collisions at $\sqrt{s} = 13$ TeV*, (2016), arXiv: [1607.00915 \[hep-ex\]](#).
- [21] CMS Collaboration, *Search for new physics in events with opposite-sign leptons, jets, and missing transverse energy in pp collisions at $\sqrt{s} = 7$ TeV*, *Phys. Lett. B* **718** (2013) 815, arXiv: [1206.3949 \[hep-ex\]](#).
- [22] ATLAS Collaboration, *The ATLAS Experiment at the CERN Large Hadron Collider*, *JINST* **3** (2008) S08003.
- [23] ATLAS Collaboration, *Early Inner Detector Tracking Performance in the 2015 Data at $\sqrt{s} = 13$ TeV*, ATL-PHYS-PUB-2015-051, 2015, URL: <http://cds.cern.ch/record/2110140>.
- [24] P. Fayet, *Supersymmetry and Weak, Electromagnetic and Strong Interactions*, *Phys. Lett. B* **64** (1976) 159.
- [25] P. Fayet, *Spontaneously Broken Supersymmetric Theories of Weak, Electromagnetic and Strong Interactions*, *Phys. Lett. B* **69** (1977) 489.
- [26] M. Cahill-Rowley et al., *ATLAS Z + missing transverse energy excess in the MSSM*, *Phys. Rev. D* **92** (2015) 075029, arXiv: [1506.05799 \[hep-ph\]](#).
- [27] ATLAS Collaboration, *Search for direct top squark pair production in events with a Z boson, b-jets and missing transverse momentum in $\sqrt{s} = 8$ TeV pp collisions with the ATLAS detector*, *Eur. Phys. J. C* **74** (2014) 2883, arXiv: [1403.5222 \[hep-ex\]](#).
- [28] ATLAS Collaboration, *Search for direct top-squark pair production in final states with two leptons in pp collisions at $\sqrt{s} = 8$ TeV with the ATLAS detector*, *JHEP* **06** (2014) 124, arXiv: [1403.4853 \[hep-ex\]](#).
- [29] D. Alves, E. Izaguirre and J. Wacker, *Where the Sidewalk Ends: Jets and Missing Energy Search Strategies for the 7 TeV LHC*, (2011), arXiv: [1102.5338 \[hep-ph\]](#).
- [30] ATLAS Collaboration, *Improved luminosity determination in pp collisions at $\sqrt{s} = 7$ TeV using the ATLAS detector at the LHC*, *Eur. Phys. J. C* **73** (2013) 2518, arXiv: [1302.4393 \[hep-ex\]](#).
- [31] ATLAS Collaboration, *Luminosity determination in pp collisions at $\sqrt{s} = 8$ TeV using the ATLAS detector at the LHC*, *Eur. Phys. J. C* (2016), arXiv: [1608.03953 \[hep-ex\]](#).
- [32] ATLAS Collaboration, *2015 start-up trigger menu and initial performance assessment of the ATLAS trigger using Run-2 data*, ATL-DAQ-PUB-2016-001, 2016, URL: <http://cds.cern.ch/record/2136007>.
- [33] J. Alwall et al., *The automated computation of tree-level and next-to-leading order differential cross sections, and their matching to parton shower simulations*, *JHEP* **07** (2014) 079, arXiv: [1405.0301 \[hep-ph\]](#).

- [34] T. Sjöstrand, S. Mrenna and P. Skands, *A Brief Introduction to PYTHIA 8.1*, *Comput. Phys. Commun.* **178** (2008) 852, arXiv: [0710.3820 \[hep-ph\]](#).
- [35] ATLAS Collaboration, *ATLAS Pythia 8 tunes to 7 TeV data*, ATL-PHYS-PUB-2014-021, 2014, URL: <http://cdsweb.cern.ch/record/1966419>.
- [36] R. D. Ball et al., *Parton distributions with LHC data*, *Nucl. Phys. B* **867** (2013) 244, arXiv: [1207.1303 \[hep-ph\]](#).
- [37] P. Nason, *A new method for combining NLO QCD with shower Monte Carlo algorithms*, *JHEP* **11** (2004) 040, arXiv: [hep-ph/0409146 \[hep-ph\]](#).
- [38] S. Frixione, P. Nason and C. Oleari, *Matching NLO QCD computations with parton shower simulations: the POWHEG method*, *JHEP* **11** (2007) 070, arXiv: [0709.2092 \[hep-ph\]](#).
- [39] S. Alioli et al., *A general framework for implementing NLO calculations in shower Monte Carlo programs: the POWHEG BOX*, *JHEP* **06** (2010) 043, arXiv: [1002.2581 \[hep-ph\]](#).
- [40] T. Sjöstrand, S. Mrenna and P. Skands, *PYTHIA 6.4 Physics and Manual*, *JHEP* **05** (2006) 026, arXiv: [hep-ph/0603175 \[hep-ph\]](#).
- [41] B. Cooper et al., *Monte Carlo tuning in the presence of Matching*, *Eur. Phys. J. C* **72** (2011) 2078, arXiv: [1109.5295 \[hep-ph\]](#).
- [42] D. J. Lange, *The EvtGen particle decay simulation package*, *Nucl. Instrum. Meth. A* **462** (2001) 152.
- [43] T. Gleisberg et al., *Event generation with Sherpa 1.1*, *JHEP* **02** (2009) 007, arXiv: [0811.4622 \[hep-ph\]](#).
- [44] S. Schumann and F. Krauss, *A Parton shower algorithm based on Catani-Seymour dipole factorisation*, *JHEP* **03** (2008) 038, arXiv: [0709.1027 \[hep-ph\]](#).
- [45] T. Gleisberg and S. Höche, *Comix, a new matrix element generator*, *JHEP* **12** (2008) 039, arXiv: [0808.3674 \[hep-ph\]](#).
- [46] F. Cascioli, P. Maierhofer and S. Pozzorini, *Scattering Amplitudes with Open Loops*, *Phys. Rev. Lett.* **108** (2012) 111601, arXiv: [1111.5206 \[hep-ph\]](#).
- [47] S. Höche et al., *QCD matrix elements + parton showers: The NLO case*, *JHEP* **04** (2013) 027, arXiv: [1207.5030 \[hep-ph\]](#).
- [48] S. Catani et al., *QCD Matrix Elements + Parton Showers*, *JHEP* **11** (2001) 063, arXiv: [hep-ph/0109231](#).
- [49] L. Lönnblad, *Correcting the Colour-Dipole Cascade Model with Fixed Order Matrix Elements*, *JHEP* **05** (2002) 046, arXiv: [hep-ph/0112284](#).
- [50] W. Beenakker et al., *Squark and gluino production at hadron colliders*, *Nucl. Phys. B* **492** (1997) 51, arXiv: [hep-ph/9610490 \[hep-ph\]](#).
- [51] A. Kulesza and L. Motyka, *Threshold resummation for squark-antisquark and gluino-pair production at the LHC*, *Phys. Rev. Lett.* **102** (2009) 111802, arXiv: [0807.2405 \[hep-ph\]](#).
- [52] A. Kulesza and L. Motyka, *Soft gluon resummation for the production of gluino-gluino and squark-antisquark pairs at the LHC*, *Phys. Rev. D* **80** (2009) 095004, arXiv: [0905.4749 \[hep-ph\]](#).

- [53] W. Beenakker et al., *Soft-gluon resummation for squark and gluino hadroproduction*, *JHEP* **12** (2009) 041, arXiv: [0909.4418 \[hep-ph\]](#).
- [54] W. Beenakker et al., *Squark and gluino hadroproduction*, *Int. J. Mod. Phys. A* **26** (2011) 2637, arXiv: [1105.1110 \[hep-ph\]](#).
- [55] ATLAS Collaboration, *The ATLAS Simulation Infrastructure*, *Eur. Phys. J. C* **70** (2010) 823, arXiv: [1005.4568 \[physics.ins-det\]](#).
- [56] S. Agostinelli et al., *GEANT4: A simulation toolkit*, *Nucl. Instrum. Meth. A* **506** (2003) 250.
- [57] ATLAS Collaboration, *Summary of ATLAS Pythia 8 tunes*, ATL-PHYS-PUB-2012-003, 2012, URL: <http://cds.cern.ch/record/1474107>.
- [58] G. Watt and R. S. Thorne, *Study of Monte Carlo approach to experimental uncertainty propagation with MSTW 2008 PDFs*, *JHEP* **08** (2012) 052, arXiv: [1205.4024 \[hep-ph\]](#).
- [59] ATLAS Collaboration, *Modelling of the $t\bar{t}H$ and $t\bar{t}V$ ($V = W, Z$) processes for $\sqrt{s} = 13$ TeV ATLAS analyses*, ATL-PHYS-PUB-2016-005, 2016, URL: <http://cds.cern.ch/record/2120826>.
- [60] M. V. Garzelli et al., *$t\bar{t}W^{+-}$ and $t\bar{t}Z$ Hadroproduction at NLO accuracy in QCD with Parton Shower and Hadronization effects*, *JHEP* **11** (2012) 056, arXiv: [1208.2665 \[hep-ph\]](#).
- [61] J. M. Campbell and R. K. Ellis, *$t\bar{t}W$ production and decay at NLO*, *JHEP* **07** (2012) 052, arXiv: [1204.5678 \[hep-ph\]](#).
- [62] A. Lazopoulos et al., *Next-to-leading order QCD corrections to $t\bar{t}Z$ production at the LHC*, *Phys. Lett. B* **666** (2008) 62, arXiv: [0804.2220 \[hep-ph\]](#).
- [63] ATLAS Collaboration, *Simulation of top quark production for the ATLAS experiment at $\sqrt{s} = 13$ TeV*, ATL-PHYS-PUB-2016-004, 2016, URL: <http://cds.cern.ch/record/2120417>.
- [64] M. Czakon, P. Fiedler and A. Mitov, *Total Top-Quark Pair-Production Cross Section at Hadron Colliders Through $O(\alpha_s^4)$* , *Phys. Rev. Lett.* **110** (2013) 252004, arXiv: [1303.6254 \[hep-ph\]](#).
- [65] M. Czakon and A. Mitov, *Top++: A Program for the Calculation of the Top-Pair Cross-Section at Hadron Colliders*, *Comput. Phys. Commun.* **185** (2014) 2930, arXiv: [1112.5675 \[hep-ph\]](#).
- [66] N. Kidonakis, *Two-loop soft anomalous dimensions for single top quark associated production with a W^- or H^-* , *Phys. Rev. D* **82** (2010) 054018, arXiv: [1005.4451 \[hep-ph\]](#).
- [67] ATLAS Collaboration, *Multi-Boson Simulation for 13 TeV ATLAS Analyses*, ATL-PHYS-PUB-2016-002, 2016, URL: <http://cds.cern.ch/record/2119986>.
- [68] J. M. Campbell and R. K. Ellis, *An update on vector boson pair production at hadron colliders*, *Phys. Rev. D* **60** (1999) 113006, arXiv: [hep-ph/9905386 \[hep-ph\]](#).
- [69] J. M. Campbell, R. K. Ellis and C. Williams, *Vector boson pair production at the LHC*, *JHEP* **07** (2011) 018, arXiv: [1105.0020 \[hep-ph\]](#).
- [70] ATLAS Collaboration, *Monte Carlo Generators for the Production of a W or Z/γ^* Boson in Association with Jets at ATLAS in Run 2*, ATL-PHYS-PUB-2016-003, 2016, URL: <http://cds.cern.ch/record/2120133>.

- [71] S. Catani et al.,
Vector boson production at hadron colliders: a fully exclusive QCD calculation at NNLO,
Phys. Rev. Lett. **103** (2009) 082001, arXiv: [0903.2120 \[hep-ph\]](#).
- [72] S. Catani and M. Grazzini, *An NNLO subtraction formalism in hadron collisions and its application to Higgs boson production at the LHC*, Phys. Rev. Lett. **98** (2007) 222002,
arXiv: [hep-ph/0703012 \[hep-ph\]](#).
- [73] ATLAS Collaboration,
Vertex Reconstruction Performance of the ATLAS Detector at $\sqrt{s} = 13$ TeV,
ATL-PHYS-PUB-2015-026, 2015, URL: <http://cds.cern.ch/record/2037717>.
- [74] ATLAS Collaboration, *Electron efficiency measurements with the ATLAS detector using the 2012 LHC proton–proton collision data*, ATLAS-CONF-2014-032, 2014,
URL: <https://cds.cern.ch/record/1706245>.
- [75] ATLAS Collaboration, *Muon reconstruction performance of the ATLAS detector in proton–proton collision data at $\sqrt{s} = 13$ TeV*, Eur. Phys. J. C **76** (2016) 292, arXiv: [1603.05598 \[hep-ex\]](#).
- [76] ATLAS Collaboration,
Topological cell clustering in the ATLAS calorimeters and its performance in LHC Run 1, (2016),
arXiv: [1603.02934 \[hep-ex\]](#).
- [77] M. Cacciari, G. P. Salam and G. Soyez, *The anti- k_t jet clustering algorithm*, JHEP **04** (2008) 063,
arXiv: [0802.1189 \[hep-ph\]](#).
- [78] M. Cacciari and G. P. Salam, *Dispelling the N^3 myth for the K_t jet-finder*,
Phys. Lett. B **641** (2006) 57, arXiv: [hep-ph/0512210](#).
- [79] ATLAS Collaboration, *Jet energy measurement and its systematic uncertainty in proton–proton collisions at $\sqrt{s} = 7$ TeV with the ATLAS detector*, Eur. Phys. J. C **75** (2015) 17,
arXiv: [1406.0076 \[hep-ex\]](#).
- [80] ATLAS Collaboration, *Jet Calibration and Systematic Uncertainties for Jets Reconstructed in the ATLAS Detector at $\sqrt{s} = 13$ TeV*, ATL-PHYS-PUB-2015-015, 2015,
URL: <http://cds.cern.ch/record/2037613>.
- [81] ATLAS Collaboration, *Tagging and suppression of pileup jets with the ATLAS detector*,
ATLAS-CONF-2014-018, 2014, URL: <http://cds.cern.ch/record/1700870>.
- [82] ATLAS Collaboration, *Characterisation and mitigation of beam-induced backgrounds observed in the ATLAS detector during the 2011 proton-proton run*, JINST **8** (2013) P07004,
arXiv: [1303.0223 \[hep-ex\]](#).
- [83] ATLAS Collaboration,
Selection of jets produced in 13TeV proton-proton collisions with the ATLAS detector,
ATLAS-CONF-2015-029, 2015, URL: <http://cds.cern.ch/record/2037702>.
- [84] ATLAS Collaboration, *Performance of b -Jet Identification in the ATLAS Experiment*,
JINST **11** (2016) P04008, arXiv: [1512.01094 \[hep-ex\]](#).
- [85] ATLAS Collaboration, *Optimisation of the ATLAS b -tagging performance for the 2016 LHC Run*,
ATL-PHYS-PUB-2016-012, 2016, URL: <http://cds.cern.ch/record/2160731>.
- [86] ATLAS Collaboration,
Electron and photon energy calibration with the ATLAS detector using LHC Run 1 data,
Eur. Phys. J. C **74** (2014) 3071, arXiv: [1407.5063 \[hep-ex\]](#).

- [87] ATLAS Collaboration, *Expected performance of missing transverse momentum reconstruction for the ATLAS detector at $\sqrt{s} = 13$ TeV*, ATL-PHYS-PUB-2015-023, 2015, URL: <http://cds.cern.ch/record/2037700>.
- [88] ATLAS Collaboration, *Performance of missing transverse momentum reconstruction for the ATLAS detector in the first proton-proton collisions at $\sqrt{s} = 13$ TeV*, ATL-PHYS-PUB-2015-027, 2015, URL: <http://cds.cern.ch/record/2037904>.
- [89] G. Cowan et al., *Asymptotic formulae for likelihood-based tests of new physics*, *Eur. Phys. J. C* **71** (2011) 1554, arXiv: [1007.1727](https://arxiv.org/abs/1007.1727) [[physics.data-an](#)].
- [90] ATLAS Collaboration, *Measurement of the differential cross-section of highly boosted top quarks as a function of their transverse momentum in $\sqrt{s} = 8$ TeV proton-proton collisions using the ATLAS detector*, *Phys. Rev. D* **93** (2016) 032009, arXiv: [1510.03818](https://arxiv.org/abs/1510.03818) [[hep-ex](#)].
- [91] CMS Collaboration, *Measurement of the integrated and differential t - \bar{t} production cross sections for high- p_T top quarks in pp collisions at $\sqrt{s} = 8$ TeV*, *Phys. Rev. D* **94** (2016) 072002, arXiv: [1605.00116](https://arxiv.org/abs/1605.00116) [[hep-ex](#)].
- [92] M. Czakon, D. Heymes and A. Mitov, *Dynamical scales for multi-TeV top-pair production at the LHC*, (2016), arXiv: [1606.03350](https://arxiv.org/abs/1606.03350) [[hep-ph](#)].
- [93] ATLAS Collaboration, *Search for squarks and gluinos in events with isolated leptons, jets and missing transverse momentum at $\sqrt{s} = 8$ TeV with the ATLAS detector*, *JHEP* **04** (2015) 116, arXiv: [1501.03555](https://arxiv.org/abs/1501.03555) [[hep-ex](#)].
- [94] M. Krämer et al., *Supersymmetry production cross sections in pp collisions at $\sqrt{s} = 7$ TeV*, (2012), arXiv: [1206.2892](https://arxiv.org/abs/1206.2892) [[hep-ph](#)].
- [95] C. Borschensky et al., *Squark and gluino production cross sections in pp collisions at $\sqrt{s} = 13, 14, 33$ and 100 TeV*, *Eur. Phys. J. C* **74** (2014) 3174, arXiv: [1407.5066](https://arxiv.org/abs/1407.5066) [[hep-ph](#)].
- [96] M. Baak et al., *HistFitter software framework for statistical data analysis*, *Eur. Phys. J. C* **75** (2014) 153, arXiv: [1410.1280](https://arxiv.org/abs/1410.1280) [[hep-ex](#)].
- [97] A. Read, *Presentation of search results: the CLs technique*, *Journal of Physics G: Nucl. Part. Phys.* **28** (2002) 2693.
- [98] ATLAS Collaboration, *ATLAS Computing Acknowledgements 2016–2017*, ATL-GEN-PUB-2016-002, 2016, URL: <https://cds.cern.ch/record/2202407>.

The ATLAS Collaboration

M. Aaboud^{137d}, G. Aad⁸⁸, B. Abbott¹¹⁵, J. Abdallah⁸, O. Abidinov¹², B. Abeloos¹¹⁹, O.S. AbouZeid¹³⁹, N.L. Abraham¹⁵¹, H. Abramowicz¹⁵⁵, H. Abreu¹⁵⁴, R. Abreu¹¹⁸, Y. Abulaiti^{148a,148b}, B.S. Acharya^{167a,167b,a}, S. Adachi¹⁵⁷, L. Adamczyk^{41a}, D.L. Adams²⁷, J. Adelman¹¹⁰, T. Adye¹³³, A.A. Affolder¹³⁹, T. Agatonovic-Jovin¹⁴, C. Agheorghiesei^{28b}, J.A. Aguilar-Saavedra^{128a,128f}, S.P. Ahlen²⁴, F. Ahmadov^{68,b}, G. Aielli^{135a,135b}, H. Akerstedt^{148a,148b}, T.P.A. Åkesson⁸⁴, A.V. Akimov⁹⁸, G.L. Alberghi^{22a,22b}, J. Albert¹⁷², M.J. Alconada Verzini⁷⁴, M. Aleksa³², I.N. Aleksandrov⁶⁸, C. Alexa^{28b}, G. Alexander¹⁵⁵, T. Alexopoulos¹⁰, M. Alhroob¹¹⁵, B. Ali¹³⁰, M. Aliev^{76a,76b}, G. Alimonti^{94a}, J. Alison³³, S.P. Alkire³⁸, B.M.M. Allbrooke¹⁵¹, B.W. Allen¹¹⁸, P.P. Allport¹⁹, A. Aloisio^{106a,106b}, A. Alonso³⁹, F. Alonso⁷⁴, C. Alpigiani¹⁴⁰, A.A. Alshehri⁵⁶, M. Alstaty⁸⁸, B. Alvarez Gonzalez³², D. Álvarez Piqueras¹⁷⁰, M.G. Alviggi^{106a,106b}, B.T. Amadio¹⁶, Y. Amaral Coutinho^{26a}, C. Amelung²⁵, D. Amidei⁹², S.P. Amor Dos Santos^{128a,128c}, A. Amorim^{128a,128b}, S. Amoroso³², G. Amundsen²⁵, C. Anastopoulos¹⁴¹, L.S. Ancu⁵², N. Andari¹⁹, T. Andeen¹¹, C.F. Anders^{60b}, J.K. Anders⁷⁷, K.J. Anderson³³, A. Andreazza^{94a,94b}, V. Andrei^{60a}, S. Angelidakis⁹, I. Angelozzi¹⁰⁹, A. Angerami³⁸, F. Anghinolfi³², A.V. Anisenkov^{111,c}, N. Anjos¹³, A. Annovi^{126a,126b}, C. Antel^{60a}, M. Antonelli⁵⁰, A. Antonov^{100,*}, D.J. Antrim¹⁶⁶, F. Anulli^{134a}, M. Aoki⁶⁹, L. Aperio Bella¹⁹, G. Arabidze⁹³, Y. Arai⁶⁹, J.P. Araque^{128a}, V. Araujo Ferraz^{26a}, A.T.H. Arce⁴⁸, F.A. Arduh⁷⁴, J-F. Arguin⁹⁷, S. Argyropoulos⁶⁶, M. Arik^{20a}, A.J. Armbruster¹⁴⁵, L.J. Armitage⁷⁹, O. Arnaez³², H. Arnold⁵¹, M. Arratia³⁰, O. Arslan²³, A. Artamonov⁹⁹, G. Artoni¹²², S. Artz⁸⁶, S. Asai¹⁵⁷, N. Asbah⁴⁵, A. Ashkenazi¹⁵⁵, B. Åsman^{148a,148b}, L. Asquith¹⁵¹, K. Assamagan²⁷, R. Astalos^{146a}, M. Atkinson¹⁶⁹, N.B. Atlay¹⁴³, K. Augsten¹³⁰, G. Avolio³², B. Axen¹⁶, M.K. Ayoub¹¹⁹, G. Azuelos^{97,d}, M.A. Baak³², A.E. Baas^{60a}, M.J. Baca¹⁹, H. Bachacou¹³⁸, K. Bachas^{76a,76b}, M. Backes¹²², M. Backhaus³², P. Bagiacchi^{134a,134b}, P. Bagnaia^{134a,134b}, Y. Bai^{35a}, J.T. Baines¹³³, M. Bajic³⁹, O.K. Baker¹⁷⁹, E.M. Baldin^{111,c}, P. Balek¹⁷⁵, T. Balestri¹⁵⁰, F. Balli¹³⁸, W.K. Balunas¹²⁴, E. Banas⁴², Sw. Banerjee^{176,e}, A.A.E. Bannoura¹⁷⁸, L. Barak³², E.L. Barberio⁹¹, D. Barberis^{53a,53b}, M. Barbero⁸⁸, T. Barillari¹⁰³, M-S Barisits³², T. Barklow¹⁴⁵, N. Barlow³⁰, S.L. Barnes⁸⁷, B.M. Barnett¹³³, R.M. Barnett¹⁶, Z. Barnovska-Blenessy^{36a}, A. Baroncelli^{136a}, G. Barone²⁵, A.J. Barr¹²², L. Barranco Navarro¹⁷⁰, F. Barreiro⁸⁵, J. Barreiro Guimarães da Costa^{35a}, R. Bartoldus¹⁴⁵, A.E. Barton⁷⁵, P. Bartos^{146a}, A. Basalae¹²⁵, A. Bassalat^{119,f}, R.L. Bates⁵⁶, S.J. Batista¹⁶¹, J.R. Batley³⁰, M. Battaglia¹³⁹, M. Bauce^{134a,134b}, F. Bauer¹³⁸, H.S. Bawa^{145,g}, J.B. Beacham¹¹³, M.D. Beattie⁷⁵, T. Beau⁸³, P.H. Beauchemin¹⁶⁵, P. Bechtel²³, H.P. Beck^{18,h}, K. Becker¹²², M. Becker⁸⁶, M. Beckingham¹⁷³, C. Becot¹¹², A.J. Beddall^{20e}, A. Beddall^{20b}, V.A. Bednyakov⁶⁸, M. Bedognetti¹⁰⁹, C.P. Bee¹⁵⁰, L.J. Beemster¹⁰⁹, T.A. Beermann³², M. Begel²⁷, J.K. Behr⁴⁵, A.S. Bell⁸¹, G. Bella¹⁵⁵, L. Bellagamba^{22a}, A. Bellerive³¹, M. Bellomo⁸⁹, K. Belotskiy¹⁰⁰, O. Beltramello³², N.L. Belyaev¹⁰⁰, O. Benary^{155,*}, D. Benckekroun^{137a}, M. Bender¹⁰², K. Bendtz^{148a,148b}, N. Benekos¹⁰, Y. Benhammou¹⁵⁵, E. Benhar Nocchioli¹⁷⁹, J. Benitez⁶⁶, D.P. Benjamin⁴⁸, J.R. Bensinger²⁵, S. Bentvelsen¹⁰⁹, L. Beresford¹²², M. Beretta⁵⁰, D. Berge¹⁰⁹, E. Bergeaas Kuutmann¹⁶⁸, N. Berger⁵, J. Beringer¹⁶, S. Berlendis⁵⁸, N.R. Bernard⁸⁹, C. Bernius¹¹², F.U. Bernlochner²³, T. Berry⁸⁰, P. Berta¹³¹, C. Bertella⁸⁶, G. Bertoli^{148a,148b}, F. Bertolucci^{126a,126b}, I.A. Bertram⁷⁵, C. Bertsche⁴⁵, D. Bertsche¹¹⁵, G.J. Besjes³⁹, O. Bessidskaia Bylund^{148a,148b}, M. Bessner⁴⁵, N. Besson¹³⁸, C. Betancourt⁵¹, A. Bethani⁵⁸, S. Bethke¹⁰³, A.J. Bevan⁷⁹, R.M. Bianchi¹²⁷, M. Bianco³², O. Biebel¹⁰², D. Biedermann¹⁷, R. Bielski⁸⁷, N.V. Biesuz^{126a,126b}, M. Biglietti^{136a}, J. Bilbao De Mendizabal⁵², T.R.V. Billoud⁹⁷, H. Bilokon⁵⁰, M. Bindi⁵⁷, A. Bingul^{20b}, C. Bini^{134a,134b}, S. Biondi^{22a,22b}, T. Bisanz⁵⁷, D.M. Bjergaard⁴⁸, C.W. Black¹⁵², J.E. Black¹⁴⁵, K.M. Black²⁴, D. Blackburn¹⁴⁰, R.E. Blair⁶, T. Blazek^{146a}, I. Bloch⁴⁵, C. Blocker²⁵, A. Blue⁵⁶, W. Blum^{86,*}, U. Blumenschein⁵⁷, S. Blunier^{34a}, G.J. Bobbink¹⁰⁹,

V.S. Bobrovnikov^{111,c}, S.S. Bocchetta⁸⁴, A. Bocci⁴⁸, C. Bock¹⁰², M. Boehler⁵¹, D. Boerner¹⁷⁸, J.A. Bogaerts³², D. Bogavac¹⁰², A.G. Bogdanchikov¹¹¹, C. Bohm^{148a}, V. Boisvert⁸⁰, P. Bokan¹⁴, T. Bold^{41a}, A.S. Boldyrev¹⁰¹, M. Bomben⁸³, M. Bona⁷⁹, M. Boonekamp¹³⁸, A. Borisov¹³², G. Borissov⁷⁵, J. Bortfeldt³², D. Bortoletto¹²², V. Bortolotto^{62a,62b,62c}, K. Bos¹⁰⁹, D. Boscherini^{22a}, M. Bosman¹³, J.D. Bossio Sola²⁹, J. Boudreau¹²⁷, J. Bouffard², E.V. Bouhova-Thacker⁷⁵, D. Boumediene³⁷, C. Bourdarios¹¹⁹, S.K. Boutle⁵⁶, A. Boveia¹¹³, J. Boyd³², I.R. Boyko⁶⁸, J. Bracinik¹⁹, A. Brandt⁸, G. Brandt⁵⁷, O. Brandt^{60a}, U. Bratzler¹⁵⁸, B. Brau⁸⁹, J.E. Brau¹¹⁸, W.D. Breaden Madden⁵⁶, K. Brendlinger¹²⁴, A.J. Brennan⁹¹, L. Brenner¹⁰⁹, R. Brenner¹⁶⁸, S. Bressler¹⁷⁵, T.M. Bristow⁴⁹, D. Britton⁵⁶, D. Britzger⁴⁵, F.M. Brochu³⁰, I. Brock²³, R. Brock⁹³, G. Brooijmans³⁸, T. Brooks⁸⁰, W.K. Brooks^{34b}, J. Brosamer¹⁶, E. Brost¹¹⁰, J.H. Broughton¹⁹, P.A. Bruckman de Renstrom⁴², D. Bruncko^{146b}, A. Bruni^{22a}, G. Bruni^{22a}, L.S. Bruni¹⁰⁹, B.H. Brunt³⁰, M. Bruschi^{22a}, N. Bruscino²³, P. Bryant³³, L. Bryngemark⁸⁴, T. Buanes¹⁵, Q. Buat¹⁴⁴, P. Buchholz¹⁴³, A.G. Buckley⁵⁶, I.A. Budagov⁶⁸, F. Buehrer⁵¹, M.K. Bugge¹²¹, O. Bulekov¹⁰⁰, D. Bullock⁸, H. Burckhart³², S. Burdin⁷⁷, C.D. Burgard⁵¹, A.M. Burger⁵, B. Burghgrave¹¹⁰, K. Burka⁴², S. Burke¹³³, I. Burmeister⁴⁶, J.T.P. Burr¹²², E. Busato³⁷, D. Büscher⁵¹, V. Büscher⁸⁶, P. Bussey⁵⁶, J.M. Butler²⁴, C.M. Buttar⁵⁶, J.M. Butterworth⁸¹, P. Butti¹⁰⁹, W. Buttinger²⁷, A. Buzatu^{35c}, A.R. Buzykaev^{111,c}, S. Cabrera Urbán¹⁷⁰, D. Caforio¹³⁰, V.M. Cairo^{40a,40b}, O. Cakir^{4a}, N. Calace⁵², P. Calafiura¹⁶, A. Calandri⁸⁸, G. Calderini⁸³, P. Calfayan⁶⁴, G. Callea^{40a,40b}, L.P. Caloba^{26a}, S. Calvente Lopez⁸⁵, D. Calvet³⁷, S. Calvet³⁷, T.P. Calvet⁸⁸, R. Camacho Toro³³, S. Camarda³², P. Camarri^{135a,135b}, D. Cameron¹²¹, R. Caminal Armadans¹⁶⁹, C. Camincher⁵⁸, S. Campana³², M. Campanelli⁸¹, A. Camplani^{94a,94b}, A. Campoverde¹⁴³, V. Canale^{106a,106b}, A. Canepa^{163a}, M. Cano Bret^{36c}, J. Cantero¹¹⁶, T. Cao¹⁵⁵, M.D.M. Capeans Garrido³², I. Caprini^{28b}, M. Caprini^{28b}, M. Capua^{40a,40b}, R.M. Carbone³⁸, R. Cardarelli^{135a}, F. Cardillo⁵¹, I. Carli¹³¹, T. Carli³², G. Carlino^{106a}, B.T. Carlson¹²⁷, L. Carminati^{94a,94b}, R.M.D. Carney^{148a,148b}, S. Caron¹⁰⁸, E. Carquin^{34b}, G.D. Carrillo-Montoya³², J.R. Carter³⁰, J. Carvalho^{128a,128c}, D. Casadei¹⁹, M.P. Casado^{13,i}, M. Casolino¹³, D.W. Casper¹⁶⁶, R. Castelijin¹⁰⁹, A. Castelli¹⁰⁹, V. Castillo Gimenez¹⁷⁰, N.F. Castro^{128a,j}, A. Catinaccio³², J.R. Catmore¹²¹, A. Cattai³², J. Caudron²³, V. Cavaliere¹⁶⁹, E. Cavallaro¹³, D. Cavalli^{94a}, M. Cavalli-Sforza¹³, V. Cavasinni^{126a,126b}, F. Ceradini^{136a,136b}, L. Cerda Alberich¹⁷⁰, A.S. Cerqueira^{26b}, A. Cerri¹⁵¹, L. Cerrito^{135a,135b}, F. Cerutti¹⁶, A. Cervelli¹⁸, S.A. Cetin^{20d}, A. Chafaq^{137a}, D. Chakraborty¹¹⁰, S.K. Chan⁵⁹, Y.L. Chan^{62a}, P. Chang¹⁶⁹, J.D. Chapman³⁰, D.G. Charlton¹⁹, A. Chatterjee⁵², C.C. Chau¹⁶¹, C.A. Chavez Barajas¹⁵¹, S. Che¹¹³, S. Cheatham^{167a,167c}, A. Chegwidan⁹³, S. Chekanov⁶, S.V. Chekulaev^{163a}, G.A. Chelkov^{68,k}, M.A. Chelstowska³², C. Chen⁶⁷, H. Chen²⁷, S. Chen^{35b}, S. Chen¹⁵⁷, X. Chen^{35c}, Y. Chen⁷⁰, H.C. Cheng⁹², H.J. Cheng^{35a}, Y. Cheng³³, A. Cheplakov⁶⁸, E. Cheremushkina¹³², R. Cherkaoui El Moursli^{137e}, V. Chernyatin^{27,*}, E. Cheu⁷, L. Chevalier¹³⁸, V. Chiarella⁵⁰, G. Chiarelli^{126a,126b}, G. Chiodini^{76a}, A.S. Chisholm³², A. Chitan^{28b}, Y.H. Chiu¹⁷², M.V. Chizhov⁶⁸, K. Choi⁶⁴, A.R. Chomont³⁷, S. Chouridou⁹, B.K.B. Chow¹⁰², V. Christodoulou⁸¹, D. Chromek-Burckhart³², J. Chudoba¹²⁹, A.J. Chuinard⁹⁰, J.J. Chwastowski⁴², L. Chytka¹¹⁷, A.K. Ciftci^{4a}, D. Cinca⁴⁶, V. Cindro⁷⁸, I.A. Cioara²³, C. Ciocca^{22a,22b}, A. Ciocio¹⁶, F. Ciotto^{106a,106b}, Z.H. Citron¹⁷⁵, M. Citterio^{94a}, M. Ciubancan^{28b}, A. Clark⁵², B.L. Clark⁵⁹, M.R. Clark³⁸, P.J. Clark⁴⁹, R.N. Clarke¹⁶, C. Clement^{148a,148b}, Y. Coadou⁸⁸, M. Cobal^{167a,167c}, A. Coccaro⁵², J. Cochran⁶⁷, L. Colasurdo¹⁰⁸, B. Cole³⁸, A.P. Colijn¹⁰⁹, J. Collot⁵⁸, T. Colombo¹⁶⁶, P. Conde Muiño^{128a,128b}, E. Coniavitis⁵¹, S.H. Connell^{147b}, I.A. Connelly⁸⁰, V. Consorti⁵¹, S. Constantinescu^{28b}, G. Conti³², F. Conventi^{106a,l}, M. Cooke¹⁶, B.D. Cooper⁸¹, A.M. Cooper-Sarkar¹²², F. Cormier¹⁷¹, K.J.R. Cormier¹⁶¹, T. Cornelissen¹⁷⁸, M. Corradi^{134a,134b}, F. Corriveau^{90,m}, A. Cortes-Gonzalez³², G. Cortiana¹⁰³, G. Costa^{94a}, M.J. Costa¹⁷⁰, D. Costanzo¹⁴¹, G. Cottin³⁰, G. Cowan⁸⁰, B.E. Cox⁸⁷, K. Cranmer¹¹², S.J. Crawley⁵⁶, G. Cree³¹, S. Crépe-Renaudin⁵⁸, F. Crescioli⁸³, W.A. Cribbs^{148a,148b}, M. Crispin Ortuzar¹²², M. Cristinziani²³, V. Croft¹⁰⁸, G. Crosetti^{40a,40b}, A. Cueto⁸⁵,

T. Cuhadar Donszelmann¹⁴¹, J. Cummings¹⁷⁹, M. Curatolo⁵⁰, J. Cúth⁸⁶, H. Czirr¹⁴³, P. Czodrowski³, G. D'amen^{22a,22b}, S. D'Auria⁵⁶, M. D'Onofrio⁷⁷, M.J. Da Cunha Sargedas De Sousa^{128a,128b}, C. Da Via⁸⁷, W. Dabrowski^{41a}, T. Dado^{146a}, T. Dai⁹², O. Dale¹⁵, F. Dallaire⁹⁷, C. Dallapiccola⁸⁹, M. Dam³⁹, J.R. Dandoy¹²⁴, N.P. Dang⁵¹, A.C. Daniells¹⁹, N.S. Dann⁸⁷, M. Danninger¹⁷¹, M. Dano Hoffmann¹³⁸, V. Dao⁵¹, G. Darbo^{53a}, S. Darmora⁸, J. Dassoulas³, A. Dattagupta¹¹⁸, T. Daubney⁴⁵, W. Davey²³, C. David⁴⁵, T. Davidek¹³¹, M. Davies¹⁵⁵, P. Davison⁸¹, E. Dawe⁹¹, I. Dawson¹⁴¹, K. De⁸, R. de Asmundis^{106a}, A. De Benedetti¹¹⁵, S. De Castro^{22a,22b}, S. De Cecco⁸³, N. De Groot¹⁰⁸, P. de Jong¹⁰⁹, H. De la Torre⁹³, F. De Lorenzi⁶⁷, A. De Maria⁵⁷, D. De Pedis^{134a}, A. De Salvo^{134a}, U. De Sanctis¹⁵¹, A. De Santo¹⁵¹, J.B. De Vivie De Regie¹¹⁹, W.J. Dearnaley⁷⁵, R. Debbe²⁷, C. Debenedetti¹³⁹, D.V. Dedovich⁶⁸, N. Dehghanian³, I. Deigaard¹⁰⁹, M. Del Gaudio^{40a,40b}, J. Del Peso⁸⁵, T. Del Prete^{126a,126b}, D. Delgove¹¹⁹, F. Deliot¹³⁸, C.M. Delitzsch⁵², A. Dell'Acqua³², L. Dell'Asta²⁴, M. Dell'Orso^{126a,126b}, M. Della Pietra^{106a,l}, D. della Volpe⁵², M. Delmastro⁵, P.A. Delsart⁵⁸, D.A. DeMarco¹⁶¹, S. Demers¹⁷⁹, M. Demichev⁶⁸, A. Demilly⁸³, S.P. Denisov¹³², D. Denysiuk¹³⁸, D. Derendarz⁴², J.E. Derkaoui^{137d}, F. Derue⁸³, P. Dervan⁷⁷, K. Desch²³, C. Deterre⁴⁵, K. Dette⁴⁶, P.O. Deviveiros³², A. Dewhurst¹³³, S. Dhaliwal²⁵, A. Di Ciaccio^{135a,135b}, L. Di Ciaccio⁵, W.K. Di Clemente¹²⁴, C. Di Donato^{106a,106b}, A. Di Girolamo³², B. Di Girolamo³², B. Di Micco^{136a,136b}, R. Di Nardo³², K.F. Di Petrillo⁵⁹, A. Di Simone⁵¹, R. Di Sipio¹⁶¹, D. Di Valentino³¹, C. Diaconu⁸⁸, M. Diamond¹⁶¹, F.A. Dias⁴⁹, M.A. Diaz^{34a}, E.B. Diehl⁹², J. Dietrich¹⁷, S. Díez Cornell⁴⁵, A. Dimitrievska¹⁴, J. Dingfelder²³, P. Dita^{28b}, S. Dita^{28b}, F. Dittus³², F. Djama⁸⁸, T. Djobava^{54b}, J.I. Djuvsland^{60a}, M.A.B. do Vale^{26c}, D. Dobos³², M. Dobre^{28b}, C. Doglioni⁸⁴, J. Dolejsi¹³¹, Z. Dolezal¹³¹, M. Donadelli^{26d}, S. Donati^{126a,126b}, P. Dondero^{123a,123b}, J. Donini³⁷, J. Dopke¹³³, A. Doria^{106a}, M.T. Dova⁷⁴, A.T. Doyle⁵⁶, E. Drechsler⁵⁷, M. Dris¹⁰, Y. Du^{36b}, J. Duarte-Campderros¹⁵⁵, E. Duchovni¹⁷⁵, G. Duckeck¹⁰², O.A. Ducu^{97,n}, D. Duda¹⁰⁹, A. Dudarev³², A.Ch. Dudder⁸⁶, E.M. Duffield¹⁶, L. Duflot¹¹⁹, M. Dührssen³², M. Dumancic¹⁷⁵, A.K. Duncan⁵⁶, M. Dunford^{60a}, H. Duran Yildiz^{4a}, M. Düren⁵⁵, A. Durglishvili^{54b}, D. Duschinger⁴⁷, B. Dutta⁴⁵, M. Dyndal⁴⁵, C. Eckardt⁴⁵, K.M. Ecker¹⁰³, R.C. Edgar⁹², N.C. Edwards⁴⁹, T. Eifert³², G. Eigen¹⁵, K. Einsweiler¹⁶, T. Ekelof¹⁶⁸, M. El Kacimi^{137c}, V. Ellajosyula⁸⁸, M. Ellert¹⁶⁸, S. Elles⁵, F. Ellinghaus¹⁷⁸, A.A. Elliot¹⁷², N. Ellis³², J. Elmsheuser²⁷, M. Elsing³², D. Emelianov¹³³, Y. Enari¹⁵⁷, O.C. Endner⁸⁶, J.S. Ennis¹⁷³, J. Erdmann⁴⁶, A. Ereditato¹⁸, G. Ernis¹⁷⁸, J. Ernst², M. Ernst²⁷, S. Errede¹⁶⁹, E. Ertel⁸⁶, M. Escalier¹¹⁹, H. Esch⁴⁶, C. Escobar¹²⁷, B. Esposito⁵⁰, A.I. Etienne¹³⁸, E. Etzion¹⁵⁵, H. Evans⁶⁴, A. Ezhilov¹²⁵, M. Ezzi^{137e}, F. Fabbri^{22a,22b}, L. Fabbri^{22a,22b}, G. Facini³³, R.M. Fakhruddinov¹³², S. Falciano^{134a}, R.J. Falla⁸¹, J. Faltova³², Y. Fang^{35a}, M. Fanti^{94a,94b}, A. Farbin⁸, A. Farilla^{136a}, C. Farina¹²⁷, E.M. Farina^{123a,123b}, T. Farooque⁹³, S. Farrell¹⁶, S.M. Farrington¹⁷³, P. Farthouat³², F. Fassi^{137e}, P. Fassnacht³², D. Fassouliotis⁹, M. Fauci Giannelli⁸⁰, A. Favareto^{53a,53b}, W.J. Fawcett¹²², L. Fayard¹¹⁹, O.L. Fedin^{125,o}, W. Fedorko¹⁷¹, S. Feigl¹²¹, L. Felgioni⁸⁸, C. Feng^{36b}, E.J. Feng³², H. Feng⁹², A.B. Fenyuk¹³², L. Feremenga⁸, P. Fernandez Martinez¹⁷⁰, S. Fernandez Perez¹³, J. Ferrando⁴⁵, A. Ferrari¹⁶⁸, P. Ferrari¹⁰⁹, R. Ferrari^{123a}, D.E. Ferreira de Lima^{60b}, A. Ferrer¹⁷⁰, D. Ferrere⁵², C. Ferretti⁹², F. Fiedler⁸⁶, A. Filipčič⁷⁸, M. Filipuzzi⁴⁵, F. Filthaut¹⁰⁸, M. Fincke-Keeler¹⁷², K.D. Finelli¹⁵², M.C.N. Fiolhais^{128a,128c}, L. Fiorini¹⁷⁰, A. Fischer², C. Fischer¹³, J. Fischer¹⁷⁸, W.C. Fisher⁹³, N. Flaschel⁴⁵, I. Fleck¹⁴³, P. Fleischmann⁹², G.T. Fletcher¹⁴¹, R.R.M. Fletcher¹²⁴, T. Flick¹⁷⁸, B.M. Flierl¹⁰², L.R. Flores Castillo^{62a}, M.J. Flowerdew¹⁰³, G.T. Forcolin⁸⁷, A. Formica¹³⁸, A. Forti⁸⁷, A.G. Foster¹⁹, D. Fournier¹¹⁹, H. Fox⁷⁵, S. Fracchia¹³, P. Francavilla⁸³, M. Franchini^{22a,22b}, D. Francis³², L. Franconi¹²¹, M. Franklin⁵⁹, M. Frate¹⁶⁶, M. Fraternali^{123a,123b}, D. Freeborn⁸¹, S.M. Fressard-Batraneanu³², D. Froidevaux³², J.A. Frost¹²², C. Fukunaga¹⁵⁸, E. Fullana Torregrosa⁸⁶, T. Fusayasu¹⁰⁴, J. Fuster¹⁷⁰, C. Gabaldon⁵⁸, O. Gabizon¹⁵⁴, A. Gabrielli^{22a,22b}, A. Gabrielli¹⁶, G.P. Gach^{41a}, S. Gadatsch³², G. Gagliardi^{53a,53b}, L.G. Gagnon⁹⁷, P. Gagnon⁶⁴, C. Galea¹⁰⁸, B. Galhardo^{128a,128c}, E.J. Gallas¹²², B.J. Gallop¹³³, P. Gallus¹³⁰, G. Galster³⁹, K.K. Gan¹¹³,

S. Ganguly³⁷, J. Gao^{36a}, Y. Gao⁷⁷, Y.S. Gao^{145.g}, F.M. Garay Walls⁴⁹, C. García¹⁷⁰,
 J.E. García Navarro¹⁷⁰, M. Garcia-Sciveres¹⁶, R.W. Gardner³³, N. Garelli¹⁴⁵, V. Garonne¹²¹,
 A. Gascon Bravo⁴⁵, K. Gasnikova⁴⁵, C. Gatti⁵⁰, A. Gaudiello^{53a,53b}, G. Gaudio^{123a}, L. Gauthier⁹⁷,
 I.L. Gavrilenko⁹⁸, C. Gay¹⁷¹, G. Gaycken²³, E.N. Gazis¹⁰, Z. Gecse¹⁷¹, C.N.P. Gee¹³³,
 Ch. Geich-Gimbel²³, M. Geisen⁸⁶, M.P. Geisler^{60a}, K. Gellerstedt^{148a,148b}, C. Gemme^{53a},
 M.H. Genest⁵⁸, C. Geng^{36a,p}, S. Gentile^{134a,134b}, C. Gentsos¹⁵⁶, S. George⁸⁰, D. Gerbaudo¹³,
 A. Gershon¹⁵⁵, S. Ghasemi¹⁴³, M. Ghneimat²³, B. Giacobbe^{22a}, S. Giagu^{134a,134b}, P. Giannetti^{126a,126b},
 S.M. Gibson⁸⁰, M. Gignac¹⁷¹, M. Gilchriese¹⁶, T.P.S. Gillam³⁰, D. Gillberg³¹, G. Gilles¹⁷⁸,
 D.M. Gingrich^{3.d}, N. Giokaris^{9,*}, M.P. Giordani^{167a,167c}, F.M. Giorgi^{22a}, P.F. Giraud¹³⁸, P. Giromini⁵⁹,
 D. Giugni^{94a}, F. Giuli¹²², C. Giuliani¹⁰³, M. Giulini^{60b}, B.K. Gjelsten¹²¹, S. Gkaitatzis¹⁵⁶, I. Gkialas¹⁵⁶,
 E.L. Gkoukousis¹³⁹, L.K. Gladilin¹⁰¹, C. Glasman⁸⁵, J. Glatzer¹³, P.C.F. Glaysher⁴⁹, A. Glazov⁴⁵,
 M. Goblirsch-Kolb²⁵, J. Godlewski⁴², S. Goldfarb⁹¹, T. Golling⁵², D. Golubkov¹³²,
 A. Gomes^{128a,128b,128d}, R. Gonçalo^{128a}, R. Goncalves Gama^{26a}, J. Goncalves Pinto Firmino Da Costa¹³⁸,
 G. Gonella⁵¹, L. Gonella¹⁹, A. Gongadze⁶⁸, S. González de la Hoz¹⁷⁰, S. Gonzalez-Sevilla⁵²,
 L. Goossens³², P.A. Gorbounov⁹⁹, H.A. Gordon²⁷, I. Gorelov¹⁰⁷, B. Gorini³², E. Gorini^{76a,76b},
 A. Gorišek⁷⁸, A.T. Goshaw⁴⁸, C. Gössling⁴⁶, M.I. Gostkin⁶⁸, C.R. Goudet¹¹⁹, D. Goujdami^{137c},
 A.G. Goussiou¹⁴⁰, N. Govender^{147b,q}, E. Gozani¹⁵⁴, L. Graber⁵⁷, I. Grabowska-Bold^{141a}, P.O.J. Gradin⁵⁸,
 P. Grafström^{22a,22b}, J. Gramling⁵², E. Gramstad¹²¹, S. Grancagnolo¹⁷, V. Gratchev¹²⁵, P.M. Gravila^{28e},
 H.M. Gray³², E. Graziani^{136a}, Z.D. Greenwood^{82,r}, C. Grefe²³, K. Gregersen⁸¹, I.M. Gregor⁴⁵,
 P. Grenier¹⁴⁵, K. Grevtsov⁵, J. Griffiths⁸, A.A. Grillo¹³⁹, K. Grimm⁷⁵, S. Grinstein^{13,s}, Ph. Gris³⁷,
 J.-F. Grivaz¹¹⁹, S. Groh⁸⁶, E. Gross¹⁷⁵, J. Grosse-Knetter⁵⁷, G.C. Grossi⁸², Z.J. Grout⁸¹, L. Guan⁹²,
 W. Guan¹⁷⁶, J. Guenther⁶⁵, F. Guescini^{163a}, D. Guest¹⁶⁶, O. Gueta¹⁵⁵, B. Gui¹¹³, E. Guido^{53a,53b},
 T. Guillemin⁵, S. Guindon², U. Gul⁵⁶, C. Gumpert³², J. Guo^{36c}, W. Guo⁹², Y. Guo^{36a}, R. Gupta⁴³,
 S. Gupta¹²², G. Gustavino^{134a,134b}, P. Gutierrez¹¹⁵, N.G. Gutierrez Ortiz⁸¹, C. Gutsche⁸¹, C. Guyot¹³⁸,
 C. Gwenlan¹²², C.B. Gwilliam⁷⁷, A. Haas¹¹², C. Haber¹⁶, H.K. Hadavand⁸, N. Haddad^{137e}, A. Hadeef⁸⁸,
 S. Hageböck²³, M. Hagihara¹⁶⁴, H. Hakobyan^{180,*}, M. Haleem⁴⁵, J. Haley¹¹⁶, G. Halladjian⁹³,
 G.D. Hallewell⁸⁸, K. Hamacher¹⁷⁸, P. Hamal¹¹⁷, K. Hamano¹⁷², A. Hamilton^{147a}, G.N. Hamity¹⁴¹,
 P.G. Hamnett⁴⁵, L. Han^{36a}, S. Han^{35a}, K. Hanagaki^{69,t}, K. Hanawa¹⁵⁷, M. Hance¹³⁹, B. Haney¹²⁴,
 P. Hanke^{60a}, R. Hanna¹³⁸, J.B. Hansen³⁹, J.D. Hansen³⁹, M.C. Hansen²³, P.H. Hansen³⁹, K. Hara¹⁶⁴,
 A.S. Hard¹⁷⁶, T. Harenberg¹⁷⁸, F. Hariri¹¹⁹, S. Harkusha⁹⁵, R.D. Harrington⁴⁹, P.F. Harrison¹⁷³,
 F. Hartjes¹⁰⁹, N.M. Hartmann¹⁰², M. Hasegawa⁷⁰, Y. Hasegawa¹⁴², A. Hasib⁴⁹, S. Hassani¹³⁸,
 S. Haug¹⁸, R. Hauser⁹³, L. Hauswald⁴⁷, M. Havranek¹³⁰, C.M. Hawkes¹⁹, R.J. Hawkins³²,
 D. Hayakawa¹⁵⁹, D. Hayden⁹³, C.P. Hays¹²², J.M. Hays⁷⁹, H.S. Hayward⁷⁷, S.J. Haywood¹³³,
 S.J. Head¹⁹, T. Heck⁸⁶, V. Hedberg⁸⁴, L. Heelan⁸, S. Heim¹²⁴, T. Heim¹⁶, B. Heinemann⁴⁵,
 J.J. Heinrich¹⁰², L. Heinrich¹¹², C. Heinz⁵⁵, J. Hejbal¹²⁹, L. Helary³², S. Hellman^{148a,148b}, C. Helsen³²,
 J. Henderson¹²², R.C.W. Henderson⁷⁵, Y. Heng¹⁷⁶, S. Henkelmann¹⁷¹, A.M. Henriques Correia³²,
 S. Henrot-Versille¹¹⁹, G.H. Herbert¹⁷, H. Herde²⁵, V. Herget¹⁷⁷, Y. Hernández Jiménez^{147c}, G. Herten⁵¹,
 R. Hertenberger¹⁰², L. Hervas³², T.C. Herwig¹²⁴, G.G. Hesketh⁸¹, N.P. Hessey¹⁰⁹, J.W. Hetherly⁴³,
 E. Higón-Rodríguez¹⁷⁰, E. Hill¹⁷², J.C. Hill³⁰, K.H. Hiller⁴⁵, S.J. Hillier¹⁹, I. Hinchliffe¹⁶, E. Hines¹²⁴,
 M. Hirose⁵¹, D. Hirschbuehl¹⁷⁸, O. Hladik¹²⁹, X. Hoad⁴⁹, J. Hobbs¹⁵⁰, N. Hod^{163a}, M.C. Hodgkinson¹⁴¹,
 P. Hodgson¹⁴¹, A. Hoecker³², M.R. Hoferkamp¹⁰⁷, F. Hoenig¹⁰², D. Hohn²³, T.R. Holmes¹⁶,
 M. Homann⁴⁶, S. Honda¹⁶⁴, T. Honda⁶⁹, T.M. Hong¹²⁷, B.H. Hooberman¹⁶⁹, W.H. Hopkins¹¹⁸,
 Y. Horii¹⁰⁵, A.J. Horton¹⁴⁴, J.-Y. Hostachy⁵⁸, S. Hou¹⁵³, A. Hoummada^{137a}, J. Howarth⁴⁵, J. Hoya⁷⁴,
 M. Hrabovsky¹¹⁷, I. Hristova¹⁷, J. Hrivnac¹¹⁹, T. Hryn'ova⁵, A. Hrynevich⁹⁶, P.J. Hsu⁶³, S.-C. Hsu¹⁴⁰,
 Q. Hu^{36a}, S. Hu^{36c}, Y. Huang^{35a}, Z. Hubacek¹³⁰, F. Hubaut⁸⁸, F. Huegging²³, T.B. Huffman¹²²,
 E.W. Hughes³⁸, G. Hughes⁷⁵, M. Huhtinen³², P. Huo¹⁵⁰, N. Huseynov^{68.b}, J. Huston⁹³, J. Huth⁵⁹,
 G. Iacobucci⁵², G. Iakovidis²⁷, I. Ibragimov¹⁴³, L. Iconomidou-Fayard¹¹⁹, Z. Idrissi^{137e}, P. Iengo³²,

O. Igonkina^{109,u}, T. Iizawa¹⁷⁴, Y. Ikegami⁶⁹, M. Ikeno⁶⁹, Y. Ilchenko^{11,v}, D. Iliadis¹⁵⁶, N. Ilic¹⁴⁵, G. Introzzi^{123a,123b}, P. Ioannou^{9,*}, M. Iodice^{136a}, K. Iordanidou³⁸, V. Ippolito⁵⁹, N. Ishijima¹²⁰, M. Ishino¹⁵⁷, M. Ishitsuka¹⁵⁹, C. Issever¹²², S. Istin^{20a}, F. Ito¹⁶⁴, J.M. Iturbe Ponce⁸⁷, R. Iuppa^{162a,162b}, H. Iwasaki⁶⁹, J.M. Izen⁴⁴, V. Izzo^{106a}, S. Jabbar³, P. Jackson¹, V. Jain², K.B. Jakobi⁸⁶, K. Jakobs⁵¹, S. Jakobsen³², T. Jakoubek¹²⁹, D.O. Jamin¹¹⁶, D.K. Jana⁸², R. Jansky⁶⁵, J. Janssen²³, M. Janus⁵⁷, P.A. Janus^{41a}, G. Jarlskog⁸⁴, N. Javadov^{68,b}, T. Javůrek⁵¹, M. Javurkova⁵¹, F. Jeanneau¹³⁸, L. Jeanty¹⁶, J. Jejelava^{54a,w}, G.-Y. Jeng¹⁵², P. Jenni^{51,x}, C. Jeske¹⁷³, S. Jézéquel⁵, H. Ji¹⁷⁶, J. Jia¹⁵⁰, H. Jiang⁶⁷, Y. Jiang^{36a}, Z. Jiang¹⁴⁵, S. Jiggins⁸¹, J. Jimenez Pena¹⁷⁰, S. Jin^{35a}, A. Jinaru^{28b}, O. Jinnouchi¹⁵⁹, H. Jivan^{147c}, P. Johansson¹⁴¹, K.A. Johns⁷, C.A. Johnson⁶⁴, W.J. Johnson¹⁴⁰, K. Jon-And^{148a,148b}, G. Jones¹⁷³, R.W.L. Jones⁷⁵, S. Jones⁷, T.J. Jones⁷⁷, J. Jongmanns^{60a}, P.M. Jorge^{128a,128b}, J. Jovicevic^{163a}, X. Ju¹⁷⁶, A. Juste Rozas^{13,s}, M.K. Köhler¹⁷⁵, A. Kaczmarska⁴², M. Kado¹¹⁹, H. Kagan¹¹³, M. Kagan¹⁴⁵, S.J. Kahn⁸⁸, T. Kaji¹⁷⁴, E. Kajomovitz⁴⁸, C.W. Kalderon⁸⁴, A. Kaluza⁸⁶, S. Kama⁴³, A. Kamenshchikov¹³², N. Kanaya¹⁵⁷, S. Kaneti³⁰, L. Kanjir⁷⁸, V.A. Kantserov¹⁰⁰, J. Kanzaki⁶⁹, B. Kaplan¹¹², L.S. Kaplan¹⁷⁶, A. Kapliy³³, D. Kar^{147c}, K. Karakostas¹⁰, A. Karamaoun³, N. Karastathis¹⁰, M.J. Kareem⁵⁷, E. Karentzos¹⁰, S.N. Karpov⁶⁸, Z.M. Karpova⁶⁸, K. Karthik¹¹², V. Kartvelishvili⁷⁵, A.N. Karyukhin¹³², K. Kasahara¹⁶⁴, L. Kashif¹⁷⁶, R.D. Kass¹¹³, A. Kastanas¹⁴⁹, Y. Kataoka¹⁵⁷, C. Kato¹⁵⁷, A. Katre⁵², J. Katzy⁴⁵, K. Kawade¹⁰⁵, K. Kawagoe⁷³, T. Kawamoto¹⁵⁷, G. Kawamura⁵⁷, V.F. Kazanin^{111,c}, R. Keeler¹⁷², R. Kehoe⁴³, J.S. Keller⁴⁵, J.J. Kempster⁸⁰, H. Keoshkerian¹⁶¹, O. Kepka¹²⁹, B.P. Kerševan⁷⁸, S. Kersten¹⁷⁸, R.A. Keyes⁹⁰, M. Khader¹⁶⁹, F. Khalil-zada¹², A. Khanov¹¹⁶, A.G. Kharlamov^{111,c}, T. Kharlamova^{111,c}, T.J. Khoo⁵², V. Khovanskiy⁹⁹, E. Khramov⁶⁸, J. Khubua^{54b,y}, S. Kido⁷⁰, C.R. Kilby⁸⁰, H.Y. Kim⁸, S.H. Kim¹⁶⁴, Y.K. Kim³³, N. Kimura¹⁵⁶, O.M. Kind¹⁷, B.T. King⁷⁷, M. King¹⁷⁰, D. Kirchmeier⁴⁷, J. Kirk¹³³, A.E. Kiryunin¹⁰³, T. Kishimoto¹⁵⁷, D. Kisieleska^{41a}, K. Kiuchi¹⁶⁴, O. Kivernyk¹³⁸, E. Kladiva^{146b}, T. Klapdor-kleingrothaus⁵¹, M.H. Klein³⁸, M. Klein⁷⁷, U. Klein⁷⁷, K. Kleinknecht⁸⁶, P. Klimek¹¹⁰, A. Klimentov²⁷, R. Klingenberg⁴⁶, T. Klioutchnikova³², E.-E. Kluge^{60a}, P. Kluit¹⁰⁹, S. Kluth¹⁰³, J. Knapik⁴², E. Kneringer⁶⁵, E.B.F.G. Knoop⁸⁸, A. Knue¹⁰³, A. Kobayashi¹⁵⁷, D. Kobayashi¹⁵⁹, T. Kobayashi¹⁵⁷, M. Kobel⁴⁷, M. Kocian¹⁴⁵, P. Kodys¹³¹, T. Koffas³¹, E. Koffeman¹⁰⁹, N.M. Köhler¹⁰³, T. Koi¹⁴⁵, H. Kolanoski¹⁷, M. Kolb^{60b}, I. Koletsou⁵, A.A. Komar^{98,*}, Y. Komori¹⁵⁷, T. Kondo⁶⁹, N. Kondrashova^{36c}, K. Köneke⁵¹, A.C. König¹⁰⁸, T. Kono^{69,z}, R. Konoplich^{112,aa}, N. Konstantinidis⁸¹, R. Kopeliansky⁶⁴, S. Koperny^{41a}, A.K. Kopp⁵¹, K. Korcyl⁴², K. Kordas¹⁵⁶, A. Korn⁸¹, A.A. Korol^{111,c}, I. Korolkov¹³, E.V. Korolkova¹⁴¹, O. Kortner¹⁰³, S. Kortner¹⁰³, T. Kosek¹³¹, V.V. Kostyukhin²³, A. Kotwal⁴⁸, A. Koulouris¹⁰, A. Kourkoumeli-Charalampidi^{123a,123b}, C. Kourkoumelis⁹, V. Kouskoura²⁷, A.B. Kowalewska⁴², R. Kowalewski¹⁷², T.Z. Kowalski^{41a}, C. Kozakai¹⁵⁷, W. Kozanecki¹³⁸, A.S. Kozhin¹³², V.A. Kramarenko¹⁰¹, G. Kramberger⁷⁸, D. Krasnopevtsev¹⁰⁰, M.W. Krasny⁸³, A. Krasznahorkay³², A. Kravchenko²⁷, M. Kretz^{60c}, J. Kretzschmar⁷⁷, K. Kreutzfeldt⁵⁵, P. Krieger¹⁶¹, K. Krizka³³, K. Kroeninger⁴⁶, H. Kroha¹⁰³, J. Kroll¹²⁴, J. Kroseberg²³, J. Krstic¹⁴, U. Kruchonak⁶⁸, H. Krüger²³, N. Krumnack⁶⁷, M.C. Kruse⁴⁸, M. Kruskal²⁴, T. Kubota⁹¹, H. Kucuk⁸¹, S. Kuday^{4b}, J.T. Kuechler¹⁷⁸, S. Kuehn⁵¹, A. Kugel^{60c}, F. Kuger¹⁷⁷, T. Kuhl⁴⁵, V. Kukhtin⁶⁸, R. Kukla¹³⁸, Y. Kulchitsky⁹⁵, S. Kuleshov^{34b}, M. Kuna^{134a,134b}, T. Kunigo⁷¹, A. Kupco¹²⁹, O. Kuprash¹⁵⁵, H. Kurashige⁷⁰, L.L. Kurchaninov^{163a}, Y.A. Kurochkin⁹⁵, M.G. Kurth^{35a}, V. Kus¹²⁹, E.S. Kuwertz¹⁷², M. Kuze¹⁵⁹, J. Kvita¹¹⁷, T. Kwan¹⁷², D. Kyriazopoulos¹⁴¹, A. La Rosa¹⁰³, J.L. La Rosa Navarro^{26d}, L. La Rotonda^{40a,40b}, C. Lacasta¹⁷⁰, F. Lacava^{134a,134b}, J. Lacey³¹, H. Lacker¹⁷, D. Lacour⁸³, E. Ladygin⁶⁸, R. Lafaye⁵, B. Laforge⁸³, T. Lagouri¹⁷⁹, S. Lai⁵⁷, S. Lammers⁶⁴, W. Lampl⁷, E. Lançon²⁷, U. Landgraf⁵¹, M.P.J. Landon⁷⁹, M.C. Lanfermann⁵², V.S. Lang^{60a}, J.C. Lange¹³, A.J. Lankford¹⁶⁶, F. Lanni²⁷, K. Lantsch²³, A. Lanza^{123a}, A. Lapertosa^{53a,53b}, S. Laplace⁸³, C. Lapoire³², J.F. Laporte¹³⁸, T. Lari^{94a}, F. Lasagni Manghi^{22a,22b}, M. Lassnig³², P. Laurelli⁵⁰, W. Lavrijsen¹⁶, A.T. Law¹³⁹, P. Laycock⁷⁷, T. Lazovich⁵⁹, M. Lazzaroni^{94a,94b}, B. Le⁹¹, O. Le Dortz⁸³, E. Le Guirriec⁸⁸,

E.P. Le Quilleuc¹³⁸, M. LeBlanc¹⁷², T. LeCompte⁶, F. Ledroit-Guillon⁵⁸, C.A. Lee²⁷, S.C. Lee¹⁵³, L. Lee¹, B. Lefebvre⁹⁰, G. Lefebvre⁸³, M. Lefebvre¹⁷², F. Legger¹⁰², C. Leggett¹⁶, A. Lehan⁷⁷, G. Lehmann Miotto³², X. Lei⁷, W.A. Leight³¹, A.G. Leister¹⁷⁹, M.A.L. Leite^{26d}, R. Leitner¹³¹, D. Lellouch¹⁷⁵, B. Lemmer⁵⁷, K.J.C. Leney⁸¹, T. Lenz²³, B. Lenzi³², R. Leone⁷, S. Leone^{126a,126b}, C. Leonidopoulos⁴⁹, S. Leontsinis¹⁰, G. Lerner¹⁵¹, C. Leroy⁹⁷, A.A.J. Lesage¹³⁸, C.G. Lester³⁰, M. Levchenko¹²⁵, J. Levêque⁵, D. Levin⁹², L.J. Levinson¹⁷⁵, M. Levy¹⁹, D. Lewis⁷⁹, M. Leyton⁴⁴, B. Li^{36a,p}, C. Li^{36a}, H. Li¹⁵⁰, L. Li⁴⁸, L. Li^{36c}, Q. Li^{35a}, S. Li⁴⁸, X. Li⁸⁷, Y. Li¹⁴³, Z. Liang^{35a}, B. Liberti^{135a}, A. Liblong¹⁶¹, P. Lichard³², K. Lie¹⁶⁹, J. Liebal²³, W. Liebig¹⁵, A. Limosani¹⁵², S.C. Lin^{153,ab}, T.H. Lin⁸⁶, B.E. Lindquist¹⁵⁰, A.E. Lioni⁵², E. Lipeles¹²⁴, A. Lipniacka¹⁵, M. Lisovyi^{60b}, T.M. Liss¹⁶⁹, A. Lister¹⁷¹, A.M. Litke¹³⁹, B. Liu^{153,ac}, H. Liu⁹², H. Liu²⁷, J. Liu^{36b}, J.B. Liu^{36a}, K. Liu⁸⁸, L. Liu¹⁶⁹, M. Liu^{36a}, Y.L. Liu^{36a}, Y. Liu^{36a}, M. Livan^{123a,123b}, A. Lleres⁵⁸, J. Llorente Merino^{35a}, S.L. Lloyd⁷⁹, F. Lo Sterzo¹⁵³, E.M. Lobodzinska⁴⁵, P. Loch⁷, F.K. Loebinger⁸⁷, K.M. Loew²⁵, A. Loginov^{179,*}, T. Lohse¹⁷, K. Lohwasser⁴⁵, M. Lokajicek¹²⁹, B.A. Long²⁴, J.D. Long¹⁶⁹, R.E. Long⁷⁵, L. Longo^{76a,76b}, K.A. Looper¹¹³, J.A. Lopez^{34b}, D. Lopez Mateos⁵⁹, B. Lopez Paredes¹⁴¹, I. Lopez Paz¹³, A. Lopez Solis⁸³, J. Lorenz¹⁰², N. Lorenzo Martinez⁶⁴, M. Losada²¹, P.J. Lösel¹⁰², X. Lou^{35a}, A. Lounis¹¹⁹, J. Love⁶, P.A. Love⁷⁵, H. Lu^{62a}, N. Lu⁹², H.J. Lubatti¹⁴⁰, C. Luci^{134a,134b}, A. Lucotte⁵⁸, C. Luedtke⁵¹, F. Luehring⁶⁴, W. Lukas⁶⁵, L. Luminari^{134a}, O. Lundberg^{148a,148b}, B. Lund-Jensen¹⁴⁹, P.M. Luzi⁸³, D. Lynn²⁷, R. Lysak¹²⁹, E. Lytken⁸⁴, V. Lyubushkin⁶⁸, H. Ma²⁷, L.L. Ma^{36b}, Y. Ma^{36b}, G. Maccarrone⁵⁰, A. Macchiolo¹⁰³, C.M. Macdonald¹⁴¹, B. Maček⁷⁸, J. Machado Miguens^{124,128b}, D. Madaffari⁸⁸, R. Madar³⁷, H.J. Maddocks¹⁶⁸, W.F. Mader⁴⁷, A. Madsen⁴⁵, J. Maeda⁷⁰, S. Maeland¹⁵, T. Maeno²⁷, A. Maevskiy¹⁰¹, E. Magradze⁵⁷, J. Mahlstedt¹⁰⁹, C. Maiani¹¹⁹, C. Maidantchik^{26a}, A.A. Maier¹⁰³, T. Maier¹⁰², A. Maio^{128a,128b,128d}, S. Majewski¹¹⁸, Y. Makida⁶⁹, N. Makovec¹¹⁹, B. Malaescu⁸³, Pa. Malecki⁴², V.P. Maleev¹²⁵, F. Malek⁵⁸, U. Mallik⁶⁶, D. Malon⁶, C. Malone³⁰, S. Maltezos¹⁰, S. Malyukov³², J. Mamuzic¹⁷⁰, G. Mancini⁵⁰, L. Mandelli^{94a}, I. Mandić⁷⁸, J. Maneira^{128a,128b}, L. Manhaes de Andrade Filho^{26b}, J. Manjarres Ramos^{163b}, A. Mann¹⁰², A. Manousos³², B. Mansoulie¹³⁸, J.D. Mansour^{35a}, R. Mantifel⁹⁰, M. Mantoani⁵⁷, S. Manzoni^{94a,94b}, L. Mapelli³², G. Marceca²⁹, L. March⁵², G. Marchiori⁸³, M. Marcisovsky¹²⁹, M. Marjanovic¹⁴, D.E. Marley⁹², F. Marroquim^{26a}, S.P. Marsden⁸⁷, Z. Marshall¹⁶, S. Marti-Garcia¹⁷⁰, T.A. Martin¹⁷³, V.J. Martin⁴⁹, B. Martin dit Latour¹⁵, M. Martinez^{13,s}, V.I. Martinez Outschoorn¹⁶⁹, S. Martin-Haugh¹³³, V.S. Martoiu^{28b}, A.C. Martyniuk⁸¹, A. Marzin³², L. Masetti⁸⁶, T. Mashimo¹⁵⁷, R. Mashinistov⁹⁸, J. Masik⁸⁷, A.L. Maslennikov^{111,c}, L. Massa^{22a,22b}, P. Mastrandrea⁵, A. Mastroberardino^{40a,40b}, T. Masubuchi¹⁵⁷, P. Mättig¹⁷⁸, J. Mattmann⁸⁶, J. Maurer^{28b}, S.J. Maxfield⁷⁷, D.A. Maximov^{111,c}, R. Mazini¹⁵³, I. Maznas¹⁵⁶, S.M. Mazza^{94a,94b}, N.C. Mc Fadden¹⁰⁷, G. Mc Goldrick¹⁶¹, S.P. Mc Kee⁹², A. McCarn⁹², R.L. McCarthy¹⁵⁰, T.G. McCarthy¹⁰³, L.I. McClymont⁸¹, E.F. McDonald⁹¹, J.A. Mcfayden⁸¹, G. Mchedlidze⁵⁷, S.J. McMahon¹³³, P.C. McNamara⁹¹, R.A. McPherson^{172,m}, M. Medinnis⁴⁵, S. Meehan¹⁴⁰, S. Mehlhase¹⁰², A. Mehta⁷⁷, K. Meier^{60a}, C. Meineck¹⁰², B. Meirose⁴⁴, D. Melini^{170,ad}, B.R. Mellado Garcia^{147c}, M. Melo^{146a}, F. Meloni¹⁸, S.B. Menary⁸⁷, L. Meng⁷⁷, X.T. Meng⁹², A. Mengarelli^{22a,22b}, S. Menke¹⁰³, E. Meoni¹⁶⁵, S. Mergelmeyer¹⁷, P. Mermod⁵², L. Merola^{106a,106b}, C. Meroni^{94a}, F.S. Merritt³³, A. Messina^{134a,134b}, J. Metcalfe⁶, A.S. Mete¹⁶⁶, C. Meyer¹²⁴, J-P. Meyer¹³⁸, J. Meyer¹⁰⁹, H. Meyer Zu Theenhausen^{60a}, F. Miano¹⁵¹, R.P. Middleton¹³³, S. Miglioranzi^{53a,53b}, L. Mijović⁴⁹, G. Mikenberg¹⁷⁵, M. Mikestikova¹²⁹, M. Mikuž⁷⁸, M. Milesi⁹¹, A. Milic²⁷, D.W. Miller³³, C. Mills⁴⁹, A. Milov¹⁷⁵, D.A. Milstead^{148a,148b}, A.A. Minaenko¹³², Y. Minami¹⁵⁷, I.A. Minashvili⁶⁸, A.I. Mincer¹¹², B. Mindur^{41a}, M. Mineev⁶⁸, Y. Minegishi¹⁵⁷, Y. Ming¹⁷⁶, L.M. Mir¹³, K.P. Mistry¹²⁴, T. Mitani¹⁷⁴, J. Mitrevski¹⁰², V.A. Mitsou¹⁷⁰, A. Miucci¹⁸, P.S. Miyagawa¹⁴¹, A. Mizukami⁶⁹, J.U. Mjörnmark⁸⁴, M. Mlynarikova¹³¹, T. Moa^{148a,148b}, K. Mochizuki⁹⁷, P. Mogg⁵¹, S. Mohapatra³⁸, S. Molander^{148a,148b}, R. Moles-Valls²³, R. Monden⁷¹, M.C. Mondragon⁹³, K. Mönig⁴⁵, J. Monk³⁹, E. Monnier⁸⁸, A. Montalbano¹⁵⁰, J. Montejo Berlingen³²,

F. Monticelli⁷⁴, S. Monzani^{94a,94b}, R.W. Moore³, N. Morange¹¹⁹, D. Moreno²¹, M. Moreno Llácer⁵⁷, P. Moretini^{53a}, S. Morgenstern³², D. Mori¹⁴⁴, T. Mori¹⁵⁷, M. Morii⁵⁹, M. Morinaga¹⁵⁷, V. Morisbak¹²¹, S. Moritz⁸⁶, A.K. Morley¹⁵², G. Mornacchi³², J.D. Morris⁷⁹, S.S. Mortensen³⁹, L. Morvaj¹⁵⁰, P. Moschovakos¹⁰, M. Mosidze^{54b}, H.J. Moss¹⁴¹, J. Moss^{145,ae}, K. Motohashi¹⁵⁹, R. Mount¹⁴⁵, E. Mountricha²⁷, E.J.W. Moyse⁸⁹, S. Muanza⁸⁸, R.D. Mudd¹⁹, F. Mueller¹⁰³, J. Mueller¹²⁷, R.S.P. Mueller¹⁰², T. Mueller³⁰, D. Muenstermann⁷⁵, P. Mullen⁵⁶, G.A. Mullier¹⁸, F.J. Munoz Sanchez⁸⁷, J.A. Murillo Quijada¹⁹, W.J. Murray^{173,133}, H. Musheghyan⁵⁷, M. Muškinja⁷⁸, A.G. Myagkov^{132,af}, M. Myska¹³⁰, B.P. Nachman¹⁶, O. Nackenhorst⁵², K. Nagai¹²², R. Nagai^{69,z}, K. Nagano⁶⁹, Y. Nagasaka⁶¹, K. Nagata¹⁶⁴, M. Nagel⁵¹, E. Nagy⁸⁸, A.M. Nairz³², Y. Nakahama¹⁰⁵, K. Nakamura⁶⁹, T. Nakamura¹⁵⁷, I. Nakano¹¹⁴, R.F. Naranjo Garcia⁴⁵, R. Narayan¹¹, D.I. Narrias Villar^{60a}, I. Naryshkin¹²⁵, T. Naumann⁴⁵, G. Navarro²¹, R. Nayyar⁷, H.A. Neal⁹², P.Yu. Nechaeva⁹⁸, T.J. Neep⁸⁷, A. Negri^{123a,123b}, M. Negrini^{22a}, S. Nektarijevic¹⁰⁸, C. Nellist¹¹⁹, A. Nelson¹⁶⁶, S. Nemecek¹²⁹, P. Nemethy¹¹², A.A. Nepomuceno^{26a}, M. Nessi^{32,ag}, M.S. Neubauer¹⁶⁹, M. Neumann¹⁷⁸, R.M. Neves¹¹², P. Nevski²⁷, P.R. Newman¹⁹, T. Nguyen Manh⁹⁷, R.B. Nickerson¹²², R. Nicolaidou¹³⁸, J. Nielsen¹³⁹, V. Nikolaenko^{132,af}, I. Nikolic-Audit⁸³, K. Nikolopoulos¹⁹, J.K. Nilsen¹²¹, P. Nilsson²⁷, Y. Ninomiya¹⁵⁷, A. Nisati^{134a}, R. Nisius¹⁰³, T. Nobe¹⁵⁷, Y. Noguchi⁷¹, M. Nomachi¹²⁰, I. Nomidis³¹, T. Nooney⁷⁹, S. Norberg¹¹⁵, M. Nordberg³², N. Norjoharuddeen¹²², O. Novgorodova⁴⁷, S. Nowak¹⁰³, M. Nozaki⁶⁹, L. Nozka¹¹⁷, K. Ntekas¹⁶⁶, E. Nurse⁸¹, F. Nuti⁹¹, D.C. O’Neil¹⁴⁴, A.A. O’Rourke⁴⁵, V. O’Shea⁵⁶, F.G. Oakham^{31,d}, H. Oberlack¹⁰³, T. Obermann²³, J. Ocariz⁸³, A. Ochi⁷⁰, I. Ochoa³⁸, J.P. Ochoa-Ricoux^{34a}, S. Oda⁷³, S. Odaka⁶⁹, H. Ogren⁶⁴, A. Oh⁸⁷, S.H. Oh⁴⁸, C.C. Ohm¹⁶, H. Ohman¹⁶⁸, H. Oide^{53a,53b}, H. Okawa¹⁶⁴, Y. Okumura¹⁵⁷, T. Okuyama⁶⁹, A. Olariu^{28b}, L.F. Oleiro Seabra^{128a}, S.A. Olivares Pino⁴⁹, D. Oliveira Damazio²⁷, A. Olszewski⁴², J. Olszowska⁴², A. Onofre^{128a,128e}, K. Onogi¹⁰⁵, P.U.E. Onyisi^{11,v}, M.J. Oreglia³³, Y. Oren¹⁵⁵, D. Orestano^{136a,136b}, N. Orlando^{62b}, R.S. Orr¹⁶¹, B. Osculati^{53a,53b,*}, R. Ospanov⁸⁷, G. Otero y Garzon²⁹, H. Otono⁷³, M. Ouchrif^{137d}, F. Ould-Saada¹²¹, A. Ouraou¹³⁸, K.P. Oussoren¹⁰⁹, Q. Ouyang^{35a}, M. Owen⁵⁶, R.E. Owen¹⁹, V.E. Ozcan^{20a}, N. Ozturk⁸, K. Pachal¹⁴⁴, A. Pacheco Pages¹³, L. Pacheco Rodriguez¹³⁸, C. Padilla Aranda¹³, S. Pagan Griso¹⁶, M. Paganini¹⁷⁹, F. Paige²⁷, P. Pais⁸⁹, K. Pajchel¹²¹, G. Palacino⁶⁴, S. Palazzo^{40a,40b}, S. Palestini³², M. Palka^{41b}, D. Pallin³⁷, E.St. Panagiotopoulou¹⁰, I. Panagoulas¹⁰, C.E. Pandini⁸³, J.G. Panduro Vazquez⁸⁰, P. Pani^{148a,148b}, S. Panitkin²⁷, D. Pantea^{28b}, L. Paolozzi⁵², Th.D. Papadopoulou¹⁰, K. Papageorgiou¹⁵⁶, A. Paramonov⁶, D. Paredes Hernandez¹⁷⁹, A.J. Parker⁷⁵, M.A. Parker³⁰, K.A. Parker¹⁴¹, F. Parodi^{53a,53b}, J.A. Parsons³⁸, U. Parzefall⁵¹, V.R. Pascuzzi¹⁶¹, E. Pasqualucci^{134a}, S. Passaggio^{53a}, Fr. Pastore⁸⁰, S. Patariaia¹⁷⁸, J.R. Pater⁸⁷, T. Pauly³², J. Pearce¹⁷², B. Pearson¹¹⁵, L.E. Pedersen³⁹, S. Pedraza Lopez¹⁷⁰, R. Pedro^{128a,128b}, S.V. Peleganchuk^{111,c}, O. Penc¹²⁹, C. Peng^{35a}, H. Peng^{36a}, J. Penwell⁶⁴, B.S. Peralva^{26b}, M.M. Perego¹³⁸, D.V. Perepelitsa²⁷, E. Perez Codina^{163a}, L. Perini^{94a,94b}, H. Pernegger³², S. Perrella^{106a,106b}, R. Peschke⁴⁵, V.D. Peshekhonov⁶⁸, K. Peters⁴⁵, R.F.Y. Peters⁸⁷, B.A. Petersen³², T.C. Petersen³⁹, E. Petit⁵⁸, A. Petridis¹, C. Petridou¹⁵⁶, P. Petroff¹¹⁹, E. Petrolo^{134a}, M. Petrov¹²², F. Petrucci^{136a,136b}, N.E. Pettersson⁸⁹, A. Peyaud¹³⁸, R. Pezoa^{34b}, P.W. Phillips¹³³, G. Piacquadio¹⁵⁰, E. Pianori¹⁷³, A. Picazio⁸⁹, E. Piccaro⁷⁹, M. Piccinini^{22a,22b}, M.A. Pickering¹²², R. Piegaia²⁹, J.E. Pilcher³³, A.D. Pilkington⁸⁷, A.W.J. Pin⁸⁷, M. Pinamonti^{167a,167c,ah}, J.L. Pinfold³, S. Pires⁸³, H. Pirumov⁴⁵, M. Pitt¹⁷⁵, L. Plazak^{146a}, M.-A. Pleier²⁷, V. Pleskot⁸⁶, E. Plotnikova⁶⁸, D. Pluth⁶⁷, R. Poettgen^{148a,148b}, L. Poggioli¹¹⁹, D. Pohl²³, G. Polesello^{123a}, A. Poley⁴⁵, A. Policicchio^{40a,40b}, R. Polifka³², A. Polini^{22a}, C.S. Pollard⁵⁶, V. Polychronakos²⁷, K. Pommès³², L. Pontecorvo^{134a}, B.G. Pope⁹³, G.A. Popeneciu^{28c}, A. Poppleton³², S. Pospisil¹³⁰, K. Potamianos¹⁶, I.N. Potrap⁶⁸, C.J. Potter³⁰, C.T. Potter¹¹⁸, G. Poulard³², J. Poveda³², V. Pozdnyakov⁶⁸, M.E. Pozo Astigarraga³², P. Pralavorio⁸⁸, A. Pranko¹⁶, S. Prell⁶⁷, D. Price⁸⁷, L.E. Price⁶, M. Primavera^{76a}, S. Prince⁹⁰, K. Prokofiev^{62c}, F. Prokoshin^{34b}, S. Protopopescu²⁷, J. Proudfoot⁶, M. Przybycien^{41a}, D. Puudu^{136a,136b}, M. Purohit^{27,ai}, P. Puzo¹¹⁹,

J. Qian⁹², G. Qin⁵⁶, Y. Qin⁸⁷, A. Quadt⁵⁷, W.B. Quayle^{167a,167b}, M. Queitsch-Maitland⁴⁵, D. Quilty⁵⁶, S. Raddum¹²¹, V. Radeka²⁷, V. Radescu¹²², S.K. Radhakrishnan¹⁵⁰, P. Radloff¹¹⁸, P. Rados⁹¹, F. Ragusa^{94a,94b}, G. Rahal¹⁸¹, J.A. Raine⁸⁷, S. Rajagopalan²⁷, M. Rammensee³², C. Rangel-Smith¹⁶⁸, M.G. Ratti^{94a,94b}, D.M. Rauch⁴⁵, F. Rauscher¹⁰², S. Rave⁸⁶, T. Ravenscroft⁵⁶, I. Ravinovich¹⁷⁵, M. Raymond³², A.L. Read¹²¹, N.P. Readioff⁷⁷, M. Reale^{76a,76b}, D.M. Rebuzzi^{123a,123b}, A. Redelbach¹⁷⁷, G. Redlinger²⁷, R. Reece¹³⁹, R.G. Reed^{147c}, K. Reeves⁴⁴, L. Rehnisch¹⁷, J. Reichert¹²⁴, A. Reiss⁸⁶, C. Rembser³², H. Ren^{35a}, M. Rescigno^{134a}, S. Resconi^{94a}, E.D. Resseguie¹²⁴, O.L. Rezanova^{111.c}, P. Reznicek¹³¹, R. Rezvani⁹⁷, R. Richter¹⁰³, S. Richter⁸¹, E. Richter-Was^{41b}, O. Ricken²³, M. Ridel⁸³, P. Rieck¹⁰³, C.J. Riegel¹⁷⁸, J. Rieger⁵⁷, O. Rifki¹¹⁵, M. Rijssenbeek¹⁵⁰, A. Rimoldi^{123a,123b}, M. Rimoldi¹⁸, L. Rinaldi^{22a}, G. Ripellino¹⁴⁹, B. Ristic⁵², E. Ritsch³², I. Riu¹³, F. Rizatdinova¹¹⁶, E. Rizvi⁷⁹, C. Rizzi¹³, R.T. Roberts⁸⁷, S.H. Robertson^{90,m}, A. Robichaud-Veronneau⁹⁰, D. Robinson³⁰, J.E.M. Robinson⁴⁵, A. Robson⁵⁶, C. Roda^{126a,126b}, Y. Rodina^{88,aj}, A. Rodriguez Perez¹³, D. Rodriguez Rodriguez¹⁷⁰, S. Roe³², C.S. Rogan⁵⁹, O. Røhne¹²¹, J. Roloff⁵⁹, A. Romaniouk¹⁰⁰, M. Romano^{22a,22b}, S.M. Romano Saez³⁷, E. Romero Adam¹⁷⁰, N. Rompotis⁷⁷, M. Ronzani⁵¹, L. Roos⁸³, E. Ros¹⁷⁰, S. Rosati^{134a}, K. Rosbach⁵¹, P. Rose¹³⁹, N.-A. Rosien⁵⁷, V. Rossetti^{148a,148b}, E. Rossi^{106a,106b}, L.P. Rossi^{53a}, J.H.N. Rosten³⁰, R. Rosten¹⁴⁰, M. Rotaru^{28b}, I. Roth¹⁷⁵, J. Rothberg¹⁴⁰, D. Rousseau¹¹⁹, A. Rozanov⁸⁸, Y. Rozen¹⁵⁴, X. Ruan^{147c}, F. Rubbo¹⁴⁵, M.S. Rudolph¹⁶¹, F. Rühr⁵¹, A. Ruiz-Martinez³¹, Z. Rurikova⁵¹, N.A. Rusakovich⁶⁸, A. Ruschke¹⁰², H.L. Russell¹⁴⁰, J.P. Rutherford⁷, N. Ruthmann³², Y.F. Ryabov¹²⁵, M. Rybar¹⁶⁹, G. Rybkin¹¹⁹, S. Ryu⁶, A. Ryzhov¹³², G.F. Rzehorz⁵⁷, A.F. Saavedra¹⁵², G. Sabato¹⁰⁹, S. Sacerdoti²⁹, H.F.-W. Sadrozinski¹³⁹, R. Sadykov⁶⁸, F. Safai Tehrani^{134a}, P. Saha¹¹⁰, M. Sahinsoy^{60a}, M. Saimpert¹³⁸, T. Saito¹⁵⁷, H. Sakamoto¹⁵⁷, Y. Sakurai¹⁷⁴, G. Salamanna^{136a,136b}, J.E. Salazar Loyola^{34b}, D. Salek¹⁰⁹, P.H. Sales De Bruin¹⁴⁰, D. Salihagic¹⁰³, A. Salnikov¹⁴⁵, J. Salt¹⁷⁰, D. Salvatore^{40a,40b}, F. Salvatore¹⁵¹, A. Salvucci^{62a,62b,62c}, A. Salzburger³², D. Sammel⁵¹, D. Sampsonidis¹⁵⁶, J. Sánchez¹⁷⁰, V. Sanchez Martinez¹⁷⁰, A. Sanchez Pineda^{106a,106b}, H. Sandaker¹²¹, R.L. Sandbach⁷⁹, M. Sandhoff¹⁷⁸, C. Sandoval²¹, D.P.C. Sankey¹³³, M. Sannino^{53a,53b}, A. Sansoni⁵⁰, C. Santoni³⁷, R. Santonico^{135a,135b}, H. Santos^{128a}, I. Santoyo Castillo¹⁵¹, K. Sapp¹²⁷, A. Saprnov⁶⁸, J.G. Saraiva^{128a,128d}, B. Sarrazin²³, O. Sasaki⁶⁹, K. Sato¹⁶⁴, E. Sauvan⁵, G. Savage⁸⁰, P. Savard^{161,d}, N. Savic¹⁰³, C. Sawyer¹³³, L. Sawyer^{82,r}, J. Saxon³³, C. Sbarra^{22a}, A. Sbrizzi^{22a,22b}, T. Scanlon⁸¹, D.A. Scannicchio¹⁶⁶, M. Scarcella¹⁵², V. Scarfone^{40a,40b}, J. Schaarschmidt¹⁴⁰, P. Schacht¹⁰³, B.M. Schachtner¹⁰², D. Schaefer³², L. Schaefer¹²⁴, R. Schaefer⁴⁵, J. Schaeffer⁸⁶, S. Schaepe²³, S. Schaezel^{60b}, U. Schäfer⁸⁶, A.C. Schaffer¹¹⁹, D. Schaile¹⁰², R.D. Schamberger¹⁵⁰, V. Scharf^{60a}, V.A. Schegelsky¹²⁵, D. Scheirich¹³¹, M. Schernau¹⁶⁶, C. Schiavi^{53a,53b}, S. Schier¹³⁹, C. Schillo⁵¹, M. Schioppa^{40a,40b}, S. Schlenker³², K.R. Schmidt-Sommerfeld¹⁰³, K. Schmieden³², C. Schmitt⁸⁶, S. Schmitt⁴⁵, S. Schmitz⁸⁶, B. Schneider^{163a}, U. Schnoor⁵¹, L. Schoeffel¹³⁸, A. Schoening^{60b}, B.D. Schoenrock⁹³, E. Schopf²³, M. Schott⁸⁶, J.F.P. Schouwenberg¹⁰⁸, J. Schovancova⁸, S. Schramm⁵², M. Schreyer¹⁷⁷, N. Schuh⁸⁶, A. Schulte⁸⁶, M.J. Schultens²³, H.-C. Schultz-Coulon^{60a}, H. Schulz¹⁷, M. Schumacher⁵¹, B.A. Schumm¹³⁹, Ph. Schune¹³⁸, A. Schwartzman¹⁴⁵, T.A. Schwarz⁹², H. Schweiger⁸⁷, Ph. Schwemling¹³⁸, R. Schwienhorst⁹³, J. Schwindling¹³⁸, T. Schwindt²³, G. Sciolla²⁵, F. Scuri^{126a,126b}, F. Scutti⁹¹, J. Searcy⁹², P. Seema²³, S.C. Seidel¹⁰⁷, A. Seiden¹³⁹, F. Seifert¹³⁰, J.M. Seixas^{26a}, G. Sekhniaidze^{106a}, K. Sekhon⁹², S.J. Sekula⁴³, N. Semprini-Cesari^{22a,22b}, C. Serfon¹²¹, L. Serin¹¹⁹, L. Serkin^{167a,167b}, M. Sessa^{136a,136b}, R. Seuster¹⁷², H. Severini¹¹⁵, T. Sfiligoy⁷⁸, F. Sforza³², A. Sfyrla⁵², E. Shabalina⁵⁷, N.W. Shaikh^{148a,148b}, L.Y. Shan^{35a}, R. Shang¹⁶⁹, J.T. Shank²⁴, M. Shapiro¹⁶, P.B. Shatalov⁹⁹, K. Shaw^{167a,167b}, S.M. Shaw⁸⁷, A. Shcherbakova^{148a,148b}, C.Y. Shehu¹⁵¹, Y. Shen¹¹⁵, P. Sherwood⁸¹, L. Shi^{153.ak}, S. Shimizu⁷⁰, C.O. Shimmin¹⁶⁶, M. Shimojima¹⁰⁴, S. Shirabe⁷³, M. Shiyakova^{68,al}, J. Shlomi¹⁷⁵, A. Shmeleva⁹⁸, D. Shoaleh Saadi⁹⁷, M.J. Shochet³³, S. Shojai^{94a}, D.R. Shope¹¹⁵, S. Shrestha¹¹³, E. Shulga¹⁰⁰, M.A. Shupe⁷, P. Sicho¹²⁹, A.M. Sickles¹⁶⁹, P.E. Sidebo¹⁴⁹, E. Sideras Haddad^{147c}, O. Sidiropoulou¹⁷⁷, D. Sidorov¹¹⁶, A. Sidoti^{22a,22b}, F. Siegert⁴⁷, Dj. Sijacki¹⁴,

J. Silva^{128a,128d}, S.B. Silverstein^{148a}, V. Simak¹³⁰, Lj. Simic¹⁴, S. Simion¹¹⁹, E. Simioni⁸⁶,
 B. Simmons⁸¹, M. Simon⁸⁶, P. Sinervo¹⁶¹, N.B. Sinev¹¹⁸, M. Sioli^{22a,22b}, G. Siragusa¹⁷⁷, I. Siral⁹²,
 S.Yu. Sivoklov¹⁰¹, J. Sjölin^{148a,148b}, M.B. Skinner⁷⁵, P. Skubic¹¹⁵, M. Slater¹⁹, T. Slavicek¹³⁰,
 M. Slawinska¹⁰⁹, K. Sliwa¹⁶⁵, R. Slovak¹³¹, V. Smakhtin¹⁷⁵, B.H. Smart⁵, L. Smestad¹⁵, J. Smiesko^{146a},
 S.Yu. Smirnov¹⁰⁰, Y. Smirnov¹⁰⁰, L.N. Smirnova^{101.am}, O. Smirnova⁸⁴, J.W. Smith⁵⁷, M.N.K. Smith³⁸,
 R.W. Smith³⁸, M. Smizanska⁷⁵, K. Smolek¹³⁰, A.A. Snesarev⁹⁸, I.M. Snyder¹¹⁸, S. Snyder²⁷,
 R. Sobie^{172.m}, F. Socher⁴⁷, A. Soffer¹⁵⁵, D.A. Soh¹⁵³, G. Sokhrannyi⁷⁸, C.A. Solans Sanchez³²,
 M. Solar¹³⁰, E.Yu. Soldatov¹⁰⁰, U. Soldevila¹⁷⁰, A.A. Solodkov¹³², A. Soloshenko⁶⁸,
 O.V. Solovyanov¹³², V. Solovyev¹²⁵, P. Sommer⁵¹, H. Son¹⁶⁵, H.Y. Song^{36a.an}, A. Sood¹⁶,
 A. Sopczak¹³⁰, V. Sopko¹³⁰, V. Sorin¹³, D. Sosa^{60b}, C.L. Sotiropoulou^{126a,126b}, R. Soualah^{167a,167c},
 A.M. Soukharev^{111.c}, D. South⁴⁵, B.C. Sowden⁸⁰, S. Spagnolo^{76a,76b}, M. Spalla^{126a,126b},
 M. Spangenberg¹⁷³, F. Spanò⁸⁰, D. Sperlich¹⁷, F. Spettel¹⁰³, T.M. Spieker^{60a}, R. Spighi^{22a}, G. Spigo³²,
 L.A. Spiller⁹¹, M. Spousta¹³¹, R.D. St. Denis^{56.*}, A. Stabile^{94a}, R. Stamen^{60a}, S. Stamm¹⁷,
 E. Stanecka⁴², R.W. Stanek⁶, C. Stanescu^{136a}, M. Stanescu-Bellu⁴⁵, M.M. Stanitzki⁴⁵, S. Stapnes¹²¹,
 E.A. Starchenko¹³², G.H. Stark³³, J. Stark⁵⁸, P. Staroba¹²⁹, P. Starovoitov^{60a}, S. Stärz³², R. Staszewski⁴²,
 P. Steinberg²⁷, B. Stelzer¹⁴⁴, H.J. Stelzer³², O. Stelzer-Chilton^{163a}, H. Stenzel⁵⁵, G.A. Stewart⁵⁶,
 J.A. Stillings²³, M.C. Stockton⁹⁰, M. Stoebe⁹⁰, G. Stoicea^{28b}, P. Stolte⁵⁷, S. Stonjek¹⁰³, A.R. Stradling⁸,
 A. Straessner⁴⁷, M.E. Stramaglia¹⁸, J. Strandberg¹⁴⁹, S. Strandberg^{148a,148b}, A. Strandlie¹²¹,
 M. Strauss¹¹⁵, P. Strizenec^{146b}, R. Ströhmer¹⁷⁷, D.M. Strom¹¹⁸, R. Stroynowski⁴³, A. Strubig¹⁰⁸,
 S.A. Stucci²⁷, B. Stugu¹⁵, N.A. Styles⁴⁵, D. Su¹⁴⁵, J. Su¹²⁷, S. Suchek^{60a}, Y. Sugaya¹²⁰, M. Suk¹³⁰,
 V.V. Sulin⁹⁸, S. Sultansoy^{4c}, T. Sumida⁷¹, S. Sun⁵⁹, X. Sun³, K. Suruliz¹⁵¹, C.J.E. Suster¹⁵²,
 M.R. Sutton¹⁵¹, S. Suzuki⁶⁹, M. Svatos¹²⁹, M. Swiatlowski³³, S.P. Swift², I. Sykora^{146a}, T. Sykora¹³¹,
 D. Ta⁵¹, K. Tackmann⁴⁵, J. Taenzer¹⁵⁵, A. Taffard¹⁶⁶, R. Tafirout^{163a}, N. Taiblum¹⁵⁵, H. Takai²⁷,
 R. Takashima⁷², T. Takeshita¹⁴², Y. Takubo⁶⁹, M. Talby⁸⁸, A.A. Talyshev^{111.c}, J. Tanaka¹⁵⁷,
 M. Tanaka¹⁵⁹, R. Tanaka¹¹⁹, S. Tanaka⁶⁹, R. Tanioka⁷⁰, B.B. Tannenwald¹¹³, S. Tapia Araya^{34b},
 S. Tapprogge⁸⁶, S. Tarem¹⁵⁴, G.F. Tartarelli^{94a}, P. Tas¹³¹, M. Tasevsky¹²⁹, T. Tashiro⁷¹, E. Tassi^{40a,40b},
 A. Tavares Delgado^{128a,128b}, Y. Tayalati^{137e}, A.C. Taylor¹⁰⁷, G.N. Taylor⁹¹, P.T.E. Taylor⁹¹,
 W. Taylor^{163b}, F.A. Teischinger³², P. Teixeira-Dias⁸⁰, K.K. Temming⁵¹, D. Temple¹⁴⁴, H. Ten Kate³²,
 P.K. Teng¹⁵³, J.J. Teoh¹²⁰, F. Tepel¹⁷⁸, S. Terada⁶⁹, K. Terashi¹⁵⁷, J. Terron⁸⁵, S. Terzo¹³, M. Testa⁵⁰,
 R.J. Teuscher^{161.m}, T. Thevenaux-Pelzer⁸⁸, J.P. Thomas¹⁹, J. Thomas-Wilsker⁸⁰, P.D. Thompson¹⁹,
 A.S. Thompson⁵⁶, L.A. Thomsen¹⁷⁹, E. Thomson¹²⁴, M.J. Tibbetts¹⁶, R.E. Ticse Torres⁸⁸,
 V.O. Tikhomirov^{98.ao}, Yu.A. Tikhonov^{111.c}, S. Timoshenko¹⁰⁰, P. Tipton¹⁷⁹, S. Tisserant⁸⁸,
 K. Todome¹⁵⁹, S. Todorova-Nova⁵, J. Tojo⁷³, S. Tokár^{146a}, K. Tokushuku⁶⁹, E. Tolley⁵⁹, L. Tomlinson⁸⁷,
 M. Tomoto¹⁰⁵, L. Tompkins^{145.ap}, K. Toms¹⁰⁷, B. Tong⁵⁹, P. Tornambe⁵¹, E. Torrence¹¹⁸, H. Torres¹⁴⁴,
 E. Torró Pastor¹⁴⁰, J. Toth^{88.aq}, F. Touchard⁸⁸, D.R. Tovey¹⁴¹, T. Trefzger¹⁷⁷, A. Tricoli²⁷,
 I.M. Trigger^{163a}, S. Trincaz-Duvold⁸³, M.F. Tripiana¹³, W. Trischuk¹⁶¹, B. Trocme⁵⁸, A. Trofymov⁴⁵,
 C. Troncon^{94a}, M. Trotter-McDonald¹⁶, M. Trovatelli¹⁷², L. Truong^{167a,167c}, M. Trzebinski⁴²,
 A. Trzupek⁴², J.C.-L. Tseng¹²², P.V. Tsiarehka⁹⁵, G. Tsipolitis¹⁰, N. Tsirintanis⁹, S. Tsiskaridze¹³,
 V. Tsiskaridze⁵¹, E.G. Tskhadadze^{54a}, K.M. Tsui^{62a}, I.I. Tsukerman⁹⁹, V. Tsulaia¹⁶, S. Tsuno⁶⁹,
 D. Tsybychev¹⁵⁰, Y. Tu^{62b}, A. Tudorache^{28b}, V. Tudorache^{28b}, T.T. Tulbure^{28a}, A.N. Tuna⁵⁹,
 S.A. Tupputi^{22a,22b}, S. Turchikhin⁶⁸, D. Turgeman¹⁷⁵, I. Turk Cakir^{4b.ar}, R. Turra^{94a,94b}, P.M. Tuts³⁸,
 G. Uccielli^{22a,22b}, I. Ueda⁶⁹, M. Ughetto^{148a,148b}, F. Ukegawa¹⁶⁴, G. Unal³², A. Undrus²⁷, G. Unel¹⁶⁶,
 F.C. Ungaro⁹¹, Y. Unno⁶⁹, C. Unverdorben¹⁰², J. Urban^{146b}, P. Urquijo⁹¹, P. Urrejola⁸⁶, G. Usai⁸,
 J. Usui⁶⁹, L. Vacavant⁸⁸, V. Vacek¹³⁰, B. Vachon⁹⁰, C. Valderanis¹⁰², E. Valdes Santurio^{148a,148b},
 N. Valencic¹⁰⁹, S. Valentini^{22a,22b}, A. Valero¹⁷⁰, L. Valery¹³, S. Valkar¹³¹, J.A. Valls Ferrer¹⁷⁰,
 W. Van Den Wollenberg¹⁰⁹, P.C. Van Der Deijl¹⁰⁹, H. van der Graaf¹⁰⁹, N. van Eldik¹⁵⁴,
 P. van Gemmeren⁶, J. Van Nieuwkoop¹⁴⁴, I. van Vulpen¹⁰⁹, M.C. van Woerden¹⁰⁹, M. Vanadia^{134a,134b},

W. Vandelli³², R. Vanguri¹²⁴, A. Vaniachine¹⁶⁰, P. Vankov¹⁰⁹, G. Vardanyan¹⁸⁰, R. Vari^{134a}, E.W. Varnes⁷, T. Varol⁴³, D. Varouchas⁸³, A. Vartapetian⁸, K.E. Varvell¹⁵², J.G. Vasquez¹⁷⁹, G.A. Vasquez^{34b}, F. Vazeille³⁷, T. Vazquez Schroeder⁹⁰, J. Veatch⁵⁷, V. Veeraraghavan⁷, L.M. Veloce¹⁶¹, F. Veloso^{128a,128c}, S. Veneziano^{134a}, A. Ventura^{76a,76b}, M. Venturi¹⁷², N. Venturi¹⁶¹, A. Venturini²⁵, V. Vercesi^{123a}, M. Verducci^{134a,134b}, W. Verkerke¹⁰⁹, J.C. Vermeulen¹⁰⁹, M.C. Vetterli^{144,d}, O. Viazlo⁸⁴, I. Vichou^{169,*}, T. Vickey¹⁴¹, O.E. Vickey Boeriu¹⁴¹, G.H.A. Viehhauser¹²², S. Viel¹⁶, L. Vigani¹²², M. Villa^{22a,22b}, M. Villaplana Perez^{94a,94b}, E. Vilucchi⁵⁰, M.G. Vincter³¹, V.B. Vinogradov⁶⁸, A. Vishwakarma⁴⁵, C. Vittori^{22a,22b}, I. Vivarelli¹⁵¹, S. Vlachos¹⁰, M. Vlasak¹³⁰, M. Vogel¹⁷⁸, P. Vokac¹³⁰, G. Volpi^{126a,126b}, M. Volpi⁹¹, H. von der Schmitt¹⁰³, E. von Toerne²³, V. Vorobel¹³¹, K. Vorobev¹⁰⁰, M. Vos¹⁷⁰, R. Voss³², J.H. Vosseveld⁷⁷, N. Vranjes¹⁴, M. Vranjes Milosavljevic¹⁴, V. Vrba¹³⁰, M. Vreeswijk¹⁰⁹, R. Vuillermet³², I. Vukotic³³, P. Wagner²³, W. Wagner¹⁷⁸, H. Wahlberg⁷⁴, S. Wahrenmund⁴⁷, J. Wakabayashi¹⁰⁵, J. Walder⁷⁵, R. Walker¹⁰², W. Walkowiak¹⁴³, V. Wallangen^{148a,148b}, C. Wang^{35b}, C. Wang^{36b,as}, F. Wang¹⁷⁶, H. Wang¹⁶, H. Wang³, J. Wang⁴⁵, J. Wang¹⁵², K. Wang⁹⁰, Q. Wang¹¹⁵, R. Wang⁶, S.M. Wang¹⁵³, T. Wang³⁸, W. Wang^{36a}, C. Wanotayaroj¹¹⁸, A. Warburton⁹⁰, C.P. Ward³⁰, D.R. Wardrope⁸¹, A. Washbrook⁴⁹, P.M. Watkins¹⁹, A.T. Watson¹⁹, M.F. Watson¹⁹, G. Watts¹⁴⁰, S. Watts⁸⁷, B.M. Waugh⁸¹, S. Webb⁸⁶, M.S. Weber¹⁸, S.W. Weber¹⁷⁷, S.A. Weber³¹, J.S. Webster⁶, A.R. Weidberg¹²², B. Weinert⁶⁴, J. Weingarten⁵⁷, C. Weiser⁵¹, H. Weits¹⁰⁹, P.S. Wells³², T. Wenaus²⁷, T. Wengler³², S. Wenig³², N. Wermes²³, M.D. Werner⁶⁷, P. Werner³², M. Wessels^{60a}, J. Wetter¹⁶⁵, K. Whalen¹¹⁸, N.L. Whallon¹⁴⁰, A.M. Wharton⁷⁵, A. White⁸, M.J. White¹, R. White^{34b}, D. Whiteson¹⁶⁶, F.J. Wickens¹³³, W. Wiedenmann¹⁷⁶, M. Wielers¹³³, C. Wiglesworth³⁹, L.A.M. Wiik-Fuchs²³, A. Wildauer¹⁰³, F. Wilk⁸⁷, H.G. Wilkens³², H.H. Williams¹²⁴, S. Williams¹⁰⁹, C. Willis⁹³, S. Willocq⁸⁹, J.A. Wilson¹⁹, I. Wingerter-Seez⁵, F. Winklmeier¹¹⁸, O.J. Winston¹⁵¹, B.T. Winter²³, M. Wittgen¹⁴⁵, M. Wobisch^{82,r}, T.M.H. Wolf¹⁰⁹, R. Wolff⁸⁸, M.W. Wolter⁴², H. Wolters^{128a,128c}, S.D. Worm¹³³, B.K. Wosiek⁴², J. Wotschack³², M.J. Woudstra⁸⁷, K.W. Wozniak⁴², M. Wu⁵⁸, M. Wu³³, S.L. Wu¹⁷⁶, X. Wu⁵², Y. Wu⁹², T.R. Wyatt⁸⁷, B.M. Wynne⁴⁹, S. Xella³⁹, Z. Xi⁹², D. Xu^{35a}, L. Xu²⁷, B. Yabsley¹⁵², S. Yacoob^{147a}, D. Yamaguchi¹⁵⁹, Y. Yamaguchi¹²⁰, A. Yamamoto⁶⁹, S. Yamamoto¹⁵⁷, T. Yamanaka¹⁵⁷, K. Yamauchi¹⁰⁵, Y. Yamazaki⁷⁰, Z. Yan²⁴, H. Yang^{36c}, H. Yang¹⁷⁶, Y. Yang¹⁵³, Z. Yang¹⁵, W-M. Yao¹⁶, Y.C. Yap⁸³, Y. Yasu⁶⁹, E. Yatsenko⁵, K.H. Yau Wong²³, J. Ye⁴³, S. Ye²⁷, I. Yeletskikh⁶⁸, E. Yildirim⁸⁶, K. Yorita¹⁷⁴, R. Yoshida⁶, K. Yoshihara¹²⁴, C. Young¹⁴⁵, C.J.S. Young³², S. Youssef²⁴, D.R. Yu¹⁶, J. Yu⁸, J. Yu⁶⁷, L. Yuan⁷⁰, S.P.Y. Yuen²³, I. Yusuf^{30,at}, B. Zabinski⁴², G. Zacharis¹⁰, R. Zaidan¹³, A.M. Zaitsev^{132,af}, N. Zakharchuk⁴⁵, J. Zalieckas¹⁵, A. Zaman¹⁵⁰, S. Zambito⁵⁹, D. Zanzi⁹¹, C. Zeitnitz¹⁷⁸, M. Zeman¹³⁰, A. Zemla^{41a}, J.C. Zeng¹⁶⁹, Q. Zeng¹⁴⁵, O. Zenin¹³², T. Ženiš^{146a}, D. Zerwas¹¹⁹, D. Zhang⁹², F. Zhang¹⁷⁶, G. Zhang^{36a,am}, H. Zhang^{35b}, J. Zhang⁶, L. Zhang⁵¹, L. Zhang^{36a}, M. Zhang¹⁶⁹, R. Zhang²³, R. Zhang^{36a,as}, X. Zhang^{36b}, Y. Zhang^{35a}, Z. Zhang¹¹⁹, X. Zhao⁴³, Y. Zhao^{36b,au}, Z. Zhao^{36a}, A. Zhemchugov⁶⁸, J. Zhong¹²², B. Zhou⁹², C. Zhou¹⁷⁶, L. Zhou⁴³, M. Zhou^{35a}, M. Zhou¹⁵⁰, N. Zhou^{35c}, C.G. Zhu^{36b}, H. Zhu^{35a}, J. Zhu⁹², Y. Zhu^{36a}, X. Zhuang^{35a}, K. Zhukov⁹⁸, A. Zibell¹⁷⁷, D. Zieminska⁶⁴, N.I. Zimine⁶⁸, C. Zimmermann⁸⁶, S. Zimmermann⁵¹, Z. Zinonos¹⁰³, M. Zinser⁸⁶, M. Ziolkowski¹⁴³, L. Živković¹⁴, G. Zobernig¹⁷⁶, A. Zoccoli^{22a,22b}, M. zur Nedden¹⁷, L. Zwalinski³².

¹ Department of Physics, University of Adelaide, Adelaide, Australia

² Physics Department, SUNY Albany, Albany NY, United States of America

³ Department of Physics, University of Alberta, Edmonton AB, Canada

⁴ (a) Department of Physics, Ankara University, Ankara; (b) Istanbul Aydin University, Istanbul; (c)

Division of Physics, TOBB University of Economics and Technology, Ankara, Turkey

⁵ LAPP, CNRS/IN2P3 and Université Savoie Mont Blanc, Annecy-le-Vieux, France

⁶ High Energy Physics Division, Argonne National Laboratory, Argonne IL, United States of America

- ⁷ Department of Physics, University of Arizona, Tucson AZ, United States of America
- ⁸ Department of Physics, The University of Texas at Arlington, Arlington TX, United States of America
- ⁹ Physics Department, National and Kapodistrian University of Athens, Athens, Greece
- ¹⁰ Physics Department, National Technical University of Athens, Zografou, Greece
- ¹¹ Department of Physics, The University of Texas at Austin, Austin TX, United States of America
- ¹² Institute of Physics, Azerbaijan Academy of Sciences, Baku, Azerbaijan
- ¹³ Institut de Física d'Altes Energies (IFAE), The Barcelona Institute of Science and Technology, Barcelona, Spain
- ¹⁴ Institute of Physics, University of Belgrade, Belgrade, Serbia
- ¹⁵ Department for Physics and Technology, University of Bergen, Bergen, Norway
- ¹⁶ Physics Division, Lawrence Berkeley National Laboratory and University of California, Berkeley CA, United States of America
- ¹⁷ Department of Physics, Humboldt University, Berlin, Germany
- ¹⁸ Albert Einstein Center for Fundamental Physics and Laboratory for High Energy Physics, University of Bern, Bern, Switzerland
- ¹⁹ School of Physics and Astronomy, University of Birmingham, Birmingham, United Kingdom
- ²⁰ ^(a) Department of Physics, Bogazici University, Istanbul; ^(b) Department of Physics Engineering, Gaziantep University, Gaziantep; ^(d) Istanbul Bilgi University, Faculty of Engineering and Natural Sciences, Istanbul, Turkey; ^(e) Bahcesehir University, Faculty of Engineering and Natural Sciences, Istanbul, Turkey, Turkey
- ²¹ Centro de Investigaciones, Universidad Antonio Narino, Bogota, Colombia
- ²² ^(a) INFN Sezione di Bologna; ^(b) Dipartimento di Fisica e Astronomia, Università di Bologna, Bologna, Italy
- ²³ Physikalisches Institut, University of Bonn, Bonn, Germany
- ²⁴ Department of Physics, Boston University, Boston MA, United States of America
- ²⁵ Department of Physics, Brandeis University, Waltham MA, United States of America
- ²⁶ ^(a) Universidade Federal do Rio De Janeiro COPPE/EE/IF, Rio de Janeiro; ^(b) Electrical Circuits Department, Federal University of Juiz de Fora (UFJF), Juiz de Fora; ^(c) Federal University of Sao Joao del Rei (UFSJ), Sao Joao del Rei; ^(d) Instituto de Fisica, Universidade de Sao Paulo, Sao Paulo, Brazil
- ²⁷ Physics Department, Brookhaven National Laboratory, Upton NY, United States of America
- ²⁸ ^(a) Transilvania University of Brasov, Brasov, Romania; ^(b) Horia Hulubei National Institute of Physics and Nuclear Engineering, Bucharest; ^(c) National Institute for Research and Development of Isotopic and Molecular Technologies, Physics Department, Cluj Napoca; ^(d) University Politehnica Bucharest, Bucharest; ^(e) West University in Timisoara, Timisoara, Romania
- ²⁹ Departamento de Física, Universidad de Buenos Aires, Buenos Aires, Argentina
- ³⁰ Cavendish Laboratory, University of Cambridge, Cambridge, United Kingdom
- ³¹ Department of Physics, Carleton University, Ottawa ON, Canada
- ³² CERN, Geneva, Switzerland
- ³³ Enrico Fermi Institute, University of Chicago, Chicago IL, United States of America
- ³⁴ ^(a) Departamento de Física, Pontificia Universidad Católica de Chile, Santiago; ^(b) Departamento de Física, Universidad Técnica Federico Santa María, Valparaíso, Chile
- ³⁵ ^(a) Institute of High Energy Physics, Chinese Academy of Sciences, Beijing; ^(b) Department of Physics, Nanjing University, Jiangsu; ^(c) Physics Department, Tsinghua University, Beijing 100084, China
- ³⁶ ^(a) Department of Modern Physics, University of Science and Technology of China, Anhui; ^(b) School of Physics, Shandong University, Shandong; ^(c) Department of Physics and Astronomy, Shanghai Key Laboratory for Particle Physics and Cosmology, Shanghai Jiao Tong University, Shanghai; (also

affiliated with PKU-CHEP), China

³⁷ Laboratoire de Physique Corpusculaire, Université Clermont Auvergne, Université Blaise Pascal, CNRS/IN2P3, Clermont-Ferrand, France

³⁸ Nevis Laboratory, Columbia University, Irvington NY, United States of America

³⁹ Niels Bohr Institute, University of Copenhagen, Kobenhavn, Denmark

⁴⁰ ^(a) INFN Gruppo Collegato di Cosenza, Laboratori Nazionali di Frascati; ^(b) Dipartimento di Fisica, Università della Calabria, Rende, Italy

⁴¹ ^(a) AGH University of Science and Technology, Faculty of Physics and Applied Computer Science, Krakow; ^(b) Marian Smoluchowski Institute of Physics, Jagiellonian University, Krakow, Poland

⁴² Institute of Nuclear Physics Polish Academy of Sciences, Krakow, Poland

⁴³ Physics Department, Southern Methodist University, Dallas TX, United States of America

⁴⁴ Physics Department, University of Texas at Dallas, Richardson TX, United States of America

⁴⁵ DESY, Hamburg and Zeuthen, Germany

⁴⁶ Lehrstuhl für Experimentelle Physik IV, Technische Universität Dortmund, Dortmund, Germany

⁴⁷ Institut für Kern- und Teilchenphysik, Technische Universität Dresden, Dresden, Germany

⁴⁸ Department of Physics, Duke University, Durham NC, United States of America

⁴⁹ SUPA - School of Physics and Astronomy, University of Edinburgh, Edinburgh, United Kingdom

⁵⁰ INFN Laboratori Nazionali di Frascati, Frascati, Italy

⁵¹ Fakultät für Mathematik und Physik, Albert-Ludwigs-Universität, Freiburg, Germany

⁵² Departement de Physique Nucleaire et Corpusculaire, Université de Genève, Geneva, Switzerland

⁵³ ^(a) INFN Sezione di Genova; ^(b) Dipartimento di Fisica, Università di Genova, Genova, Italy

⁵⁴ ^(a) E. Andronikashvili Institute of Physics, Iv. Javakhishvili Tbilisi State University, Tbilisi; ^(b) High Energy Physics Institute, Tbilisi State University, Tbilisi, Georgia

⁵⁵ II Physikalisches Institut, Justus-Liebig-Universität Giessen, Giessen, Germany

⁵⁶ SUPA - School of Physics and Astronomy, University of Glasgow, Glasgow, United Kingdom

⁵⁷ II Physikalisches Institut, Georg-August-Universität, Göttingen, Germany

⁵⁸ Laboratoire de Physique Subatomique et de Cosmologie, Université Grenoble-Alpes, CNRS/IN2P3, Grenoble, France

⁵⁹ Laboratory for Particle Physics and Cosmology, Harvard University, Cambridge MA, United States of America

⁶⁰ ^(a) Kirchhoff-Institut für Physik, Ruprecht-Karls-Universität Heidelberg, Heidelberg; ^(b)

Physikalisches Institut, Ruprecht-Karls-Universität Heidelberg, Heidelberg; ^(c) ZITI Institut für technische Informatik, Ruprecht-Karls-Universität Heidelberg, Mannheim, Germany

⁶¹ Faculty of Applied Information Science, Hiroshima Institute of Technology, Hiroshima, Japan

⁶² ^(a) Department of Physics, The Chinese University of Hong Kong, Shatin, N.T., Hong Kong; ^(b)

Department of Physics, The University of Hong Kong, Hong Kong; ^(c) Department of Physics and Institute for Advanced Study, The Hong Kong University of Science and Technology, Clear Water Bay, Kowloon, Hong Kong, China

⁶³ Department of Physics, National Tsing Hua University, Taiwan, Taiwan

⁶⁴ Department of Physics, Indiana University, Bloomington IN, United States of America

⁶⁵ Institut für Astro- und Teilchenphysik, Leopold-Franzens-Universität, Innsbruck, Austria

⁶⁶ University of Iowa, Iowa City IA, United States of America

⁶⁷ Department of Physics and Astronomy, Iowa State University, Ames IA, United States of America

⁶⁸ Joint Institute for Nuclear Research, JINR Dubna, Dubna, Russia

⁶⁹ KEK, High Energy Accelerator Research Organization, Tsukuba, Japan

⁷⁰ Graduate School of Science, Kobe University, Kobe, Japan

⁷¹ Faculty of Science, Kyoto University, Kyoto, Japan

- 72 Kyoto University of Education, Kyoto, Japan
- 73 Department of Physics, Kyushu University, Fukuoka, Japan
- 74 Instituto de Física La Plata, Universidad Nacional de La Plata and CONICET, La Plata, Argentina
- 75 Physics Department, Lancaster University, Lancaster, United Kingdom
- 76 ^(a) INFN Sezione di Lecce; ^(b) Dipartimento di Matematica e Fisica, Università del Salento, Lecce, Italy
- 77 Oliver Lodge Laboratory, University of Liverpool, Liverpool, United Kingdom
- 78 Department of Experimental Particle Physics, Jožef Stefan Institute and Department of Physics, University of Ljubljana, Ljubljana, Slovenia
- 79 School of Physics and Astronomy, Queen Mary University of London, London, United Kingdom
- 80 Department of Physics, Royal Holloway University of London, Surrey, United Kingdom
- 81 Department of Physics and Astronomy, University College London, London, United Kingdom
- 82 Louisiana Tech University, Ruston LA, United States of America
- 83 Laboratoire de Physique Nucléaire et de Hautes Energies, UPMC and Université Paris-Diderot and CNRS/IN2P3, Paris, France
- 84 Fysiska institutionen, Lunds universitet, Lund, Sweden
- 85 Departamento de Física Teórica C-15, Universidad Autónoma de Madrid, Madrid, Spain
- 86 Institut für Physik, Universität Mainz, Mainz, Germany
- 87 School of Physics and Astronomy, University of Manchester, Manchester, United Kingdom
- 88 CPPM, Aix-Marseille Université and CNRS/IN2P3, Marseille, France
- 89 Department of Physics, University of Massachusetts, Amherst MA, United States of America
- 90 Department of Physics, McGill University, Montreal QC, Canada
- 91 School of Physics, University of Melbourne, Victoria, Australia
- 92 Department of Physics, The University of Michigan, Ann Arbor MI, United States of America
- 93 Department of Physics and Astronomy, Michigan State University, East Lansing MI, United States of America
- 94 ^(a) INFN Sezione di Milano; ^(b) Dipartimento di Fisica, Università di Milano, Milano, Italy
- 95 B.I. Stepanov Institute of Physics, National Academy of Sciences of Belarus, Minsk, Republic of Belarus
- 96 Research Institute for Nuclear Problems of Byelorussian State University, Minsk, Republic of Belarus
- 97 Group of Particle Physics, University of Montreal, Montreal QC, Canada
- 98 P.N. Lebedev Physical Institute of the Russian Academy of Sciences, Moscow, Russia
- 99 Institute for Theoretical and Experimental Physics (ITEP), Moscow, Russia
- 100 National Research Nuclear University MEPhI, Moscow, Russia
- 101 D.V. Skobeltsyn Institute of Nuclear Physics, M.V. Lomonosov Moscow State University, Moscow, Russia
- 102 Fakultät für Physik, Ludwig-Maximilians-Universität München, München, Germany
- 103 Max-Planck-Institut für Physik (Werner-Heisenberg-Institut), München, Germany
- 104 Nagasaki Institute of Applied Science, Nagasaki, Japan
- 105 Graduate School of Science and Kobayashi-Maskawa Institute, Nagoya University, Nagoya, Japan
- 106 ^(a) INFN Sezione di Napoli; ^(b) Dipartimento di Fisica, Università di Napoli, Napoli, Italy
- 107 Department of Physics and Astronomy, University of New Mexico, Albuquerque NM, United States of America
- 108 Institute for Mathematics, Astrophysics and Particle Physics, Radboud University Nijmegen/Nikhef, Nijmegen, Netherlands
- 109 Nikhef National Institute for Subatomic Physics and University of Amsterdam, Amsterdam, Netherlands

- ¹¹⁰ Department of Physics, Northern Illinois University, DeKalb IL, United States of America
- ¹¹¹ Budker Institute of Nuclear Physics, SB RAS, Novosibirsk, Russia
- ¹¹² Department of Physics, New York University, New York NY, United States of America
- ¹¹³ Ohio State University, Columbus OH, United States of America
- ¹¹⁴ Faculty of Science, Okayama University, Okayama, Japan
- ¹¹⁵ Homer L. Dodge Department of Physics and Astronomy, University of Oklahoma, Norman OK, United States of America
- ¹¹⁶ Department of Physics, Oklahoma State University, Stillwater OK, United States of America
- ¹¹⁷ Palacký University, RCPTM, Olomouc, Czech Republic
- ¹¹⁸ Center for High Energy Physics, University of Oregon, Eugene OR, United States of America
- ¹¹⁹ LAL, Univ. Paris-Sud, CNRS/IN2P3, Université Paris-Saclay, Orsay, France
- ¹²⁰ Graduate School of Science, Osaka University, Osaka, Japan
- ¹²¹ Department of Physics, University of Oslo, Oslo, Norway
- ¹²² Department of Physics, Oxford University, Oxford, United Kingdom
- ¹²³ ^(a) INFN Sezione di Pavia; ^(b) Dipartimento di Fisica, Università di Pavia, Pavia, Italy
- ¹²⁴ Department of Physics, University of Pennsylvania, Philadelphia PA, United States of America
- ¹²⁵ National Research Centre "Kurchatov Institute" B.P.Konstantinov Petersburg Nuclear Physics Institute, St. Petersburg, Russia
- ¹²⁶ ^(a) INFN Sezione di Pisa; ^(b) Dipartimento di Fisica E. Fermi, Università di Pisa, Pisa, Italy
- ¹²⁷ Department of Physics and Astronomy, University of Pittsburgh, Pittsburgh PA, United States of America
- ¹²⁸ ^(a) Laboratório de Instrumentação e Física Experimental de Partículas - LIP, Lisboa; ^(b) Faculdade de Ciências, Universidade de Lisboa, Lisboa; ^(c) Department of Physics, University of Coimbra, Coimbra; ^(d) Centro de Física Nuclear da Universidade de Lisboa, Lisboa; ^(e) Departamento de Física, Universidade do Minho, Braga; ^(f) Departamento de Física Teórica y del Cosmos and CAFPE, Universidad de Granada, Granada (Spain); ^(g) Dep Física and CEFITEC of Faculdade de Ciências e Tecnologia, Universidade Nova de Lisboa, Caparica, Portugal
- ¹²⁹ Institute of Physics, Academy of Sciences of the Czech Republic, Praha, Czech Republic
- ¹³⁰ Czech Technical University in Prague, Praha, Czech Republic
- ¹³¹ Faculty of Mathematics and Physics, Charles University in Prague, Praha, Czech Republic
- ¹³² State Research Center Institute for High Energy Physics (Protvino), NRC KI, Russia
- ¹³³ Particle Physics Department, Rutherford Appleton Laboratory, Didcot, United Kingdom
- ¹³⁴ ^(a) INFN Sezione di Roma; ^(b) Dipartimento di Fisica, Sapienza Università di Roma, Roma, Italy
- ¹³⁵ ^(a) INFN Sezione di Roma Tor Vergata; ^(b) Dipartimento di Fisica, Università di Roma Tor Vergata, Roma, Italy
- ¹³⁶ ^(a) INFN Sezione di Roma Tre; ^(b) Dipartimento di Matematica e Fisica, Università Roma Tre, Roma, Italy
- ¹³⁷ ^(a) Faculté des Sciences Ain Chock, Réseau Universitaire de Physique des Hautes Energies - Université Hassan II, Casablanca; ^(b) Centre National de l'Energie des Sciences Techniques Nucleaires, Rabat; ^(c) Faculté des Sciences Semlalia, Université Cadi Ayyad, LPHEA-Marrakech; ^(d) Faculté des Sciences, Université Mohamed Premier and LPTPM, Oujda; ^(e) Faculté des sciences, Université Mohammed V, Rabat, Morocco
- ¹³⁸ DSM/IRFU (Institut de Recherches sur les Lois Fondamentales de l'Univers), CEA Saclay (Commissariat à l'Energie Atomique et aux Energies Alternatives), Gif-sur-Yvette, France
- ¹³⁹ Santa Cruz Institute for Particle Physics, University of California Santa Cruz, Santa Cruz CA, United States of America
- ¹⁴⁰ Department of Physics, University of Washington, Seattle WA, United States of America

- ¹⁴¹ Department of Physics and Astronomy, University of Sheffield, Sheffield, United Kingdom
- ¹⁴² Department of Physics, Shinshu University, Nagano, Japan
- ¹⁴³ Fachbereich Physik, Universität Siegen, Siegen, Germany
- ¹⁴⁴ Department of Physics, Simon Fraser University, Burnaby BC, Canada
- ¹⁴⁵ SLAC National Accelerator Laboratory, Stanford CA, United States of America
- ¹⁴⁶ ^(a) Faculty of Mathematics, Physics & Informatics, Comenius University, Bratislava; ^(b) Department of Subnuclear Physics, Institute of Experimental Physics of the Slovak Academy of Sciences, Kosice, Slovak Republic
- ¹⁴⁷ ^(a) Department of Physics, University of Cape Town, Cape Town; ^(b) Department of Physics, University of Johannesburg, Johannesburg; ^(c) School of Physics, University of the Witwatersrand, Johannesburg, South Africa
- ¹⁴⁸ ^(a) Department of Physics, Stockholm University; ^(b) The Oskar Klein Centre, Stockholm, Sweden
- ¹⁴⁹ Physics Department, Royal Institute of Technology, Stockholm, Sweden
- ¹⁵⁰ Departments of Physics & Astronomy and Chemistry, Stony Brook University, Stony Brook NY, United States of America
- ¹⁵¹ Department of Physics and Astronomy, University of Sussex, Brighton, United Kingdom
- ¹⁵² School of Physics, University of Sydney, Sydney, Australia
- ¹⁵³ Institute of Physics, Academia Sinica, Taipei, Taiwan
- ¹⁵⁴ Department of Physics, Technion: Israel Institute of Technology, Haifa, Israel
- ¹⁵⁵ Raymond and Beverly Sackler School of Physics and Astronomy, Tel Aviv University, Tel Aviv, Israel
- ¹⁵⁶ Department of Physics, Aristotle University of Thessaloniki, Thessaloniki, Greece
- ¹⁵⁷ International Center for Elementary Particle Physics and Department of Physics, The University of Tokyo, Tokyo, Japan
- ¹⁵⁸ Graduate School of Science and Technology, Tokyo Metropolitan University, Tokyo, Japan
- ¹⁵⁹ Department of Physics, Tokyo Institute of Technology, Tokyo, Japan
- ¹⁶⁰ Tomsk State University, Tomsk, Russia, Russia
- ¹⁶¹ Department of Physics, University of Toronto, Toronto ON, Canada
- ¹⁶² ^(a) INFN-TIFPA; ^(b) University of Trento, Trento, Italy, Italy
- ¹⁶³ ^(a) TRIUMF, Vancouver BC; ^(b) Department of Physics and Astronomy, York University, Toronto ON, Canada
- ¹⁶⁴ Faculty of Pure and Applied Sciences, and Center for Integrated Research in Fundamental Science and Engineering, University of Tsukuba, Tsukuba, Japan
- ¹⁶⁵ Department of Physics and Astronomy, Tufts University, Medford MA, United States of America
- ¹⁶⁶ Department of Physics and Astronomy, University of California Irvine, Irvine CA, United States of America
- ¹⁶⁷ ^(a) INFN Gruppo Collegato di Udine, Sezione di Trieste, Udine; ^(b) ICTP, Trieste; ^(c) Dipartimento di Chimica, Fisica e Ambiente, Università di Udine, Udine, Italy
- ¹⁶⁸ Department of Physics and Astronomy, University of Uppsala, Uppsala, Sweden
- ¹⁶⁹ Department of Physics, University of Illinois, Urbana IL, United States of America
- ¹⁷⁰ Instituto de Física Corpuscular (IFIC) and Departamento de Física Atómica, Molecular y Nuclear and Departamento de Ingeniería Electrónica and Instituto de Microelectrónica de Barcelona (IMB-CNM), University of Valencia and CSIC, Valencia, Spain
- ¹⁷¹ Department of Physics, University of British Columbia, Vancouver BC, Canada
- ¹⁷² Department of Physics and Astronomy, University of Victoria, Victoria BC, Canada
- ¹⁷³ Department of Physics, University of Warwick, Coventry, United Kingdom
- ¹⁷⁴ Waseda University, Tokyo, Japan

- ¹⁷⁵ Department of Particle Physics, The Weizmann Institute of Science, Rehovot, Israel
- ¹⁷⁶ Department of Physics, University of Wisconsin, Madison WI, United States of America
- ¹⁷⁷ Fakultät für Physik und Astronomie, Julius-Maximilians-Universität, Würzburg, Germany
- ¹⁷⁸ Fakultät für Mathematik und Naturwissenschaften, Fachgruppe Physik, Bergische Universität Wuppertal, Wuppertal, Germany
- ¹⁷⁹ Department of Physics, Yale University, New Haven CT, United States of America
- ¹⁸⁰ Yerevan Physics Institute, Yerevan, Armenia
- ¹⁸¹ Centre de Calcul de l'Institut National de Physique Nucléaire et de Physique des Particules (IN2P3), Villeurbanne, France
- ^a Also at Department of Physics, King's College London, London, United Kingdom
- ^b Also at Institute of Physics, Azerbaijan Academy of Sciences, Baku, Azerbaijan
- ^c Also at Novosibirsk State University, Novosibirsk, Russia
- ^d Also at TRIUMF, Vancouver BC, Canada
- ^e Also at Department of Physics & Astronomy, University of Louisville, Louisville, KY, United States of America
- ^f Also at Physics Department, An-Najah National University, Nablus, Palestine
- ^g Also at Department of Physics, California State University, Fresno CA, United States of America
- ^h Also at Department of Physics, University of Fribourg, Fribourg, Switzerland
- ⁱ Also at Departament de Física de la Universitat Autònoma de Barcelona, Barcelona, Spain
- ^j Also at Departamento de Física e Astronomia, Faculdade de Ciências, Universidade do Porto, Portugal
- ^k Also at Tomsk State University, Tomsk, Russia, Russia
- ^l Also at Università di Napoli Parthenope, Napoli, Italy
- ^m Also at Institute of Particle Physics (IPP), Canada
- ⁿ Also at Horia Hulubei National Institute of Physics and Nuclear Engineering, Bucharest, Romania
- ^o Also at Department of Physics, St. Petersburg State Polytechnical University, St. Petersburg, Russia
- ^p Also at Department of Physics, The University of Michigan, Ann Arbor MI, United States of America
- ^q Also at Centre for High Performance Computing, CSIR Campus, Rosebank, Cape Town, South Africa
- ^r Also at Louisiana Tech University, Ruston LA, United States of America
- ^s Also at Institutio Catalana de Recerca i Estudis Avancats, ICREA, Barcelona, Spain
- ^t Also at Graduate School of Science, Osaka University, Osaka, Japan
- ^u Also at Institute for Mathematics, Astrophysics and Particle Physics, Radboud University Nijmegen/Nikhef, Nijmegen, Netherlands
- ^v Also at Department of Physics, The University of Texas at Austin, Austin TX, United States of America
- ^w Also at Institute of Theoretical Physics, Ilia State University, Tbilisi, Georgia
- ^x Also at CERN, Geneva, Switzerland
- ^y Also at Georgian Technical University (GTU), Tbilisi, Georgia
- ^z Also at Ochadai Academic Production, Ochanomizu University, Tokyo, Japan
- ^{aa} Also at Manhattan College, New York NY, United States of America
- ^{ab} Also at Academia Sinica Grid Computing, Institute of Physics, Academia Sinica, Taipei, Taiwan
- ^{ac} Also at School of Physics, Shandong University, Shandong, China
- ^{ad} Also at Departamento de Física Teórica y del Cosmos and CAFPE, Universidad de Granada, Granada (Spain), Portugal
- ^{ae} Also at Department of Physics, California State University, Sacramento CA, United States of America
- ^{af} Also at Moscow Institute of Physics and Technology State University, Dolgoprudny, Russia
- ^{ag} Also at Département de Physique Nucléaire et Corpusculaire, Université de Genève, Geneva, Switzerland
- ^{ah} Also at International School for Advanced Studies (SISSA), Trieste, Italy

- ai* Also at Department of Physics and Astronomy, University of South Carolina, Columbia SC, United States of America
- aj* Also at Institut de Física d'Altes Energies (IFAE), The Barcelona Institute of Science and Technology, Barcelona, Spain
- ak* Also at School of Physics, Sun Yat-sen University, Guangzhou, China
- al* Also at Institute for Nuclear Research and Nuclear Energy (INRNE) of the Bulgarian Academy of Sciences, Sofia, Bulgaria
- am* Also at Faculty of Physics, M.V.Lomonosov Moscow State University, Moscow, Russia
- an* Also at Institute of Physics, Academia Sinica, Taipei, Taiwan
- ao* Also at National Research Nuclear University MEPhI, Moscow, Russia
- ap* Also at Department of Physics, Stanford University, Stanford CA, United States of America
- aq* Also at Institute for Particle and Nuclear Physics, Wigner Research Centre for Physics, Budapest, Hungary
- ar* Also at Giresun University, Faculty of Engineering, Turkey
- as* Also at CPPM, Aix-Marseille Université and CNRS/IN2P3, Marseille, France
- at* Also at University of Malaya, Department of Physics, Kuala Lumpur, Malaysia
- au* Also at LAL, Univ. Paris-Sud, CNRS/IN2P3, Université Paris-Saclay, Orsay, France
- * Deceased